

https://dspace.org/

The isomerization of –androstene-3,17-dione by hGST A3-3: the pursuit of catalytic perfection in proton abstraction reactions of 3-ketosteroids

Daka, Jonathan Lembelani

2015-05-07
http://hdl.handle.net/10539/17659

Downloaded from a DSpace repository. https://dspace.org/

The isomerization of Δ^5–androstene-3,17-dione by hGST A3-3: the pursuit of catalytic perfection in proton abstraction reactions of 3-ketosteroids

Jonathan Lembelani Daka

A dissertation submitted to the Faculty of Science, University of the Witwatersrand, Johannesburg, in fulfillment of the requirements for the degree of Master of Science.

Johannesburg, 2015



Supervisor: Professor Heini Dirr

Advisor: Dr Ikechukwu Achilonu

Research Output

Original research Publication	Daka, L. J., Achilonu, I., and Dirr, W. H. (2014) The Isomerization of Δ^5–Androstene-3,17-dione by the Human Glutathione Transferase A3-3 Proceeds via a Conjugated Heteroannular Diene Intermediate. *J. Biol. Chem. 289, 32243-32252*
Conference presentations	The evolution of enzyme function and catalytic efficiency (2014). The Mellon Mays Annual Graduate Student Summer Conference. Emory University, Atlanta, U.S.A
	The Isomerization of Δ^5–Androstene-3,17-dione by the Human Glutathione Transferase A3-3 (2014) The South African Society for Biochemistry and Molecular Biology. Cape Town , South Africa
	The Isomerization of Δ^5–Androstene-3,17-dione by the Human Glutathione Transferase A3-3 Proceeds via a Conjugated Heteroannular Diene Intermediate (2014) The Post Graduate Cross Faculty Symposium. University of the Witwatersrand, Johannesburg, South Africa.

Declaration

I declare that this dissertation is my own, unaided work. It is being submitted for the degree of Master of Science in the University of the Witwatersrand, Johannesburg. It has not been submitted for any other degree or examination at any other University.

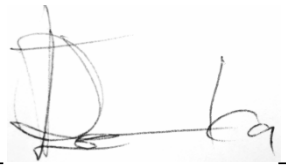

_____

Jonathan L. Daka

___10th____ day of___Februay_____, 2015

Abstract

The seemingly simple proton abstraction reactions underpin many chemical transformations including isomerization reactions and are thus of immense biological significance. Despite the energetic cost, enzyme-catalyzed proton abstraction reactions show remarkable rate enhancements. The pathways leading to these accelerated rates are numerous and on occasion partly enigmatic. The isomerization of the steroid, Δ^5-androstene-3,17-dione by the human glutathione transferase A3-3 in mammals was investigated to gain insight into the mechanism. Particular emphasis was placed on the nature of the transition state, the intermediate suspected of aiding this process and the hydrogen bonds postulated to be the stabilizing forces of these transient species. Kinetics studies on Δ^5-androstene-17-one, a substrate that is incapable of forming hydrogen bonds reveal that such stabilizing forces are not a requirement to explain the observed rate enhancements. The UV-Vis detection of the intermediate places this specie in the catalytic pathway while fluorescence spectroscopy is used to obtain the binding constant of the intermediate analogue equilenin. Analysis of the kinetics data in terms of the Marcus formalism indicates that the human glutathione transferase A3-3 lowers the intrinsic kinetic barrier by 3 kcal/mole. The results lead to the conclusion that this reaction proceeds through an enforced concerted mechanism in which the barrier to product formation is kinetically insignificant.

“His true monument lies not on the shelves of libraries, but in the thoughts of men, and in the history of more than one science.”

Rudolph Clausius on Josiah Willard Gibbs

ACKNOWLEDGMENTS

A higher power I call God, who does not play dice with the world but has the option to.

My mother and grandmother to whom I owe a debt of gratitude for their unwavering support and belief in me.

Professor H.W. Dirr for his amazing support and guidance throughout my endeavours and for the opportunity to work with extraordinary individuals in his laboratory.

Dr I. Achilonu for his support in and out of the laboratory.

All of my current and past colleagues of the Protein-Structure Function Research Unit.

The National Research Foundation for the financial assistance.

Finally to my friends, Lungile Ndlovu, Buhle Zwane and Sandile Buthelezi that have supported me and shown me the value of life.

Contents

Research Output i

Declaration ii

Abstract iii

ACKNOWLEDGMENTS v

List of abbreviations x

Chapter 1 Introduction 1

1.0 The GSTs 1

1.1 Steroid biosynthesis 2

1.2 Isomerisation of Δ^5-AD by GSTs 4

1.3 Stepwise versus single step reaction pathways 7

1.4 Dual functionality in enzymes 9

1.5 Aim 10

1.6 Objectives 11

CHAPTER 2: EXPERIMENTAL PROCEDURES 13

2.1 Materials 13

2.2 Heterologous Protein Expression and Purification 13

2.3 Thrombin cleavage 14

2.4 Kinetic Measurements 14

2.5 Steady-state kinetics 15

2.6 Determination of the pK_a of the thiol group of free and enzyme bound GSH 16

2.7 Fluorescence measurements with equilenin 17

2.8 Absorbance measurements with 19-nortestosterone 18

2.9 Detection of the dienolate intermediate 18

2.10 Determination of the activation energy 19

2.11 Solvent isotope effects with Δ^5–AD 19

CHAPTER 3: RESULTS 21

3.1 Sequence identity 21

3.2 Over-expression and purification 22

3.2.1 Ion metal affinity chromatography 22

3.2.2 Thrombin cleavage 23

3.2.3 Purification of his-tag free hGSTA3-3 protein 24

3.3 Functional characterization 25
3.3.1 Enzyme activity 25
3.4 Steady state kinetics of hGSTA3-3 with Δ^5–AD and Δ^5–AO 28
3.4.1 Michaelis-Menten kinetics for Δ^5–AD 28
3.4.2 Determination of kinetic parameters k_{cat} and k_{cat}/K_M 28
3.4.3 Michaelis-Menten kinetics for Δ^5–AO 29
3.4.4 Determination of kinetic parameters k_{cat} and k_{cat}/K_M 30
3.4.5 Steady-State kinetics with varying [GSH] and saturating [Δ^5-AD] and [Δ^5-AO] 30
3.5 The pK_a value of GSH upon binding 32
3.6 The nature of the intermediate at the active site of hGST A3-3 33
3.7 UV-Vis detection of the intermediate 35
3.8 The activation energy of reaction 36
3.9 The binding constant of equilenin to hGST A3-3 37
3.9 Solvent isotope effects 39
3.9.1 Isotopic exchange at 238 nm in D_2O 39
3.9.2 Determination of the kinetic parameters k_{cat} and k_{cat}/K_M at 238 nm in D_2O 39
3.9.3 Michaelis-Menten kinetics at 238 nm in H_2O 41
3.9.4 Determination of the kinetic parameters k_{cat} and k_{cat}/K_M at 238 nm in H_2O 41
3.9.5 Isotopic exchange at 248 nm in D_2O 43
3.9.6 Determination of the kinetic parameters k_{cat} and k_{cat}/K_M at 248 nm in D_2O 43
Chapter 4 Discussion 46
5 Conclusion 55
References 57
Appendix 61

List of figures

Figure 1. The GST fold 2

Figure 2. The basic steroid structure. 2

Figure 3. The biosynthesis of steroid hormones. 3

Figure 4. The conversion of Δ^5-AD to Δ^4-AD 4

Figure 5. Protein sequence alignment. 4

Figure 6. The catalytic mechanism of KSI 5

Figure 7. Proposed reaction mechanisms for Δ^5-AD isomerization by hGST A3-3 6

Figure 8. The crystal structure of the ternary complex of hGST A3-3 7

Figure 9. Concerted and stepwise reaction mechanisms. 8

Figure 10. The molecular structures of Δ^5-AO and Δ^5-AD 10

Figure 11. The positions of double bonds after proton abstraction 11

Figure 12: The progression of the enzyme catalysed reaction via the intermediate 19

Figure 13: Solvent isotope exchange between D_2O and the dienolate intermediate. 20

Figure 14: Plasmid sequencing 21

Figure 15. Elution profile of hGST A3-3 22

Figure 16. Protein mobility as characterised by SDS-PAGE 23

Figure. 17 and 18: Thrombin cleavage 24

Figure 19. A progress curve for the isomerisation of Δ^5- AD to Δ^4- AD observed at 248 nm 26

Figure 20. A progress curve for the isomerisation of Δ^5- AO observed at 248 nm 27

Figure 21. Michaelis-Menten Kinetics for Δ^5-AD 28

Figure 22. The k_{cat} /K_M values for Δ^5-AD isomerisation 29

Figure 23. Michaelis-Menten Kinetics for Δ^5-AO 29

Figure 24. The kinetic parameters k_{cat} and k_{cat} /K_M values for Δ^5-AO 30

Figure 25. The Michaelis-Menten Plot with a constant concentration of Δ^5-AD 31

Figure 26. The pK_a of GSH upon binding 33

Figure 27. Fluorescence emission and absorbance spectra of equilenin and 19-nortestosterone 34

Figure 28. The absorbance spectrum of Δ^5-AO 36

Figure 29. The Arrhenius plots at 248 nm and 238 nm 37

Figure 30. The binding constant of equilenin 38

Figure 31. Solvent isotope effects 39

Figure 32. The kinetic parameters k_{cat} and k_{cat}/K_M at 238 nm in D_2O 40
Figure 33. The k_{cat}/K_M values obtained for Δ^5-AD 42
Figure 34. Isotopic exchange at 248 nm in D_2O 43
Figure 35. The kinetic parameters k_{cat} and k_{cat}/K_M at 248 nm in D_2O 44
Figure 36. The proposed reaction pathway for the isomerization of Δ^5–AD by hGST A3-3 52
Figure 37. Free energy profiles illustrating the Albery and Knowles analysis 55

List of tables

TABLE 3-1. Kinetic parameters of hGST A3-3 with two different substrates Δ^5–AD and Δ^5–AO 32
TABLE 3-2. Solvent isotope exchange with Δ^5–AD at 238 nm and 248 nm. 45

List of abbreviations

A280	Absorbance at 280 nm
Δ^5-AD	Δ^5-androstene-3,17-dione
Δ^5-AO	Δ^5-androstene-17-one
ΔG^0	Gibbs free energy of reaction
$\Delta G^{\ddagger}$	Gibbs free energy of activation
ΔG_{int}	Intrinsic kinetic barrier
Amp	Ampicillin
EDTA	Ethylenediaminetetra-acetic acid
GSH	Reduced glutathione
G-site	Glutathione binding site
GST	Glutathione transferase
hGST A3-3	Human class alpha glutathione transferase with two type 3 subunits
H-site	Hydrophobic electrophilic binding site
IPTG	Isopropyl-β-D-thio-galactoside
k_{cat}	Catalytic constant
k_{cat}/K_M	Catalytic efficiency
kDa	Kilodalton
K_M	Michaelis-Menten constant
LB	Luria-Bertani
L-site	Non-substrate ligand binding site
*M*r	Relative molecular mass
NaCl	Sodium chloride
OD	Optical density
ORF	Open reading frame
PDB	Protein Data Bank
rpm	Revolutions per minute
SDS-PAGE	Sodium dodecyl Sulfate polyacrylamide gel electrophoresis
UV	ultraviolet
*V*m	Maximum velocity
ε_{280}	Molar extinction coefficient at 280 nm
ln	The natural logarithm
R	Molar gas constant given as $1.987204118 \times 10^{-3}$ kcal K^{-1} mol^{-1}
T	Temperature in Kelvin
E_a	The energy of activation
$\Delta H^{\ddagger}$	Enthalpy of reaction
kcal/mol	Kilocalories per mole

The IUPAC-IUBMB one and three letter codes for amino acids are used
Enzyme: Glutathione Transferase (EC 2.5.1.18).

Chapter 1 Introduction

1.0 The GSTs

The glutathione transferases (GSTs) (EC 2.5.1.18) encompass a physiologically important and diverse group of enzymes present in both eukaryotes and prokaryotes (Mannervik, 2005). Present in either the monomeric or dimeric state; the enzymes play a pivotal homeostatic role in detoxification by nucleophilicaly tethering the tripeptide glutathione (GSH), to variations of hydrophobic xenobiotic alkylating agents (Allardyce *et al*., 1999; Dirr and Wallace, 1999). Furthermore these enzymes are implicated in the biosynthesis of essential molecules such as prostaglandins, leukotriene A, testosterone and progesterone (Armstrong, 1997) and in the transportation of non-ligand substrates (Listowski, 1993).

There are three major families of GSTs, namely the cytosolic GSTs, the mitochondrial GSTs and the microsomal GSTs now referred to as the membrane-associated proteins in eicosanoid and glutathione metabolism (MAPEGS). The largest of these groups is the cytosolic GSTs with eight subdivisions that are based on sequence similarity and substrate specificity (Wallace and Dirr, 1999) In spite of the diversity within the cytosolic GSTs, they all function as dimers and have evolved additional functions unique to them. They are able to catalyse the isomerisation of Δ^5-3-ketosteroids, 13-*cis*-retinoic acid and maleylacetoacetate (Oakley, 2005). The GSTs possess a canonical fold consisting of two linker-bound domains within each subunit (Dirr *et al*., 1994; Wilce and Parker 1994). Domain 1, known as the N-terminal domain incorporates an ancestral thioredoxin fold that has been conserved over evolutionary time and has the glutathione (GSH) binding site known as the G-site, while domain 2 referred to as the C-terminal domain shows variability within its structure and forms the distinguishing feature between isoenzymes (Figure 1) (Allardyce *et al*., 1999). This domain forms the binding site for highly hydrophobic substrates (H-site) and also provides a ligandin site for non-substrate compounds (Listowski, 1993). The C-terminal domain is also the binding site of steroids such as Δ^5-AD.



Figure 1. The hGST homodimer (with subunits green and cyan) and its thioredoxin fold, showing the N-terminal domain (magenta) and an all-alpha helical C-terminal domain (green) (PDB code 1PKZ).. Image generated with PyMOL (DeLano Scientific, San Carlos).

1.1 Steroid biosynthesis

Steroids are a class of organic compounds which perform diverse homeostatic functions such as: the regulation of metabolic pathways, stress reactions, salt balance and sexual development and function. These compounds possess a characteristic arrangement of four fused rings, three of which are cyclohexane rings and an additional cyclopentane ring (Moss, 1989) .The three fused cyclohexane rings are known as a phenanthrene molecule and as such all steroids possess a skeleton of cyclopentaphenanthrene (Figure 2).

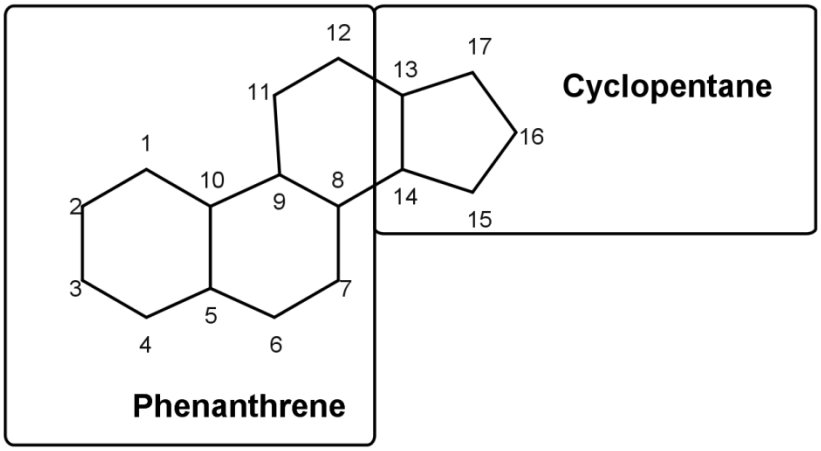

Figure 2: The basic steroid structure. The structure has a phenanthrene moiety (composed of three fused cyclohexanes, A, B and C) and a cyclopentane moiety (D). This skeleton is known as a cyclopentaphenanthrene with the IUPAC recommended ring lettering and carbon atom numbering.

The production of steroid hormones such as testosterone and progesterone from cholesterol proceeds via a complex series of oxidation and isomerization reactions (Figure 3) (Montgomery *et al.*, 1996). A critical step in this biosynthetic pathway is the isomerization of the β,γ double

bond of Δ^5-androstene-3,17-dione (Δ^5-AD) to the α, β isomer Δ^4-androstene-3,17-dione (Δ^4-AD), a labile hydrogen from C4 adjacent to the carbonyl functional group of Δ^5–AD is abstracted and transferred to C6 (Figure 4). In bacteria this conversion is catalyzed by ketosteroid isomerase (KSI) (Talalay *et al*., 1955) while mammalian steroid hormone biosynthesis appears to be more complex, were Δ^4–AD is produced directly from dehydroepiandrosterone (DHEA) by the enzyme 3-β hydroxysteroid dehydrogenase (3βHSD) (Miller and Auchus, 2011). Other studies, however, indicate that hGST A3-3 may play a role in mammalian steroidogenesis (Raffalli-Mathieu, 2008). Although the KSI catalyzed conversion of Δ^5–AD has been elucidated (Hawkinson *et al*., 1991), the hGST A3-3 catalyzed reaction remains enigmatic.

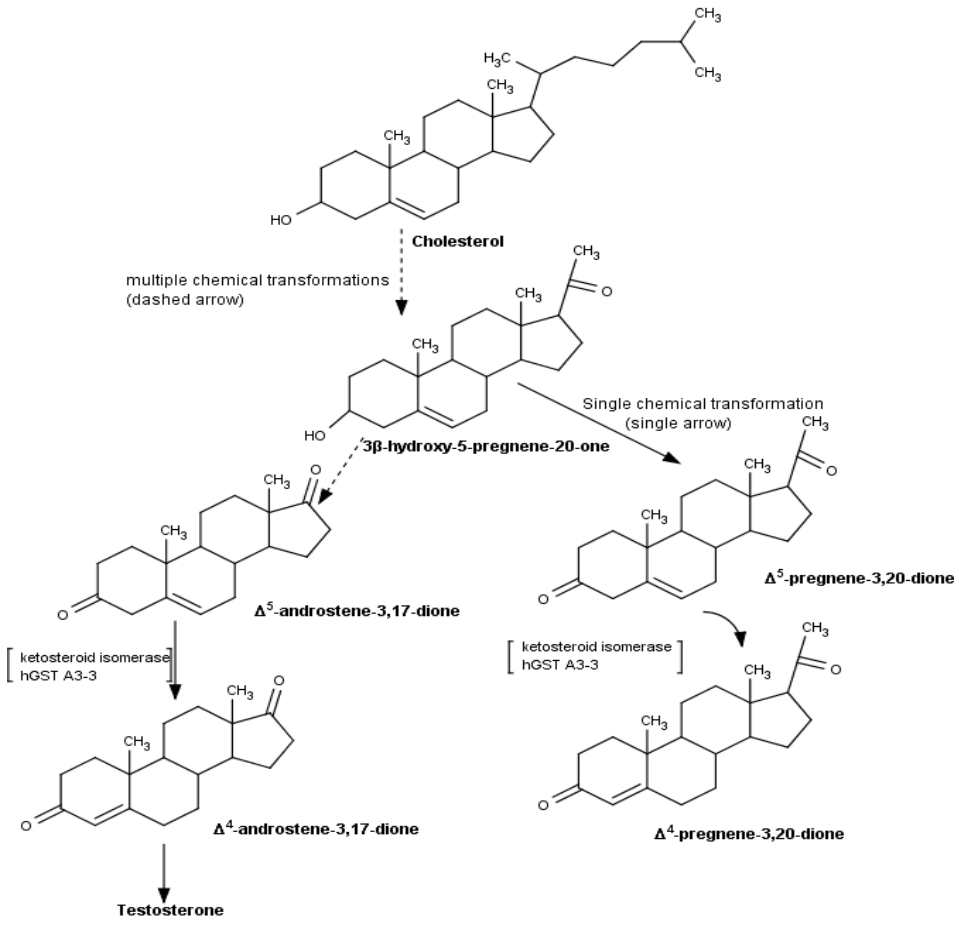

Figure 3: The biosynthesis of steroid hormones as adapted from Montgomery *et al.* (1996). The end product in Δ^5-AD isomerisation in this schematic is the hormone testosterone belonging to the androgens. A diverse group of other hormones belonging to other classes are produced but have not been shown for clarity. Ketosteroid isomerase (KSI) and hGST A3-3 (shown in square brackets) both catalyse the formation of $\Delta^{\mathbf{4}}$–androstene-3,17-dione (Δ^4-AD) and $\Delta^{\mathbf{4}}$–pregnene-3,20-dione .

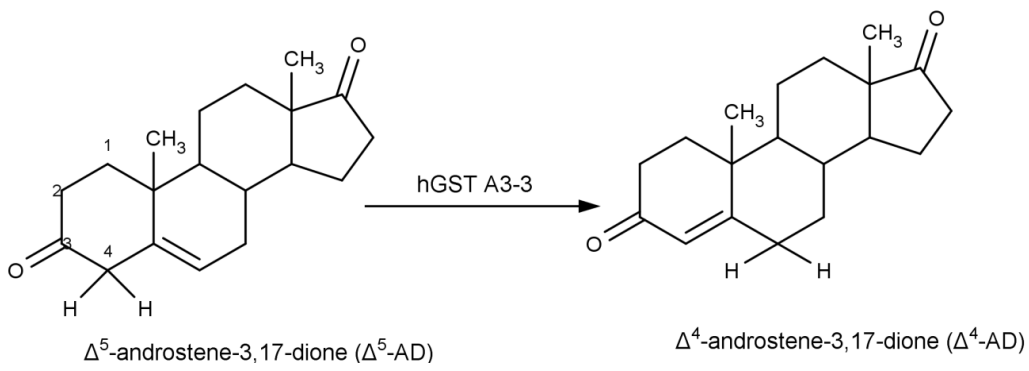

Δ5-androstene-3,17-dione (Δ5-AD)

Δ4-androstene-3,17-dione (Δ4-AD)

Figure 4. The conversion of Δ^5-AD (with carbon atoms labelled 1 to 4) to Δ^4-AD showing the GST mediated double bond isomerisation in the biosynthesis of testosterone and progesterone.

1.2 Isomerisation of Δ^5-AD by GSTs

In 1976 Benson and Talalay showed that a major GSH-dependant enzyme displays high isomerase activity with 3-ketosteroids (Benson and Talalay, 1976) and 25 years later Johansson and Mannervik (Johansson and Mannervik, 2001) identified the human glutathione transferase A3-3 (hGST A3-3) as displaying the highest isomerase activity over other members of the same class due to amino acid variations in the H-site (Figure 5).

```
GSTA3_HUMAN   MAGKPKLHYFNGRGRMEPIRWLLAAAGVEFEEKFIGURESAEDLGKLRNDGSLMFQQVPMVEI
GSTA1_HUMAN   MAEKPKLHYFNARGRMESTRWLLAAAGVEFEEKFIKSAEDLDKLRNDGYLMFQQVPMVEI
KSI           ----------------------------MNTPEHMTAVVQRYVAALNAGDLDGIVALFADD

                        70        80        90       100       110       120
                         |         |         |         |         |         |
GSTA3_HUMAN   DGMKLVQTRAILNYIASKYNLYGKDIKERALIDMYTEGMADLNEMILLLPLCRPEEKDAK
GSTA1_HUMAN   DGMKLVQTRAILNYIASKYNLYGKDIKERALIDMYIEGIADLGEMILLLPVCPPEEKDAK
KSI           ATVEDPVGSEPRSGTAAIREFYANSLKLPLAVELTQEVRAVANEAAFAFTVSFEYQGRKT

        130       140       150       160       170       180
                   |         |         |         |         |         |
GSTA3_HUMAN   IALIKEKTKSRYFPAFEKVLQSHGQDYLVGNKLSRADISLVELLYYVEELDSSLISNFPL
GSTA1_HUMAN   LALIKEKIKNRYFPAFEKVLKSHGQDYLVGNKLSRADIHLVELLYYVEELDSSLISSFPL
KSI           VVAPIDHFRFNGAGKVVSMRALFGEKNIHAGA----------------------------

                       190       200       210       220
                         |         |         |         |
GSTA3_HUMAN   LKALKTRISNLPTVKKFLQPGSPRKPPADAKALEEARKIFRF
GSTA1_HUMAN   LKALKTRISNLPTVKKFLQPGSPRKPPMDEKSLEEARKIFRF
KSI    ----------------------------------------
```

Figure 5: Protein sequence alignment. An alignment of hGST A3-3, hGST A1-1 and KSI; Red represents identical residues, blue represents residues with similar properties and green represents identical residues only to the hGSTs. The residues forming part of the H-site of the alpha GSTs and the corresponding residues in KSI are highlighted in rectangles. Alignment generated by MULTALIN –multiple sequence alignment with hierarchical clustering (Corpet, 1988).

The GSTs with the highest isomerase activity belonging to the alpha class are hGST A3-3 and hGST A1-1 (Johansson and Mannervik, 2001). There is a 91% sequence identity between hGST A3-3 and hGST A1-1 with three different amino acids in the H-site (the binding site of Δ^5-AD) between the two isoenzymes (Figure 4). There is a 43% sequence homology between both hGSTs and ketosteroid isomerase (KSI).

Two mechanisms of Δ^5-AD isomerisation have been suggested with the only commonality between them being the role of GSH as a Brønsted base, abstracting a proton from position 4 in the Δ^5-AD substrate. This is in contrast to the well-established functions of GSH as a nucleophile in conjugation reactions which proceed via a Meisenheimer complex (Arvanites and Boerth, 2001). A very thin line exists between basicity and nucleophilicity, thus, this could be suggestive of a change in the environment of the GSH, or the lack of a proper leaving group in the substrate acting as a kinetic barrier for nucleophilicity. Other enzymes such as KSI perform a similar role, also proceeding by initial proton abstraction with diffusion controlled catalytic efficiency (Pollack, 2004). This suggests that KSI has evolved a highly efficient mechanism of transition state stabilization, allowing its activity to be two-orders of magnitude greater than GST A3-3. The greater rate enhancement in KSI stems from its oxyanion hole (Figure 6) with the tyrosine and aspartic acid side chains stabilizing the dienolate transition state by strong hydrogen bonds (Wu *et al.*, 1997).

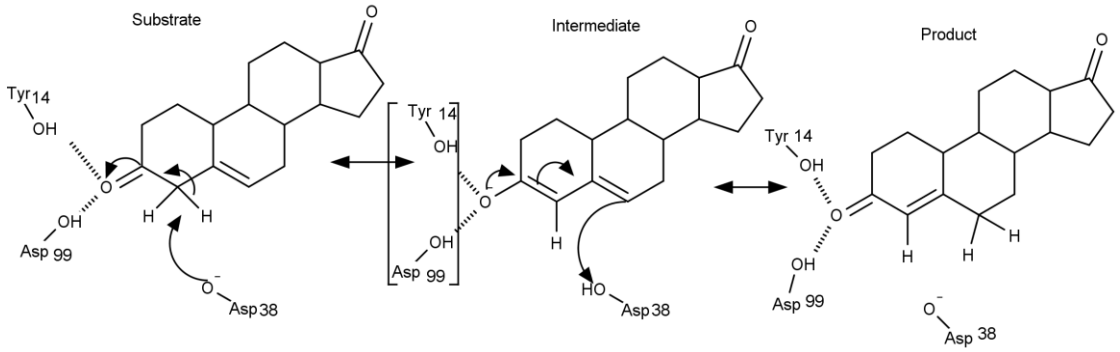

Figure 6: The catalytic mechanism of KSI. The reaction as adapted from Pollack (2004) proceeds by initial proton abstraction on carbon-4 by Asp 38. The resulting dienolate intermediate is stabilized by two hydrogen bonds formed between the carbonyl oxygen and Tyr14 and Asp 99. The abstracted proton is then transferred to carbon-6.

There has been much contention over the GST A3-3 catalytic conversion of Δ^5-AD to Δ^4-AD. Ji and co-workers have proposed a mechanism shown in scheme I (Figure 7) that proceeds by a step-wise pathway via the formation of a dienolate intermediate, stabilized by electron delocalization through a conjugate system of vacant p-orbitals along O-C3-C4-C5-C6 (Gu *et al*., 2004). It is thought that electron delocalization alone is insufficient to explain the observed catalytic rates and a water molecule that would act as a hydrogen bond donor to the carbonyl oxygen to further stabilize the dienolate intermediate has been proposed. Structural evidence based on the crystal structure of a ternary complex of hGST A3-3, GSH and the product Δ^4 –AD (Figure 8) provided no evidence of such a stabilising water molecule prompting Mannervik and co-workers (Tars *et al*., 2010) to suggest that both the bond breaking process at C4 and the bond making process at C6 is concerted and is devoid of a stable dienolate intermediate as shown in scheme II (Figure 8). The implication is that the carbonyl oxygen plays no role in the stabilization process and electron delocalization proceeds directly from C3 to C6 in concert with proton transfer to C6.

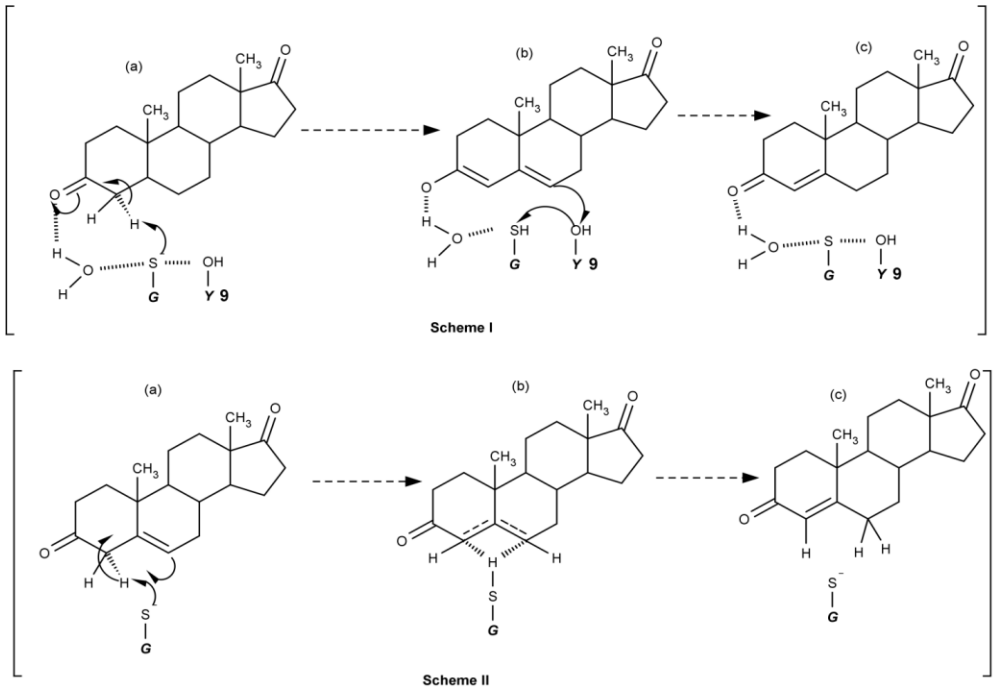

Figure 7. Proposed reaction mechanisms for Δ^5–AD isomerization by hGST A3-3. In scheme I, adapted from Gu *et al.* (2004), GSH abstracts the carbon 4 proton and a water molecule acts as a hydrogen bond donor, stabilizing the negative charge on the dienolate intermediate (a) and (b). The keto form is regenerated by the transfer of negative charge via a conjugation system of pi bonds with Tyr9 acting as a proton shuttle (c). In scheme II, adapted from Tars *et al.* (2010), GSH abstracts a proton from carbon 4 while simultaneously transferring it to carbon 6.

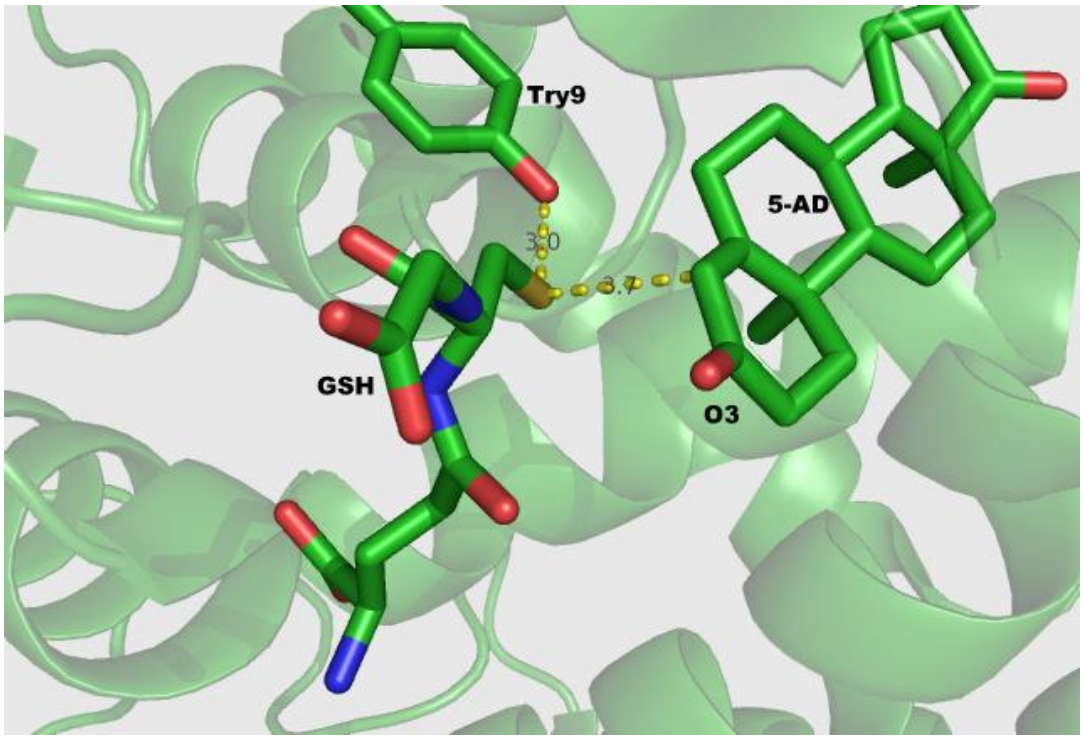

Figure 8. The crystal structure of the ternary complex of hGST A3-3 (PDB code: 2VCV) with GSH and Δ^4–AD. The spatial arrangement shows the position of GSH with respect to Δ^4–AD and Tyr9 (distances shown in yellow dashes). There is no amino acid residue in proximity to the Δ^4–AD oxygen atom labeled O3 that can stabilize the developing negative charge. Image rendered using PyMOL v0.99 (DeLano Scientific, 2006).

1.3 Stepwise versus single step reaction pathways

The critical difference between the two suggested mechanisms is the stepwise/concerted reaction paradigm. A stepwise reaction is defined as a reaction that occurs in two or more steps producing a stable intermediate that decomposes to product; while a concerted reaction has no intermediate, occurring only in one step with a single transition state (Figure 9) (Williams, 1994). Many enzymes have been shown to follow either the concerted or stepwise pathway in catalysis (Fried and Boxer, 2011; Heaps and Poulter, 2011). It is therefore necessary to analyze the energetic contributions (advantages/disadvantages) of each pathway.

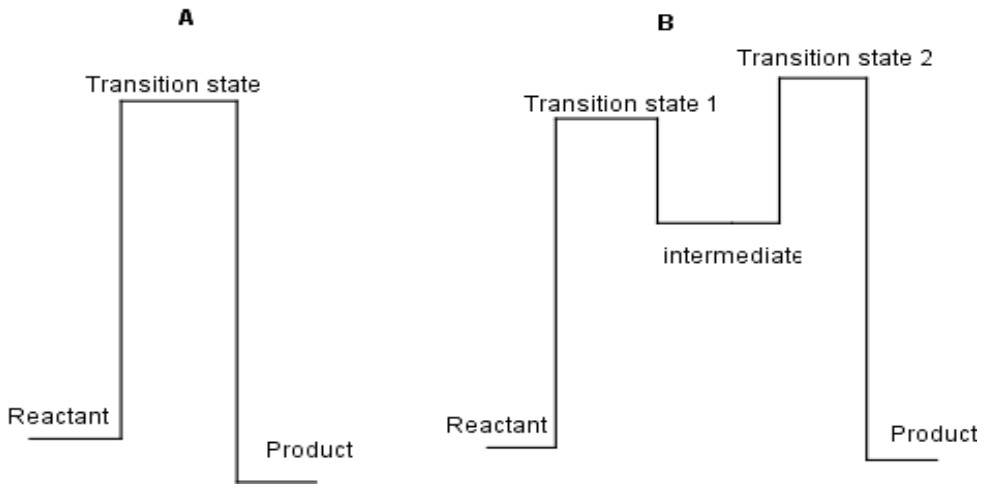

Figure 9. Concerted and stepwise reaction mechanisms. The stepwise mechanism (B) has a stable intermediate (I) with two transitions while the concerted mechanism (A) has one transition.

In the case of carbon acids having a keto group, abstraction of an alpha proton adjacent to the keto functional group results in negative charge development. The resulting anionic intermediate becomes more basic than the substrate and without a counteracting positive charge (whether by an acid catalysis or by hydrogen bonding) the charge imbalance in the transition results in electronic instability (Gerlt and Gassman, 1993). One approach used by enzymes is to posses the right amino acid residues that can reduce the negative charge imbalance of the transition state (through acid catalysis or hydrogen bonding). The reduction in instability increases the lifetime of the intermediate allowing it to decompose into products via a stepwise reaction mechanism. The second approach is to employ a concerted reaction mechanism in which a proton is simultaneously abstracted and transferred within the substrate. The timing however has to be synchronous without a substantial delay between bond breaking and bond formation (Williams, 1994). If the delay is substantial, charge imbalance develops. If the timing is synchronous, there is no significant build up of charge in the transition state because the abstracted proton is soon replaced. The advantage of a concerted mechanism is that it does not require stabilizing active site residues. Additionally the bond breaking process is aided by the energy released from bond formation which occurs simultaneously (Williams, 1994).

It is evident, however, that the mechanism of Δ^5-AD isomerisation is still unsettled. The proposals by the two groups appear radically different and while scheme I (Figure 7) is well articulated and follows a stepwise mechanism; without a stabilizing factor such as a water

molecule, or an alternative hydrogen bond donor or acid catalyst, the developing localized charge on the oxygen of the dienolate would greatly destabilize the transition state. The isomerisation of Δ^5-AD is predominantly catalysed by α-ketosteroid isomerase, an enzyme whose catalytic efficiency approaches the diffusion controlled limit and is two orders of magnitude greater than hGSTA3-3 activity (Pollack, 2004). However this enzyme possesses an oxyanion hole that stabilizes the transition state. An attempt is made to rescue a similar mechanism in hGSTA3-3 by invoking a contested water molecule to act as the stabilizing factor (Gu *et al.*, 2004). Mechanism 2 provides the easier option that can account for the absence of stabilizing residues. If a concerted reaction is assumed, then the catalytic power of hGST A3-3 stems from the timely abstraction and transfer of the proton rather than the stabilization of the transition by charged residues via a stepwise process. Scheme II however suggests that GSH acts as both the base that abstracts the proton and the acid that transfers it to position 6 synchronously. However, earlier studies have indicated that even in the absence of GSH, hGST A3-3 is still able to catalyse the reaction significantly (Pettersson and Mannervik, 2001).

1.4 Dual functionality in enzymes

It is within the realms of expectation that proteins that belong to the same super family should display similar reaction chemistry and perhaps a common mechanistic pathway of reducing the free energy associated with the rate-determining transition state (Babbitt and Gerlt, 1997). Indeed all members of the serine-protease super family, for example were known to utilize a similar mechanism of peptide bond hydrolysis which proceeded via a stabilised sp3 hybridized tetrahedral transition (Bornscheuer and Kazlauskas, 2004). However, promiscuity within enzyme homologues has evolved and it is now known that proteins with a common structural scaffold can catalyse distinct chemical reactions (Babbitt and Gerlt, 1997). The term "enzyme promiscuity" is shrouded in ambiguity and may require a clear and concise definition. Khersonsky and Tawfik define promiscuity as the ability of enzymes to catalyse reactions for which they were not initially designed for (Tawfik and Khersonsky, 2010). In this definition, enzymes that bind numerous substrates but follow a catalytic pathway inherent to their Enzyme Commission number (EC) (that is a similar mechanism in catalyzing the numerous substrates) are simply considered to be multispecific and not promiscuous. As in the example of most proteases that can hydrolyse both amide and ester bonds (C-O and C-N) where the substrates are different but the same catalytic mechanism of initial nucleophillic attack on an electron deficient

carbon atom is employed in both substrates. However, Bornscheuer and Kazlauskas clarify this when they define enzyme promiscuity as the ability of enzyme active sites to either catalyse different functional groups with the same catalytic mechanism or to pursue a different mechanistic pathway altogether (Bornscheuer and Kazlauskas, 2004; Oakley, 2005). The concept of enzyme plasticity is then used to describe these changes at the active site that result in promiscuity. According to this principle, point mutations at less well conserved regions of the active site result in the divergent evolution of new functions, while the better conserved regions maintain the signature reaction mechanisms common to all members of the super family (Todd *et al*., 2002; Oakley, 2005). Plasticity can further be extended from point mutations to repacking of tertiary contacts where structural or dynamic changes at specific enzyme regions invoke promiscuity as is the case with hGST A1-1 (Honaker *et al.*, 2011). Both definitions of enzyme promiscuity incorporate an alternative reaction chemistry which may not be shared by other members of a super family. This distinct chemical transformation is in turn, a product of divergent evolution driven by point mutations, gene duplications and tertiary rearrangements creating slight alterations at the active site.

1.5 Aim

The aim was to investigate the two proposed mechanisms in order to establish the most plausible reaction pathway. To achieve this, the substrate Δ^5-androstene-17-one (Δ^5–AO) (Figure 10) was used and the kinetic rate constants associated with this substrate were compared to those obtained with Δ^5–AD. The critical difference between these two substrates is the presence of the carbonyl functional group at C3 in Δ^5–AD.

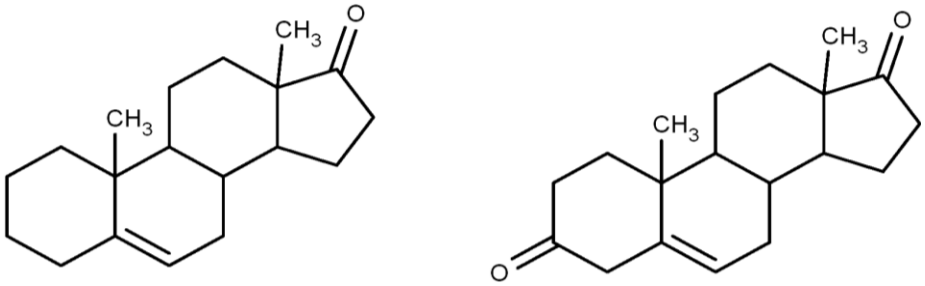

Δ^5–androstene-17-one (Δ^5–AO) Δ^5–androstene-3, 17-dione (Δ^5–AD)

Figure 10. The molecular structures of Δ^5–AO and Δ^5–AD indicate a major difference on the C3 position, with the keto group absent at this position in Δ^5–AO.

The hypothesis is that if the model proposed by Mannervik and co-workers is correct, there should be no significant differences in the observed rate constants between the two substrates and no evidence of intermediate formation. The absence of a carbonyl group at C3 in Δ^5-AO has two implications, (i) the molecule is incapable of forming any hydrogen bonding interactions with the proposed water molecule at that position and (ii), the transitioning from reactant to product can only be stabilized by a conjugate system of p-orbitals, which the molecule forms by the preferential C3 - C4 double bond over the C4 - C5 (Figure 11). The resulting stable intermediate (1) would be $\Delta^{3:5}$-androstadiene-17-one.

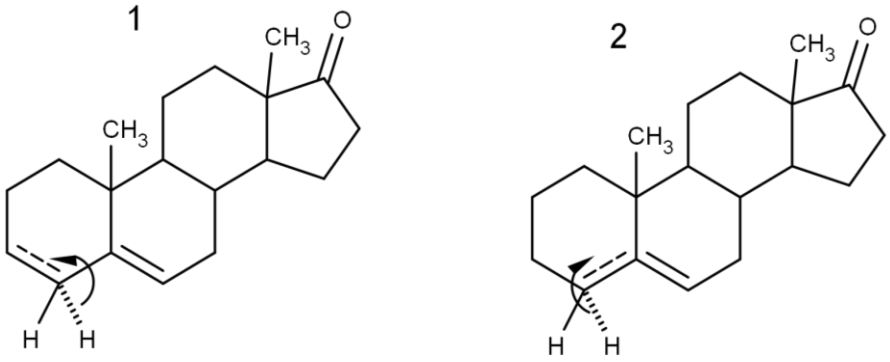

Figure 11. The positions of double bonds after proton abstraction at C4 of Δ^5 –AO in which the pathway labeled 1 is the most stable, forming a conjugate system. Pathway 2 creates 5 bonds at C5 making such a structure unlikely.

This allowed the implications of such energetic contributions to the hGST A3-3 catalyzed reaction to be deciphered. Furthermore, we obtain the dissociation constant (K_D) for the intermediate analogue, equilenin and use this value to approximate the relative stabilities of the bound substrate and the proposed intermediate. This information, together with the pK_a values of both the free and the enzyme-bound GSH is used to explain how the hGST A3-3 enhances the rate of proton abstraction reactions in steroidogenesis, where the frameworks of Albery and Knowles (Albery and Knowles, 1977) with the Marcus formalism (Marcus, 1969) are employed. We further provide a molecular mechanism consistent with these results that fully explains the observed rate enhancements, with particular focus on the nature of the contentious intermediate.

1.6 Objectives

The objectives were four-fold, firstly the wild type hGST A3-3 was to be expressed and purified successfully. Secondly, to obtain kinetic constants associated with the two subtstrates Δ^5-AD and

Δ^5-AO. Thirdly, to use spectroscopic techniques (absorbance and fluorescence) to verify/disprove the existence of an intermediate, probe the nature of the intermediate (if present) at the active site and obtain the binding constant of the proposed intermediate. Lastly, to generate an energy profile using solvent isotope effects that accurately describes the hGST A3-3 mediated isomerisation reaction.

CHAPTER 2: EXPERIMENTAL PROCEDURES

2.1 Materials

The target insert sequence encoding hGST A3-3 was cloned at the Ndel and BamHI restriction sites of the pET11a vector (GenScript, Inc). Sequencing of the target insert to confirm its identity was conducted by Inqaba Biotech (Pretoria, South Africa) using both the T7 promoter and T7 terminator primers. The chemicals GSH, equilenin, D_2O and K_2DPO_4 were purchased from Sigma-Aldrich (St. Louis, MO USA). The steroids Δ^5-androstene-3,17-dione and Δ^5- androstene-17-one were obtained from Steraloids Inc (Newport, RI). All other reagents were of analytical grade. All data fitting were done using Sigma Plot version 11 (Systat Software Inc., California,USA).

2.2 Heterologous Protein Expression and Purification

High level expression of the wild-type hGST A3-3 was based on the pET11a vector in BL21 (DE3) pLysS *Escherichia coli* cells (Lucigen, Middleton, WI, USA). The sequence landmarks of the vector include a 16 base pairs T7 promoter that facilitates strong transcription factor binding, an ampicillin resistance selection marker and a T7 terminator flanking the multiple cloning site (MCS). The cells were transformed as described by Chung *et al* (1989) and grown in 2×TY (1.6% (w/v) tryptone, 1% (w/v) yeast extract, 0.5% (w/v) NaCl) at 37 °C to an A_{600} of 0.4 at 230 rpm. A final concentration of 1 mM isopropyl-β-D-thiogalactoside (IPTG) was used to induce protein expression. The pLysS vector in the BL21 (DE3) expression system has the T7 RNA polymerase gene that is activated upon IPTG addition and induces T7 promoter driven expression. After 4 h of growth, the cells were harvested by centrifugation (5000 × g for 15 min) and re-suspended in 20 mM Tris-HCl, 1 mM EDTA and 0.02% NaN_3 at pH 7.4. The sample was frozen and thawed with the addition of 10 mg/ml of both DNAse I and lysozyme. The cells were lysed by ultrasonication (Misonix Inc. (model: XL-2020), Farmingdale, NY, USA) on ice for 6 cycles of 10 seconds with 50 % pulse intensity. The lysed cells were centrifuged at 4 ^oC at 16000 × g for 30 min and samples of whole cell extracts, the supernatant and pellet were run on 12% SDS-PAGE (Laemmli, 1970).

Protein purification was by immobilized metal affinity chromatography using nickel-Sepharose (Amersham Pharmacia Biotech). The column was washed with 5 column volumes of distilled water prior to use and charged with 1 column volume of 0.2 M $NiSO_4$. The column was washed a second time with 5 column volumes of distilled water to remove any unbound metal

ions. The column was equilibrated with 5 column volumes of 20 mM Tris-HCl, 200 mM NaCl at pH 7.4 and protein was eluted with 20 mM Tris-HCl buffer containing 0.5 M imadazole at pH 7.4 in a continuous gradient. The purification was done on an ÄKTAprime system attached to a computer with PrimeView 1.0 software (GEHealthcare Life Sciences, Uppsala, Sweden). The concentration of the dimer was determined at 280 nm using the protein subunit molar extinction coefficient of 23900 M^{-1} cm^{-1} (Johansson and Mannervik, 2001).

2.3 Thrombin cleavage

Eluted protein was dialysed in 20 mM Tris-HCl, 200 mM NaCl, 5 mM $CaCl_2$ at pH 8. Cleavage trials were conducted at room temperature on 500 µl of 5.2 mg/ml protein using 10 µl of thrombin from a stock concentration of 1 unit/µl. A sample volume of 10 µl was taken every 15 min and mixed with an equal volume of reducing sample buffer (which stopped the reaction by denaturing thrombin). The reduced sample was run on a 12% SDS-PAGE and complete cleavage of the N-terminal poly histidines was achieved after 1 h. The total protein volume of 10 ml was treated with the same amount of thrombin (10 µl of 1 unit/µl) at room temperature. Since complete cleavage of 500 µl of 5.2 mg/ml protein was achieved in 1 h, the cleavage of 10 ml of the protein with the same concentration was carried out overnight (20 hrs). An additional purification step using benzamidine-Sepharose produced thrombin-free pure protein. The purity of protein at each stage was determined using 12% SDS-PAGE and the protein was dialyzed against 20 mM sodium phosphate buffer, pH 8, containing 1 mM EDTA and 0.02% NaN_3 (w/v). The concentration of the dimer was determined at 280 nm using the protein subunit molar extinction coefficient of 23900 M^{-1} cm^{-1}.

2.4 Kinetic Measurements

The specific activity of hGST A3-3 toward Δ^5-AD for the isomerization reaction was determined at 248 nm, with a molar extinction coefficient of 16300 M^{-1} cm^{-1} for the product Δ^4-AD (Benson *et al*., 1977). The specific activity toward Δ^5-AO was determined at 248 nm with a molar extinction coefficient of 13600 M^{-1} cm^{-1} (Dorfman, 1953) or at 235 nm with a molar extinction coefficient of 18100 M^{-1} cm^{-1} (Burrows *et al*., 1937) for the detection of the suspected intermediate specie $\Delta^{3:5}$-androstadiene-17-one. Proton abstraction at carbon 4 of Δ^5-AO would result in two possible electron rearrangements; (1) the arrangement would result in the formation of two transient conjugated heteroannular ethylenic bonds (2), or adjacent double bonds that would result in an overcommitted carbon 5 atom with 5 bonds making this electronic

configuration unlikely. Conjugated double bonds are chromophoric and would be detected spectrophotometrically. The reaction of Δ^5-AO follows the formation of the two conjugated ethylenic bonds in the heteroannular carbanion intermediate. The calculated principle absorption band for the formation of this heteroannular diene is 235 nm or 248 nm (Dorfman, 1953; Woodward, 1941).

Stock concentrations of 20 mM GSH (in 20 mM sodium phosphate, pH 8.0) and 9.1 mM of both Δ^5-AD and Δ^5-AO (in 100% methanol) were prepared and enzyme concentrations ranging from 1-9 nM (Habig and Jakoby 1981) were used. The reaction was initiated by the addition of enzyme to 100 µl of GSH and 11 µl of Δ^5-AD or Δ^5-AO to create a final assay concentration of 2 mM GSH and 100 µM for either Δ^5-AD or Δ^5-AO in a final volume of 1 ml. Linear progress curves were followed on the Jasco V-630 UV-VIS spectrophotometer (Jasco Inc.,Tokyo, Japan) with a correction for non enzymatic reaction rates. The initial rates in absorbance units per second were converted to µmoles of product formed per second per milligram of enzyme using the aforementioned extinction coefficients. All measurements were done in triplicate in 25 mM sodium phosphate buffer, pH 8.0, 1 mM EDTA and 0.02% sodium azide in a semi-micro 1 cm quartz cuvette.

2.5 Steady-state kinetics

Kinetic parameters for both the isomerization of Δ^5-AD and Δ^5-AO were determined at pH 8.0 and 20 ^{o}C in 25 mM sodium phosphate buffer. Experiments were conducted in which GSH, Δ^5-AD and Δ^5–AO were varied independently. The data were fitted to equation 1 describing a random sequential mechanism that is characteristic of GST's (Pettersson and Mannervik, 2001).

$$v = \frac{V[\mathrm{A}][\mathrm{B}]}{K_{\mathrm{M}}{}^{\mathrm{B}} K_{\mathrm{S}}{}^{\mathrm{A}} + K_{\mathrm{M}}{}^{\mathrm{B}}[\mathrm{A}] + K_{\mathrm{M}}{}^{\mathrm{A}}[\mathrm{B}] + [\mathrm{A}][\mathrm{B}]} \qquad \text{equation 1}$$

Where, $K_{\mathrm{S}}{}^{\mathrm{A}}$ is the dissociation constant for the non-varied substrate while $K_{\mathrm{M}}^{\mathrm{A}}$ and $K_{\mathrm{M}}^{\mathrm{B}}$ are the Michaelis constants for the non-varied and varied substrates (Cleland, 1963). This approach of varying the GSH cofactor concentration independently, allows the actual dissociation constant for the substrate ($K_{\mathrm{S}}{}^{\mathrm{A}}$) to be found in addition to its apparent dissociation constant ($K_{\mathrm{M}}^{\mathrm{A}}$) in a random sequential mechanism. Initially, the concentrations of Δ^5-AD and Δ^5-AO were varied

from 0.5 to 100 µM (Johansson and Mannervik, 2001) in two separate experiments, while the GSH concentration remained constant at 2 mM in both experiments. The initial rates data were fit to equation 1 thereby obtaining the apparent dissociation constant K_M^B for the specific substrate and the real (K_S^A) and apparent (K_M^A) dissociation constants for GSH. The concentration of GSH was then varied from 0.05 to 10 mM (Balchin *et al*., 2010) while Δ^5-AD and Δ^5-AO were kept constant at concentrations of 200 µM (the two substrates are less soluble at concentrations exceeding this value). The initial rates data were fit to equation 1 thereby obtaining the apparent dissociation constant K_M^B for GSH and the real (K_S^A) and apparent (K_M^A) dissociation constants for the two substrates.

Independent experiments were conducted in order to obtain the catalytic efficiency k_{cat}/K_M, in which both substrate concentrations were varied within the non-saturating range of 0.5 µM to 5 µM with the GSH saturating concentration of 2 mM. The GSH concentration was varied within the non-saturating range of 20 to 100 µM while maintaining the concentration of both substrates Δ^5-AD and Δ^5-AO at 200 µM. The catalytic efficiency k_{cat}/K_M was then calculated from the slope given by equation 3 by fitting the data to a linear regression of initial velocity versus substrate concentration.

$$v_o = \frac{k_{cat}}{K_M}[E_T][S] \qquad \text{equation 3}$$

where v_o is the initial rate, $[E_T]$ is the total enzyme concentration used and $[S]$ is the substrate concentration under non-saturating conditions. Experiments to obtain the catalytic turnover k_{cat} were conducted with GSH and the two substrates, Δ^5-AD and Δ^5-AO under saturating conditions. The concentration of both Δ^5-AD and Δ^5-AO was kept at 200 µM with a saturating GSH concentration of 2mM and the enzyme concentration varied between 1-9 nM. Linear regression analysis was performed and the data were fit to equation 4.

$$V_{max} = k_{cat}[E_T] \qquad \text{equation 4}$$

2.6 Determination of the pK_a of the thiol group of free and enzyme bound GSH

To determine the pK_a of GSH in the enzyme active-site, the protein was dialyzed in 5 mM sodium phosphate buffer at pH 7.4 and a stock GSH concentration of 2.5 mM was made using the same buffer. The low ionic strength dialysis phosphate buffer served two purposes (i) it minimized the effect of the storage buffer pH on p*K*a determination (since pH was the

independent variable), therefore pH could be varied by using a buffer of high ionic strength and (ii) since the phosphate buffer system was used to obtain the pK_a, a phosphate storage buffer provided identical ionic species. The phosphate buffer system is triprotic with three ionizable hydrogen atoms dissociating as follows:

$$H_3PO_4 \xrightleftharpoons{pKa=2.16} H_2PO_4^- \xrightleftharpoons{pKa=7.21} HPO_4^{2-} \xrightleftharpoons{pKa=12.32} PO_4^{3-}$$

The absorbance of free GSH in solution was obtained at different pH values ranging from 6.5-11, the last two pH values (pH 10 and 11) were obtained by using the HPO_4^{2-}/PO_4^{3-} buffer system while the rest of the values were obtained by the $H_2PO_4^-/HPO_4^{2-}$ buffer system; a stock volume of 500 ml with a concentration of 100 mM was made for each buffer system with reference pH values of 7.8 for the $H_2PO_4^-/HPO_4^{2-}$ system and 11 for the HPO_4^{2-}/PO_4^{3-} system. The Henderson-Hasselbalch equation was used to calculate the amounts of acid and conjugate base required for the reference pH values. From the stock buffer systems 25 ml was aliquoted into different beakers corresponding to the different experimental pH values and adjusted to the required pH with NaOH and H_3PO_4. A volume of 30 µl stock GSH and 270 µl of buffer from the beakers of each pH value were added to corresponding eppendorf tubes to a final volume of 300 µl and a final GSH concentration of 250 µM. The samples were mixed and incubated for 30 min and the ionization of the thiol group was monitored by measuring the absorbance of the thiolate at 239 nm (Pettersson and Mannervik, 2001). The absorbance of GSH bound to hGST A3-3 was obtained within the pH range 5.2-8. Protein and GSH were mixed in eppendorf tubes and their concentrations adjusted to 9 µM and 250 µM respectively, with their corresponding buffers to a final volume of 300 µl and incubated for the same time period. The absorbance was corrected for both free GSH and free enzyme by subtracting the absorbance of free GSH within this pH range and free enzyme (9 µM) at the storage buffer pH of 7.4 from the enzyme-bound absorbance readings. In both preparations the GSH concentration was kept at 250 µM and all measurements were done in 100 mM sodium phosphate.

2.7 Fluorescence measurements with equilenin

All fluorescence measurements were done at 20 ^oC with a scan rate of 200 nm/min using the Jasco FP-6300 fluorimeter. The excitation and emission slit widths were set at 5 nm and 10 nm, respectively. Any increase in the excitation slit width resulted in fluorescence decay over time.

The emission spectrum was obtained from 300 nm to 500 nm with an average of 3 scans and all spectra were corrected for buffer. The nature of the intermediate at the active-site of hGST A3-3 was probed using an excitation wavelength of 292 nm in 25 mM sodium phosphate buffer at pH 8 and pH 11, in a total volume of 300 µl with 1% methanol. The equilenin and protein concentrations used were 3 µM and 9 µM, respectively. The dissociation constant for the binding of equilenin to hGST A3-3 was determined by fluorescence titration of 3 µM equilenin with varying enzyme concentrations ranging between 1 - 15 µM in 25 mM sodium phosphate buffer pH 8, with 1% methanol (v/v). The dependent variable was the emission of free equilenin measured at 363 nm after excitation at 292 nm.

2.8 Absorbance measurements with 19-nortestosterone

All spectral measurements were made in 25 mM sodium phosphate buffer, pH 8, with 1% methanol (v/v) in quartz cuvettes, with a 1 cm light path. A concentration of 33 µM of 19-nortestosterone with 19.6 µM enzyme were used. The spectrum of the ketosteroid was measured against a 25 mM sodium phosphate buffer blank in 1% methanol. The spectrum of the mixture of 19-nortestosterone and enzyme was measured against a blank containing 19.6 µM of the enzyme in the aforementioned buffer.

2.9 Detection of the dienolate intermediate

Zeng and Pollack (Zeng and Pollack, 1991) determined the maximum absorbance wavelength for the externally generated dienolate intermediate to be 238 nm (Figure 12). The UV-Vis spectroscopic detection of the dienolate intermediate was followed at 238 nm in 25 mM sodium phosphate buffer at 20 ^{o}C and pH 8.0. A total concentration of 10 µM was used for the substrate with 1 µM enzyme concentration. The principle chromophore at this wavelength is the conjugated heteroannular diene. Ionization to the enolate frees the O-H bonding electrons which make the $n \rightarrow \pi^{*}$ transition. This transition shifts the λ_{max} to 256 nm with a corresponding hyperchromic shift from 13800 M^{-1} cm^{-1} to 15000 M^{-1} cm^{-1} (Pollack *et al*., 1989).

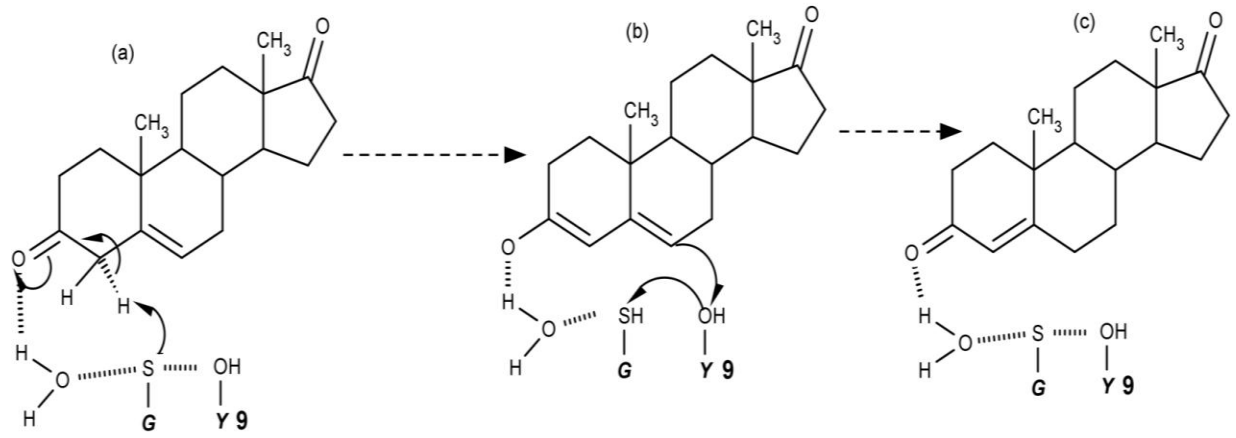

Figure 12: The possible progression of the hGST A3-3-catalysed reaction via the formation of the intermediate (b). The intermediate possesses the conjugated heteroannular double bonds which would be the principle chromophoric regions absorbing at 238 nm. Ionization to the enolate results in a wavelength shift to 256 nm as described by Pollack *et al.* (1989).

2.10 Determination of the activation energy

Isomerase activity was recorded from 15 ^{0}C to 40 ^{0}C in a thermostated Varian Cary UV-Vis spectrophotometer with a Cary dual cell peltier accessory. Steady-state kinetic parameters were obtained at 248 nm and 238 nm with three replicate measures collected for each temperature. The activation energy was determined as described by Tian *et al* (1993) by use of the Arrhenius equation ($\ln k = \ln A - E_a/RT$), where k is the rate constant (catalytic turnover), R is the molar gas constant, T is the temperature in Kelvin, E_a is the activation energy and A is the pre-exponential factor. Linear Plots of In k versus $1/T$ yield a slope of $-E_a/R$ from which E_a can be obtained directly. The relationship between the Arrhenius equation and Eyring's transition state equation $k_BT/h \exp(-\Delta G^{\ddagger}/RT)$ yields $\Delta H^{\ddagger} = E_a - RT$, were k_B is the Boltzmann constant, h is the Plank constant, $\Delta G^{\ddagger}$ is the Gibbs free energy of activation and $\Delta H^{\ddagger}$ is the enthalpy of activation.

2.11 Solvent isotope effects with Δ^5–AD

Solvent isotope effects were employed to determine the rate limiting step in the isomerization of Δ^5-AD. Two critical steps in the reaction pathway are the abstraction of the carbon 4 proton and its subsequent transfer to carbon 6. The progression of this reaction would allow isotopic exchange at the intermediate stage with D_2O, facilitating the transfer of the deuterium from the solvent to either carbon 6 to form product or back to carbon 4 in the reverse reaction, forming the substrate (Hawkinson *et al*., 1991), as shown in Figure 13. This exchange with solvent would

have the consequence of creating a primary isotopic effect at the proton transfer step if this step were rate limiting.

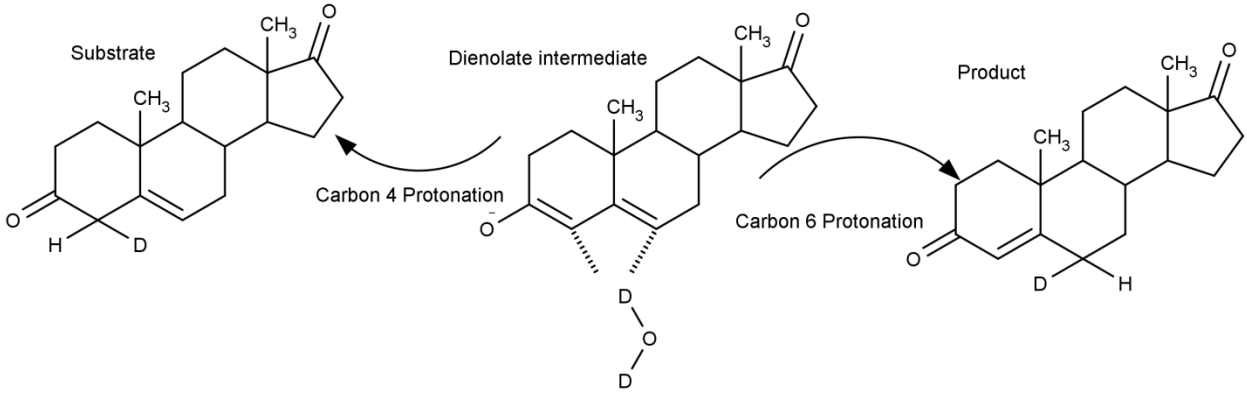

Figure 13: Solvent isotope exchange between D_2O and the dienolate intermediate as adapted from Hawkinson *et al.* (1991). The exchange results in either the formation of product after protonation at carbon 6 or reactant after carbon 4 protonation. A primary isotope effect for the formation of product would be observed if the proton transfer step to carbon 6 was rate limiting.

Steady state kinetic parameters were obtained at 238 nm and 248 nm respectively, in both D_2O and H_2O in 25 mM phosphate buffer, at 20 ^oC (using potassium deuterium phosphate for D_2O with a pD of 8.0). The concentrations of substrate were varied from 0.5 to 100 µM. The data were fitted to the Michaelis-Menten equation. The isomerisation of Δ^5-AD followed the formation of product when observed at 248 nm with a molar extinction coefficient of 16300 M^{-1} cm^{-1} (Benson *et al.*, 1977) and followed the formation of the dienolate intermediate when observed at 238 nm with an extinction coefficient of 13800 M^{-1} cm^{-1} (Zeng and Pollack, 1991). All measurements were done with 2 mM GSH, at pH 8.

CHAPTER 3: RESULTS

3.1 Sequence identity

The pET11a plasmid with the open reading frame containing the hGST A3-3 gene insert was sequenced and a segment of the sequence results is shown in Figure 14(a) with the NCBI sequence information in Figure 14(b). The results indicate that the gene insert is that encoding the wild-type hGST A3-3 and possesses no mutations.

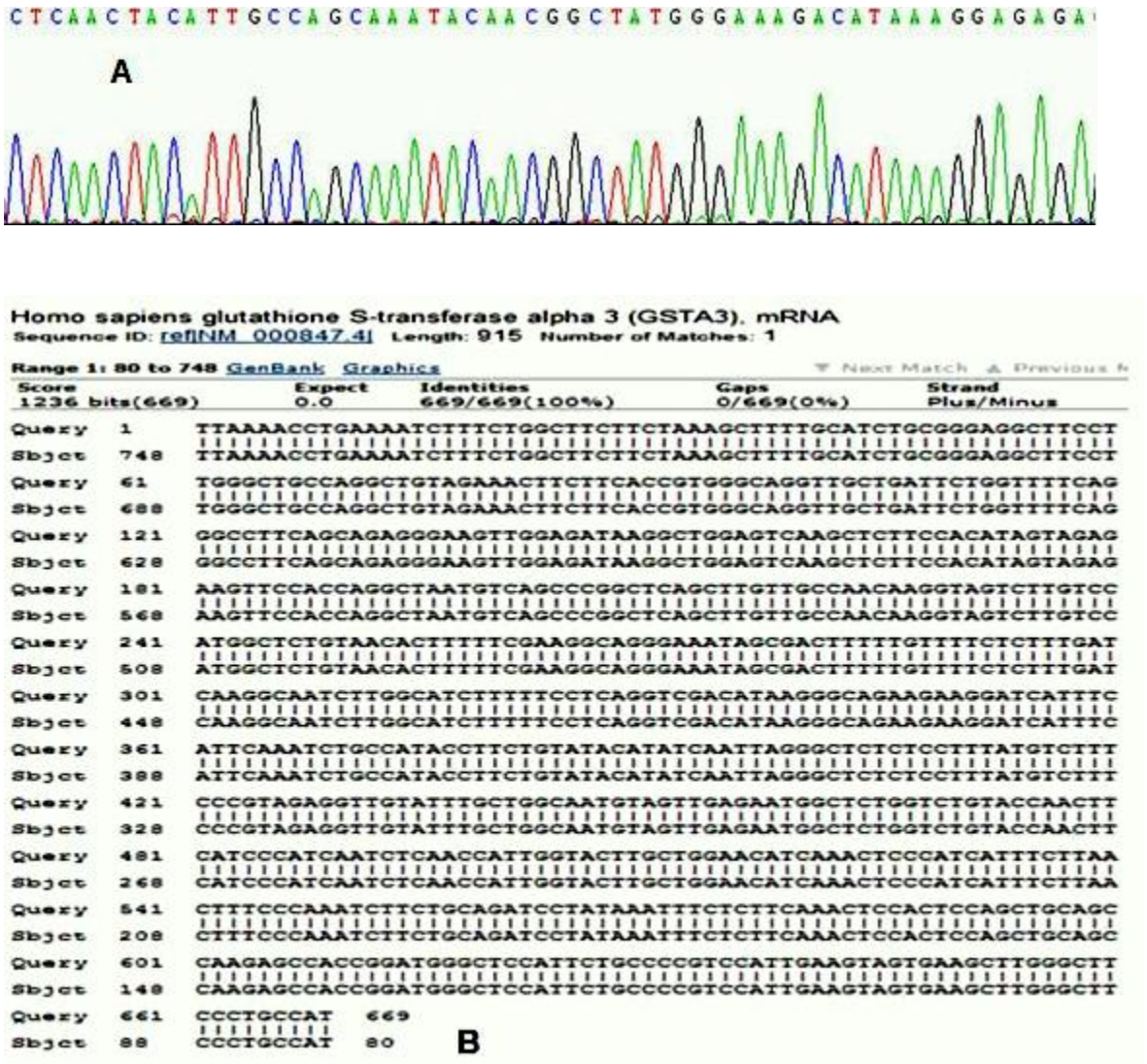

Figure 14: Plasmid sequencing results for a selected segment of the hGST A3-3 gene (A) The sequencing results were viewed using the program Finch TV version 1.4.0 (http://www.geospiza.com/FinchTV: Geospiza Inc.). NCBI information summary for the sequenced gene (B), indicating that it is that of hGST A3-3 and no mutations are present.

3.2 Over-expression and purification

3.2.1 Ion metal affinity chromatography

Optimum expression of hGST A3-3 revolved around manipulating the expression system, time and temperature while keeping the IPTG concentration constant. From this initial assessment, expression was conducted in two expression systems, *E. coli* BL21 (DE3)/pLysS and *E. coli* T7 Express I^q for 19 hrs and 4 hrs for both expression systems after induction with 1mM IPTG. The best expression system was the *E. coli* BL21 (DE3)/pLysS. Cells were grown to an A_{600} of 0.4 with optimal expression at 37 ^{0}C for 4 h after induction. The use of an immobilized metal affinity column (IMAC) allows coordination between imidazole groups on histidine and transition metals bound to the stationary phase resins. The poly histidines were placed at the N-terminus and zinc was used as the metal in the stationary phase. Some naturally occurring proteins may have histidines and this may result in non specific binding. A higher pH in the equilibration buffer enhances non specific binding. Optimization was thus done at two different pH values of equilibration buffer; pH 8 and pH 7.4. Non-specific binding was eliminated by reducing the equilibration buffer pH to 7.4. The optimum conditions for expression and purification were therefore 1 mM IPTG, in *E. coli* BL21 (DE3)/pLysS for 4 h with 20 mM Tris-HCl, 200 mM NaCl at pH 7.4 (Figure 15 and 16).

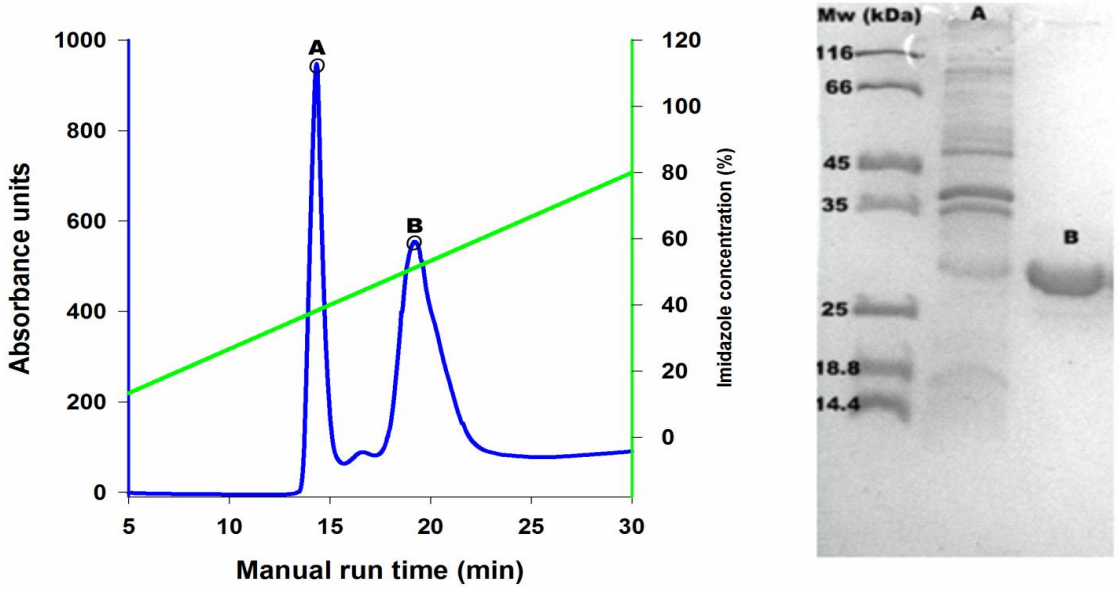

Figure 15. Elution profile of hGST A3-3 observed at A_{280} (blue axis) using Nickel affinity chromatography. The peak labelled A contains many proteins which elutes at 36 % imidazole concentration (green axis) while that labelled B corresponds to the electrophoretic mobility of pure hGST A3-3 and elutes at 48.5% imidazole concentration.

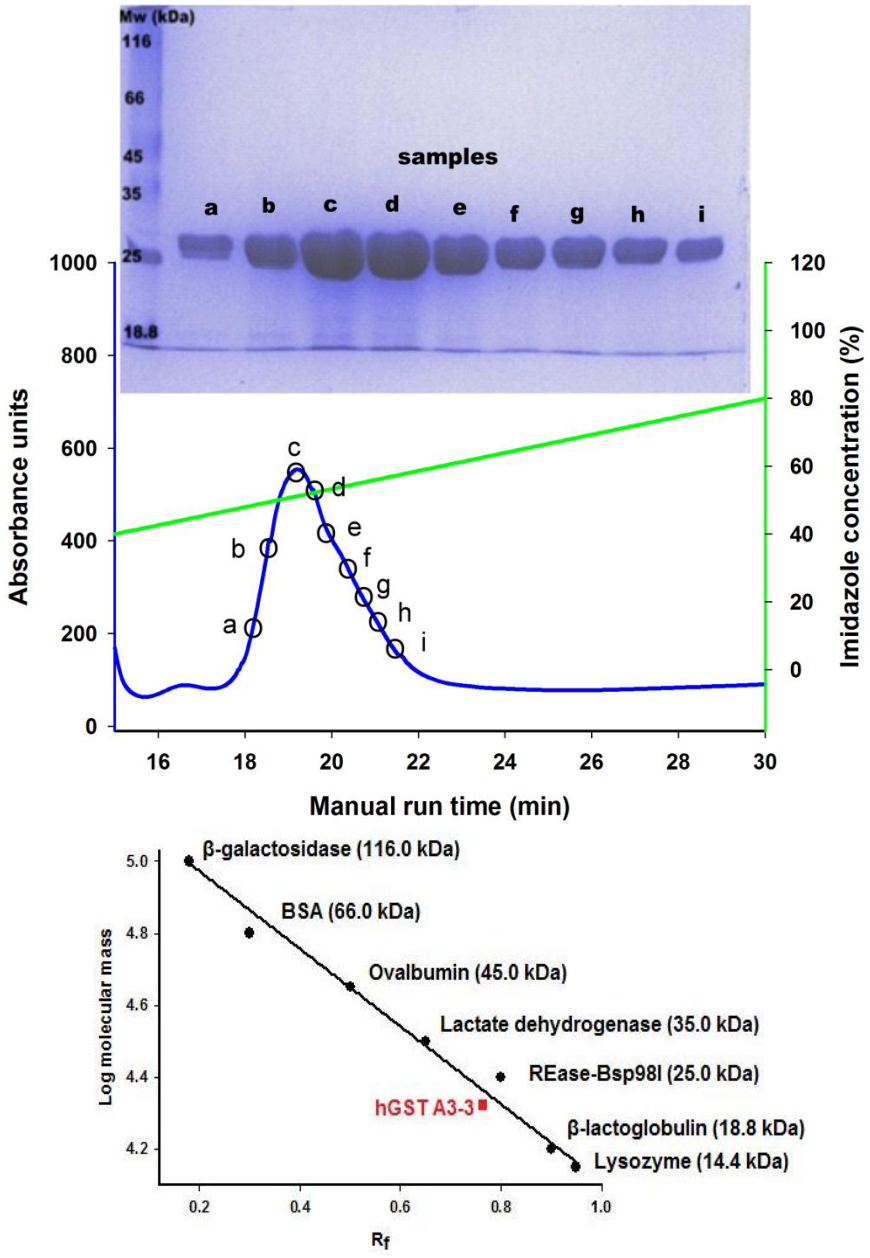

Figure 16. Protein mobility as characterised by SDS-PAGE analysis with a calibration curve. The names and sizes of the marker proteins are indicated on a calibration curve and the hGST A3-3 migration corresponds to 26 kDa.

3.2.2 Thrombin cleavage

The cleavage of the hexa-histidine peptide tag at the N-terminus of hGST A3-3 was carried out at room temperature. The cleavage process was quenched by the addition of reducing sample buffer containing β-mercaptoethanol and sodium dodecyl sulphate (SDS). The reaction was

observed by analyzing SDS-PAGE gel shifts at specific time intervals. Complete cleavage was observed after 1hr of exposure to thrombin (Figure 17).

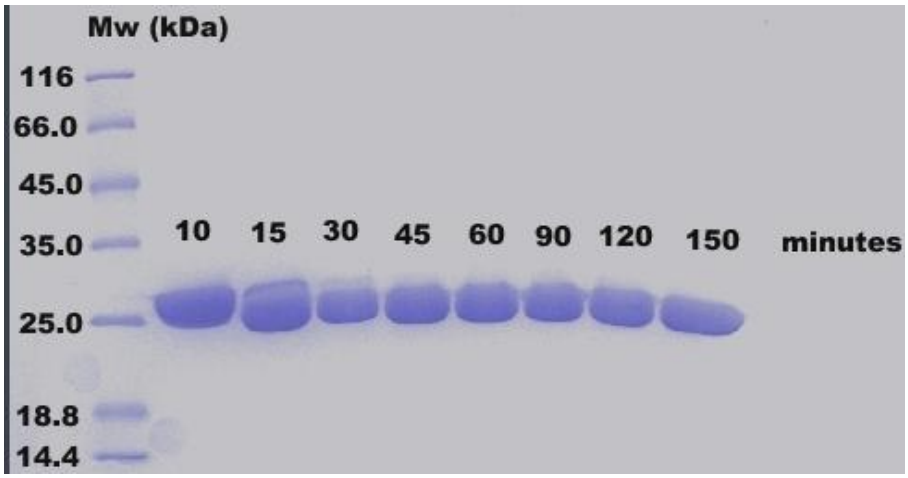

Figure 17. SDS-PAGE gel shifts after thrombin cleavage with time. At 15 min, there is equilibrium of cleaved and uncleaved protein and after 60 min cleavage is complete.

3.2.3 Purification of his-tag free hGSTA3-3 protein

The thrombin-cleavage products contained thrombin, cleaved hexa-histidines and histidine-free hGSTA3-3. Benzamidine is a reversible competitive inhibitor of proteases and when covalently attached to a Sepharose matrix will bind thrombin to the column. A further purification step using a Nickel affinity column separated the free histidines from the protein. The flow through sample was run on an SDS-PAGE gel for purity determination (Figure 18).

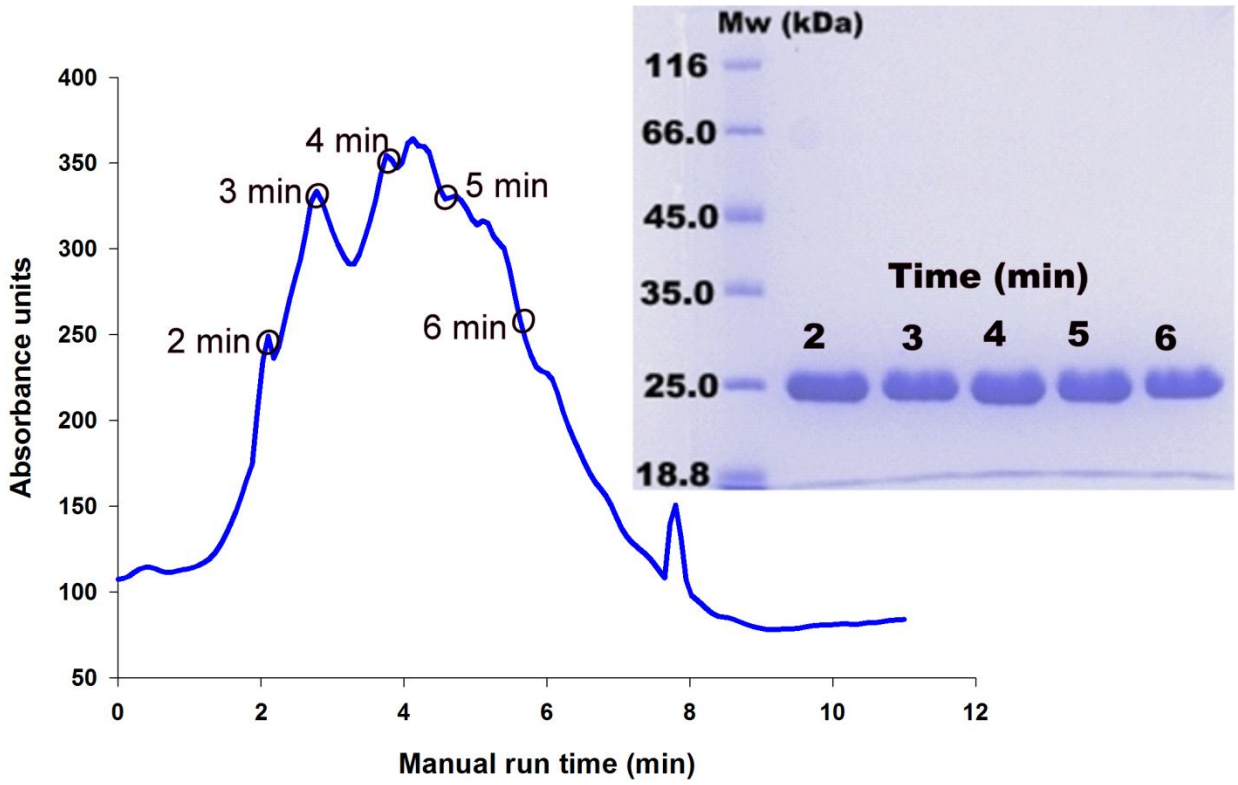

Figure. 18. Purity of his-tag-free hGST A3-3 after running the sample through a benzamadine sepharose column (to bind thrombin) in tandem with a nickel affinity column (to bind the cleaved poly histidines). The protein was collected as the flow through and samples at 2, 3, 4, 5 and 6 minutes were run on an SDS-PAGE.

3.3 Functional characterization

3.3.1 Enzyme activity

The substrates Δ^5-AD and Δ^5-AO were used to observe the catalytic functionality of the protein. The reported absorbance wavelength for monitoring product formation in Δ^5-AD isomerisation is 248 nm as cited in the experimental procedures. Activity was confirmed at this wavelength as shown in Figure 19(a) and specific the specific activity was calculated as shown in Figure 19(b).

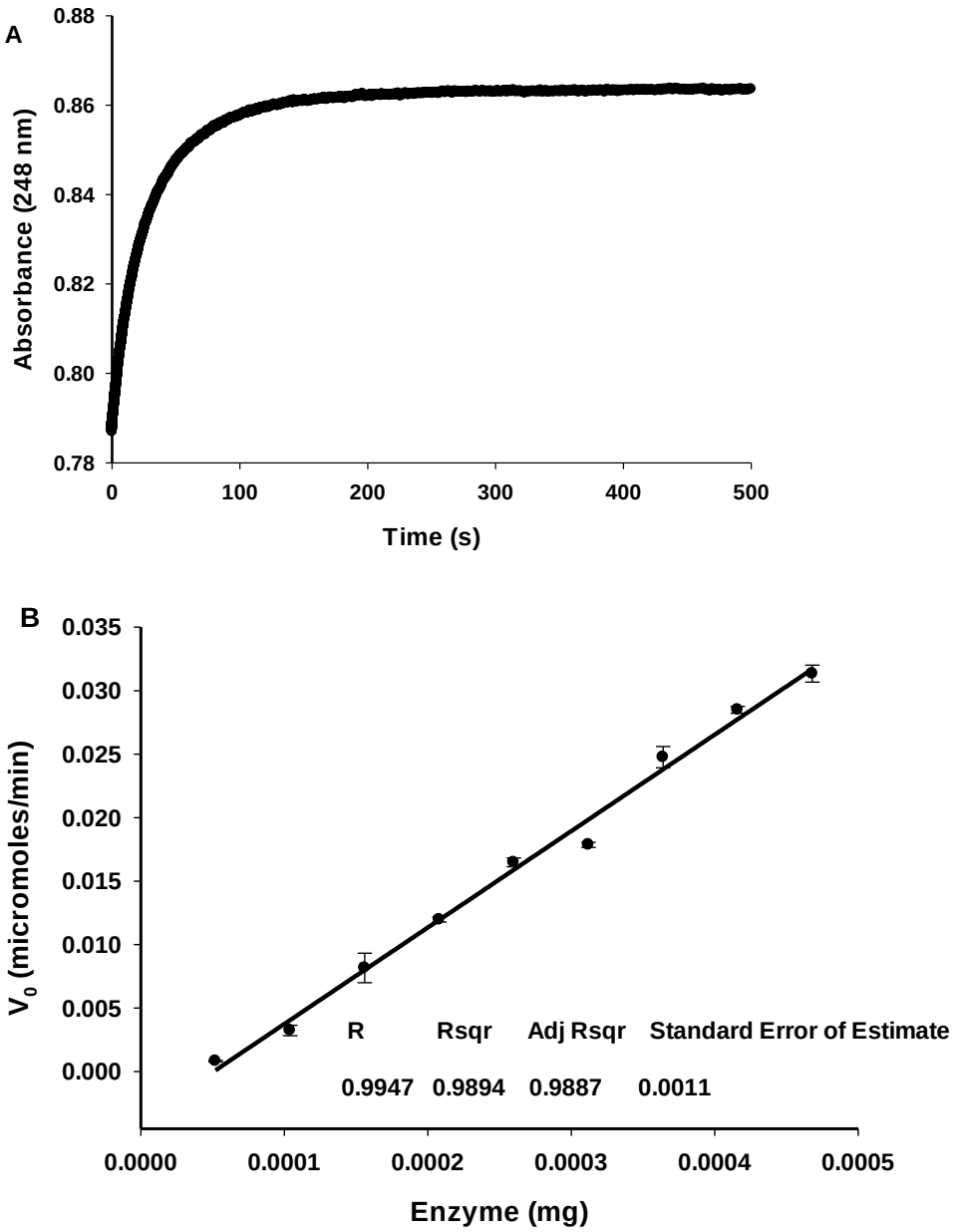

Figure 19(a). A progress curve for the isomerization of Δ^5- AD to Δ^4- AD observed at 248 nm (A). An enzyme subunit concentration of 0.5 μM was used with 20 μM of Δ^5- AD at a saturating GSH concentration of 2 mM. **(b)** The reaction was carried out at room temperature (20 ^{0}C). The specific activity was calculated to be 76 ± 2 μmol mg^{-1} min^{-1}.

To monitor the activity of hGST A3-3 in the isomerisation of Δ^5-AO an absorbance wavelength for product formation was required. The reported absorbance wavelength for the Δ^5 to Δ^4 shift in the double bond position for various androstenes has been 248 nm; however this wavelength has not been specific to Δ^5-AO. The reaction was followed at either 248 nm (Figure

20a) or 235 nm. Rather than follow the suspected product which is devoid of any conjugated double bonds, the reaction followed the formation of the transient intermediate specie suspected of having the conjugated chromophoric heteroannular double bonds. The specific activity was calculated as shown in Figure 20b

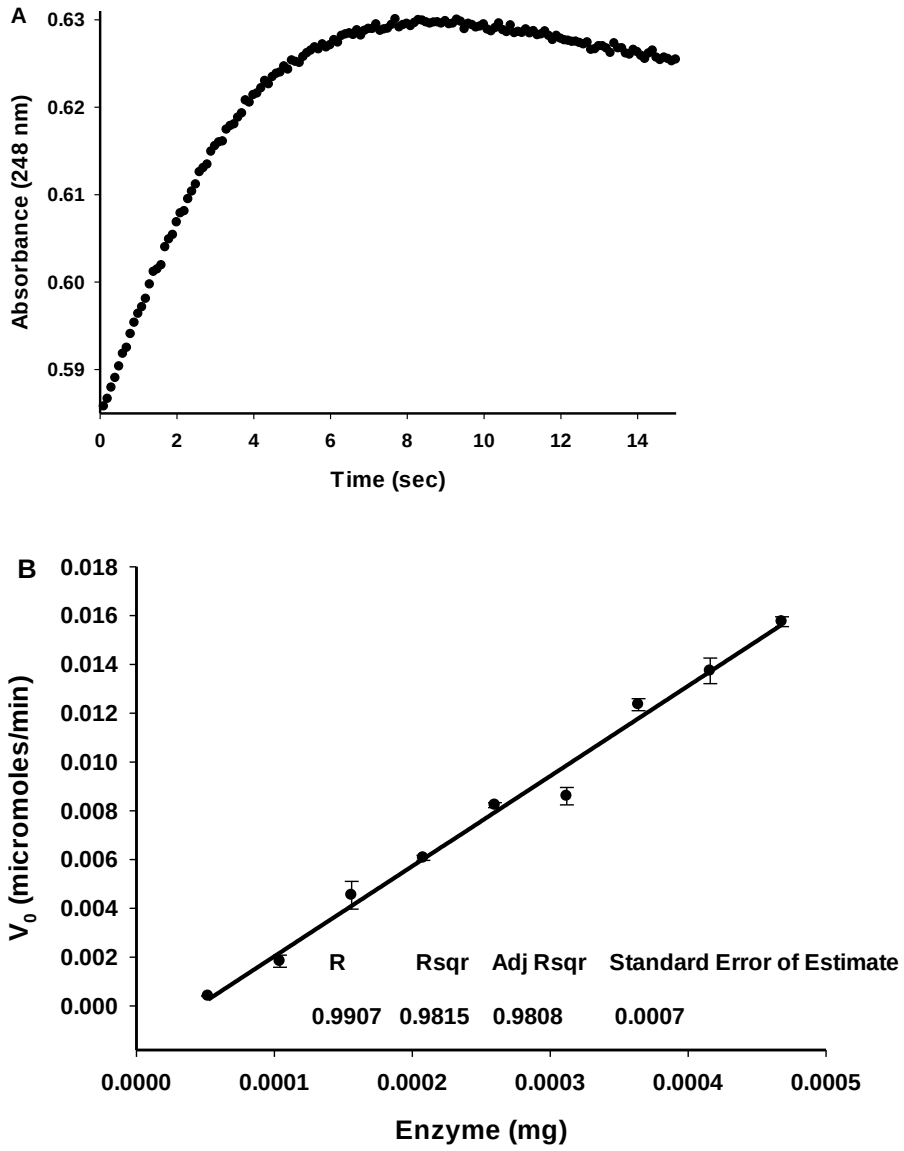

Figure 20.(a) A progress curve for the isomerization of Δ^5- AO to the suspected product Δ^4- AO observed at 248 nm (A). An enzyme subunit concentration of 0.5 µM was used with 9 µM of Δ^5- AO at a saturating GSH concentration of 2 mM. **(b)** The reaction was carried out at room temperature (20 ^{0}C). The specific activity was calculated to be 31 ± 2 µmol mg^{-1} min $^{-1}$.

3.4 Steady state kinetics of hGSTA3-3 with Δ^5–AD and Δ^5–AO

3.4.1 Michaelis-Menten kinetics for Δ^5–AD

Experiments were conducted in which Δ^5–AD and GSH were varied independently. The data were fitted to an equation describing a random sequential mechanism that is characteristic of GST's as explained in the materials and methods section. The results are shown in Figure 21.

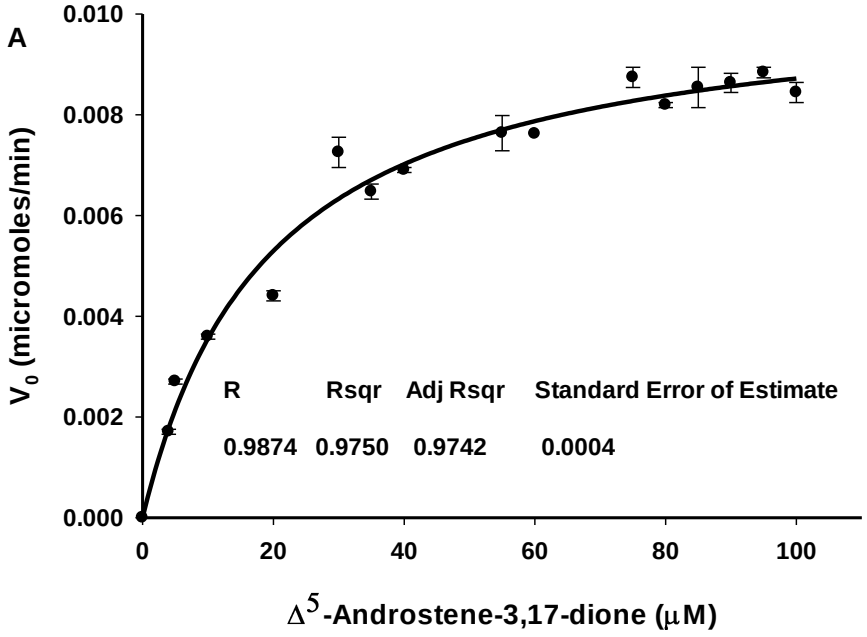

Figure 21. Michaelis-Menten Kinetics for a random sequential mechanism were [Δ^5-AD] is varied between 0.5 µM-100 µM and [GSH] is kept constant at saturating conditions of 2mM.

3.4.2 Determination of kinetic parameters k_{cat} and k_{cat}/K_M

Separate experiments were conducted to obtain the k_{cat} and k_{cat}/K_M values as described under Materials and Methods. The k_{cat} value obtained was 51 ± 3 s^{-1} and the k_{cat}/K_M was 1100 ± 100 mM^{-1} s^{-1} as shown in Figure 22.

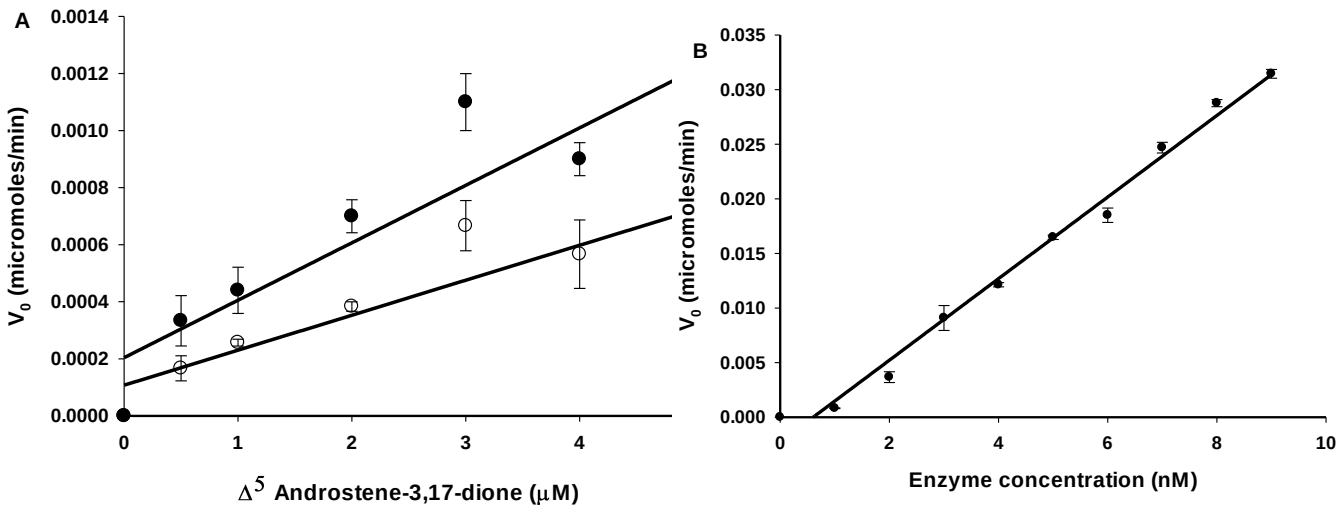

Figure 22. (A) The k_{cat}/K_M values obtained for Δ^5-AD at two different enzyme concentrations 9 nM (●) and 4 nM (O). **(B)** The k_{cat} obtained for Δ^5-AD under varying enzyme concentrations of 1-9 nM with both GSH and Δ^5-AD saturating at 2 nM and 200 µM respectively. The k_{cat} value obtained was 51 ± 3 s^{-1} and the k_{cat}/K_M was 1100 ± 100 mM^{-1} s^{-1}.

3.4.3 Michaelis-Menten kinetics for Δ⁵–AO

The isomerisation reaction of Δ^5–AO was followed as described in the materials and methods and its kinetic constants were obtained (Figure 23).

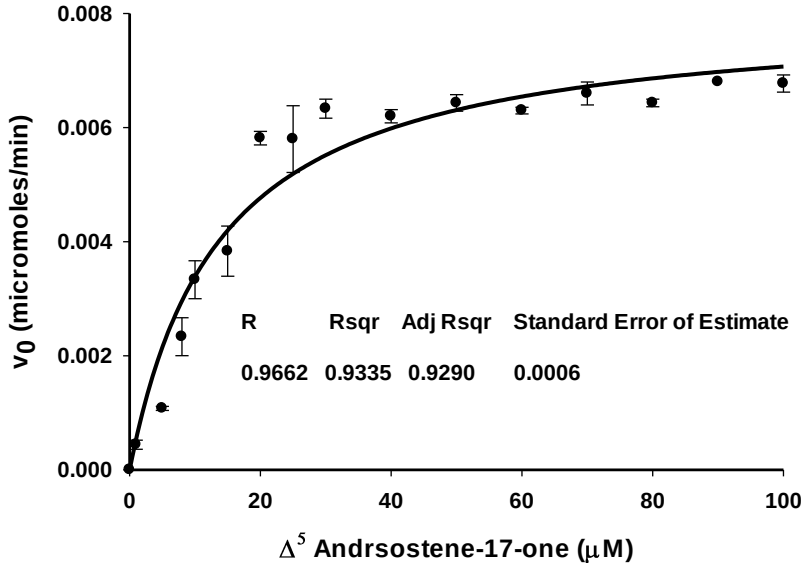

Figure 23. Michaelis-Menten Kinetics for a random sequential mechanism were [Δ^5-AO] is varied between 0.5 µM-100 µM and [GSH] is kept constant at saturating conditions of 2mM.

3.4.4 Determination of kinetic parameters k_{cat} and k_{cat}/K_M

Separate experiments were conducted to obtain the k_{cat} and k_{cat}/K_M values for Δ^5-AO as described in the materials and methods (Figure 24a). The k_{cat} value obtained was 20 ± 2 s^{-1} and the k_{cat}/K_M was 600 ± 9.7 mM^{-1} s^{-1} (Figure 24b).

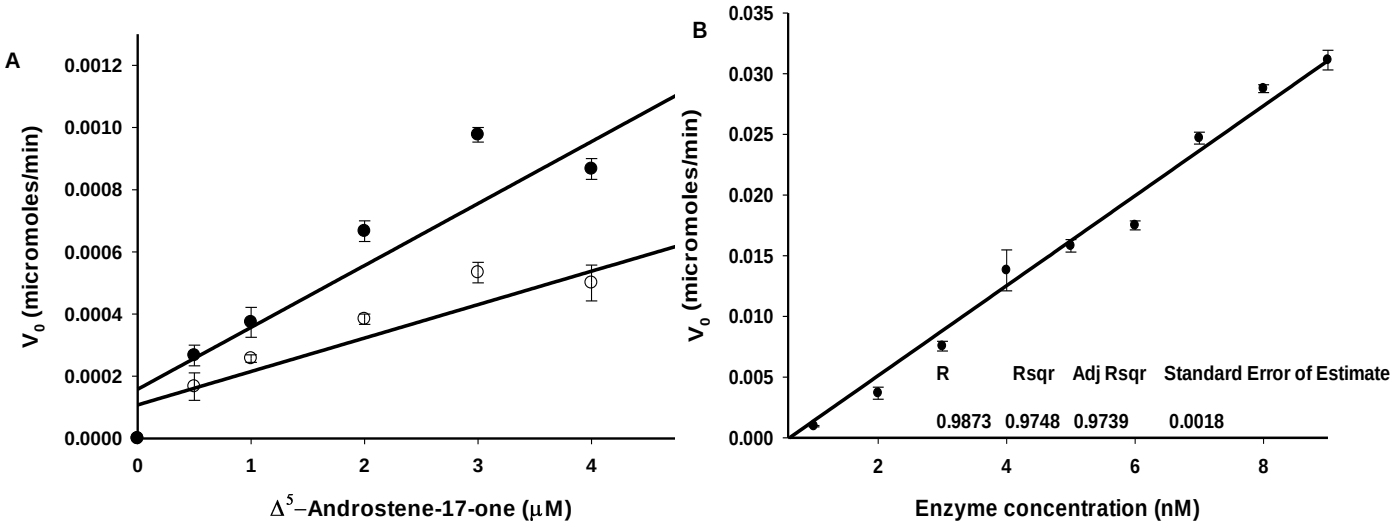

Figure 24. (A) The k_{cat}/K_M values obtained for Δ^5-AO at two different enzyme concentrations 9 nM (●) and 4 nM (○). **(B)** The k_{cat} obtained for Δ^5-AO under varying enzyme concentrations of 1-9 nM with both GSH and Δ^5-AD saturating at 2 nM and 200 μM respectively. The k_{cat} value obtained was 20 ± 2 s^{-1} and the k_{cat}/K_M was 600 ± 9.7 mM^{-1} s^{-1}.

3.4.5 Steady-State kinetics with varying [GSH] and saturating [Δ⁵-AD] and [Δ⁵-AO]

GSH concentrations were varied while both the Δ^5-AD and Δ^5-AO concentrations were kept constant as described in the materials and methods (Figure 25a). The kinetic parameters k_{cat}/K_M for GSH under these substrate concentrations were obtained and were calculated to be 370 ± 60 s^{-1} for constant [Δ^5-AD] and 100 ± 23 s^{-1} for constant [Δ^5-AO] (Figure 25b).

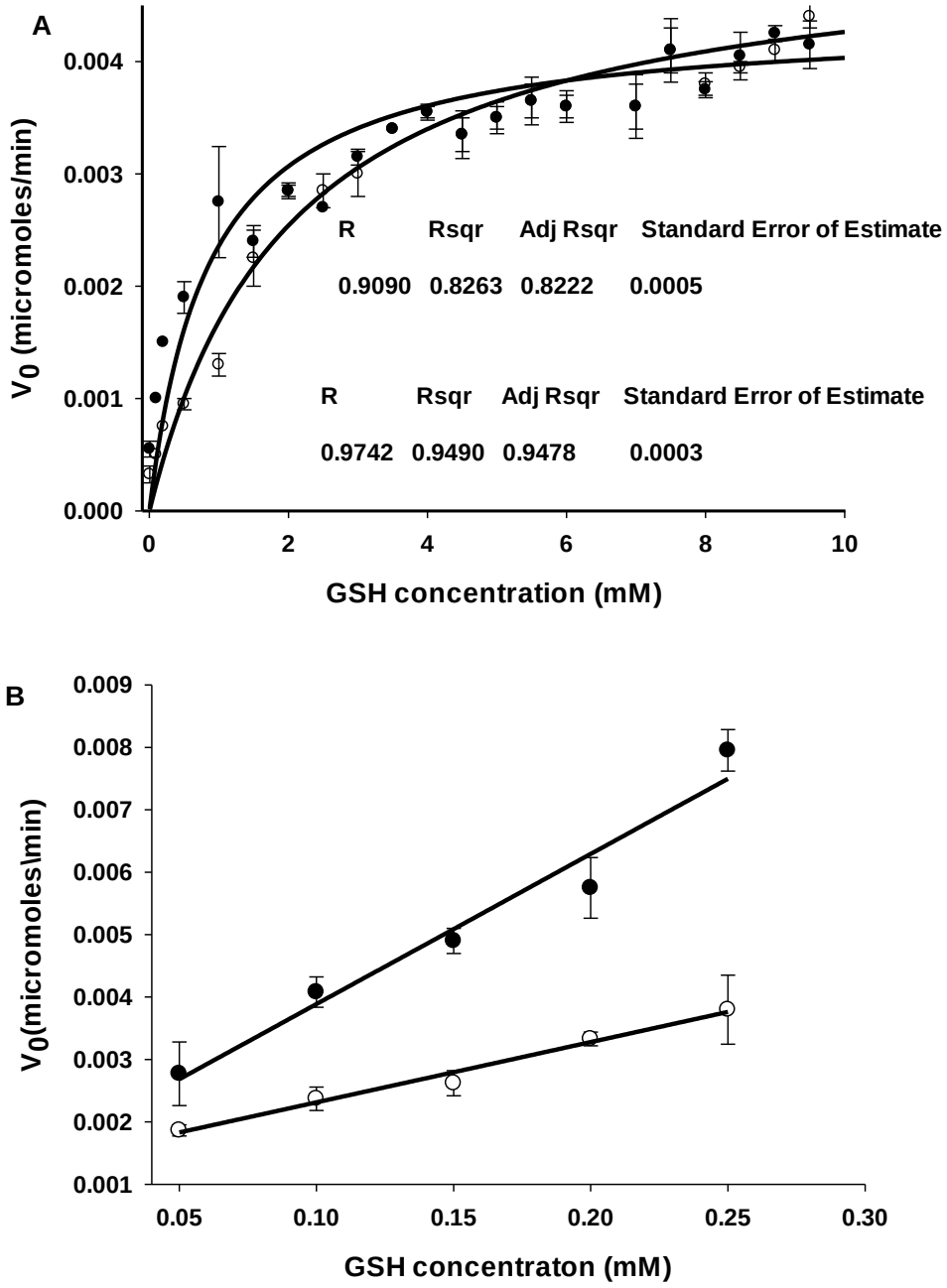

Figure 25. (A) The Michaelis-Menten Plot was obtained with varying concentrations of GSH and a constant concentration of Δ^5–AD (●) and Δ^5–AO (○). **(B)** The k_{cat} /K_M values were obtained for Δ^5-AD (●) and Δ^5–AO (○) at a single enzyme concentration of 9 nM. Both reactions were conducted with varying GSH concentrations between 20 -100 µM and saturating steroid concentrations of 200 µM.

TABLE 3-1. *Kinetic parameters of hGST A3-3 with two different substrates Δ^5–AD and Δ^5–AO*
The parameter k_{cat} is calculated per enzyme subunit while the K_M value refers to the substrate of varied concentration with the non varied substrate at saturating amounts. The enzyme activity with both substrates was measured with 2mM saturating GSH at $20^o C$, *p*H 8.0.

Substrate/Cofactor (conditions; pH 8.0, 20 °C)	Specific activity (μmol mg^{-1} min^{-1})	K_S (μM)	k_{cat} (s^{-1})	K_M (μM)	$\frac{k_{cat}}{K_M}$ (mM^{-1} s^{-1})
Δ^5–AD	76 ± 2	9.3 ± 2.2[a]	51 ± 3	22.5 ± 4.3	2000± 198
Δ^5–AO	31 ± 2	7.6 ± 1.3[b]	20 ± 2	16.5 ± 1.5	600 ± 9.7
GSH	NA	50 ± 10[c]	NA	130 ± 21	370 ± 60
		53 ± 8[d]	NA	129 ± 30	100 ± 23

NA, not applicable
[a]Determined with a constant Δ^5-AD concentration of 200 μM and varying GSH concentration
[b]Determined with a constant Δ^5-AO concentration of 200 μM and varying GSH concentration
[c]Determined with a constant GSH concentration of 2 mM and varying Δ^5-AD concentration.
[d]Determined with a constant GSH concentration of 2 mM and varying Δ^5-AO concentration.

3.5 The pK_a value of GSH upon binding

The binding of the cofactor GSH to the enzyme results in a reduction of the thiol pK_a from the solution value of 9.1 to 6.3 in the active site (Figure 26). Previous studies on hGST A1-1 indicate a similar reduction for both the isomerization reaction (Pettersson and Mannervik 2001) and the typical conjugation reaction (Caccuri *et al*., 1999), equivalent to a reduction in ΔG^o of 3.8 kcal/ mol ($\Delta G^o = 2.303RT\Delta pK_a$).

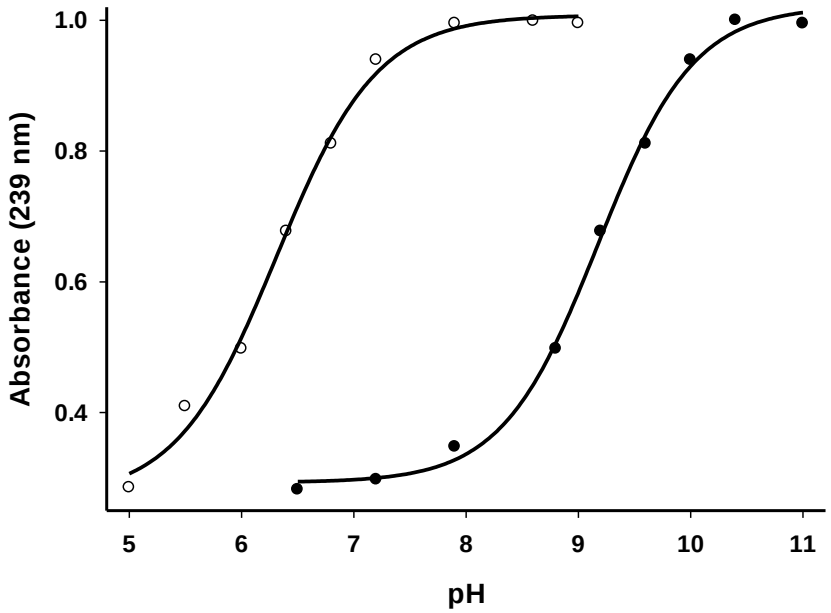

FIGURE 26. The deprotonation of GSH expressed as a function of pH, in the presence and absence of hGST A3-3. Non-linear regression analysis of the data yielded a pK_a value of 9.17 ± 0.04 for free GSH (●) and a pK_a value of 6.31 ± 0.07 for the active site-bound GSH (O).

3.6 The nature of the intermediate at the active site of hGST A3-3

At pH 8.0, free equilenin displays a λ_{max} of 362 nm with a resulting red-shift at pH 11 to 425 nm (Figure 26a). The ionization of the aromatic phenol results in the release of electrons previously held in the O-H sigma bond, thereby increasing the number of non bonding electrons capable of making the $n \rightarrow \pi^*$ electronic transition. In the presence of hGST A3-3, the fluorescence emission spectrum resembles the protonated state with a slight shift to 350 nm (Figure 27a). The α,β-unsaturated ketosteroid 19-nortestosterone has a principle absorption maximum at 248 nm in water. A 10 nm shift is observed when the enone chromophore is exposed to 10M HCl. In the presence of enzyme, the shift is not observed and the absorption maximum remains at 248 nm with a reduction in the concentration of free ligand (Figure 27b).

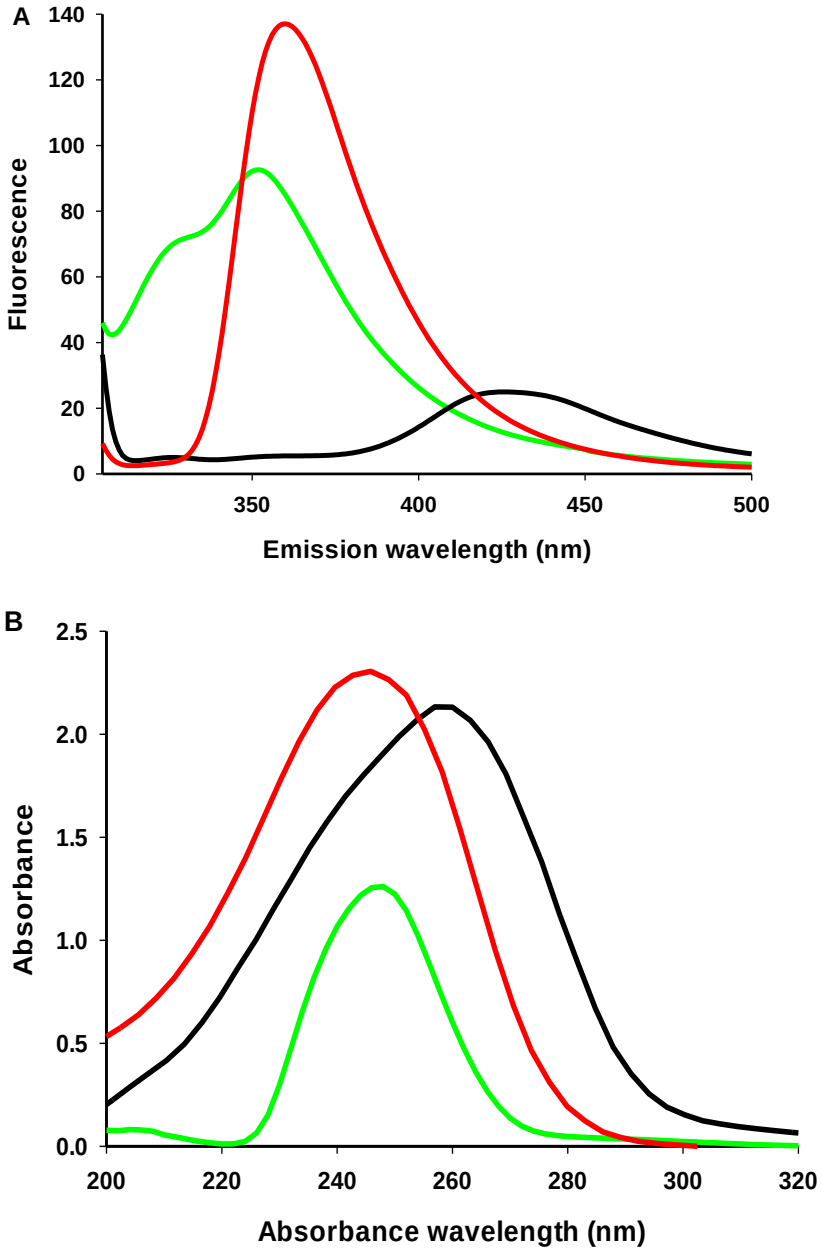

FIGURE 27. Fluorescence emission spectra of equilenin as an indicator of the intermediate ionization state at the active site (A). Free equilenin (3.8 µM) observed at pH 8.0 (red), pH 11.0 (black) and in the presence of 9 µM enzyme (green). Equilenin was in 1% methanol and excitation set at 292 nm. The absorbance spectra of 19-nortestosterone (36.6 µM) observed in solution at pH 8.0 (red), in 10 M HCl (black) and in the presence of 19 µM enzyme (green).(B).

3.7 UV-Vis detection of the intermediate

The substrate Δ^5–AD displays a λ_{max} of 200 nm with an extinction coefficient of 3800 M^{-1} cm^{-1} due to the isolated double bond at carbon 5 and two isolated keto groups at carbon 3 and carbon 17 (Figure 28a.) The dienolate intermediate from Δ^5-AD has been found to have a λ_{max} of 238 nm as cited in the experimental procedures. The principle chromophore at this wavelength is the conjugated heteroannular diene. Ionization to the enolate frees the O-H bonding electrons which make the $n \rightarrow \pi^*$ transition. This transition shifts λ_{max} to 256 nm with a corresponding hyperchromic shift from 13800 M^{-1} cm^{-1} to 15000 M^{-1} cm^{-1} (Pollack *et al*., 1989). The reaction of Δ^5-AO follows the formation of the two conjugated ethylenic bonds in the heteroannular carbanion intermediate. The calculated principle absorption band for the formation of this heteroannular diene is 235 nm (Dorfman, 1953; Woodward, 1941). The substrate Δ^5-AO has two chromophoric regions; (i) an isolated carbon 17 keto group with an extinction coefficient of 43 M^{-1} cm^{-1} (λ_{max}=294 nm) (ii) an isolated trisubstituted ethylenic chromophore at Carbon 5 with an extinction coefficient of 335.4 M^{-1} cm^{-1}(λ= 209 nm) (Figure 28c). Both reactions produce an initial rise in the absorbance followed by a gradual decay corresponding to a decrease in intermediate concentrations. The enzymatic conversion of Δ^5-AD was followed at 238 nm, 256 nm and 248 nm (Figure 28b). The reaction at 248 nm for Δ^5-AD follows product formation with the chromophoric region being the conjugated α,β-3-ketone isomer. Therefore the reaction does not show a decrease in absorbance. The enzymatic reaction of Δ^5-AO was followed at 235 nm which is the reported λ_{max} for the formation of the suspected intermediate specie $\Delta^{3:5}$-androstadiene-17-one and 248 nm (Figure 28d), a wavelength in which heteroannular dienes absorb strongly as cited in the experimental procedures.

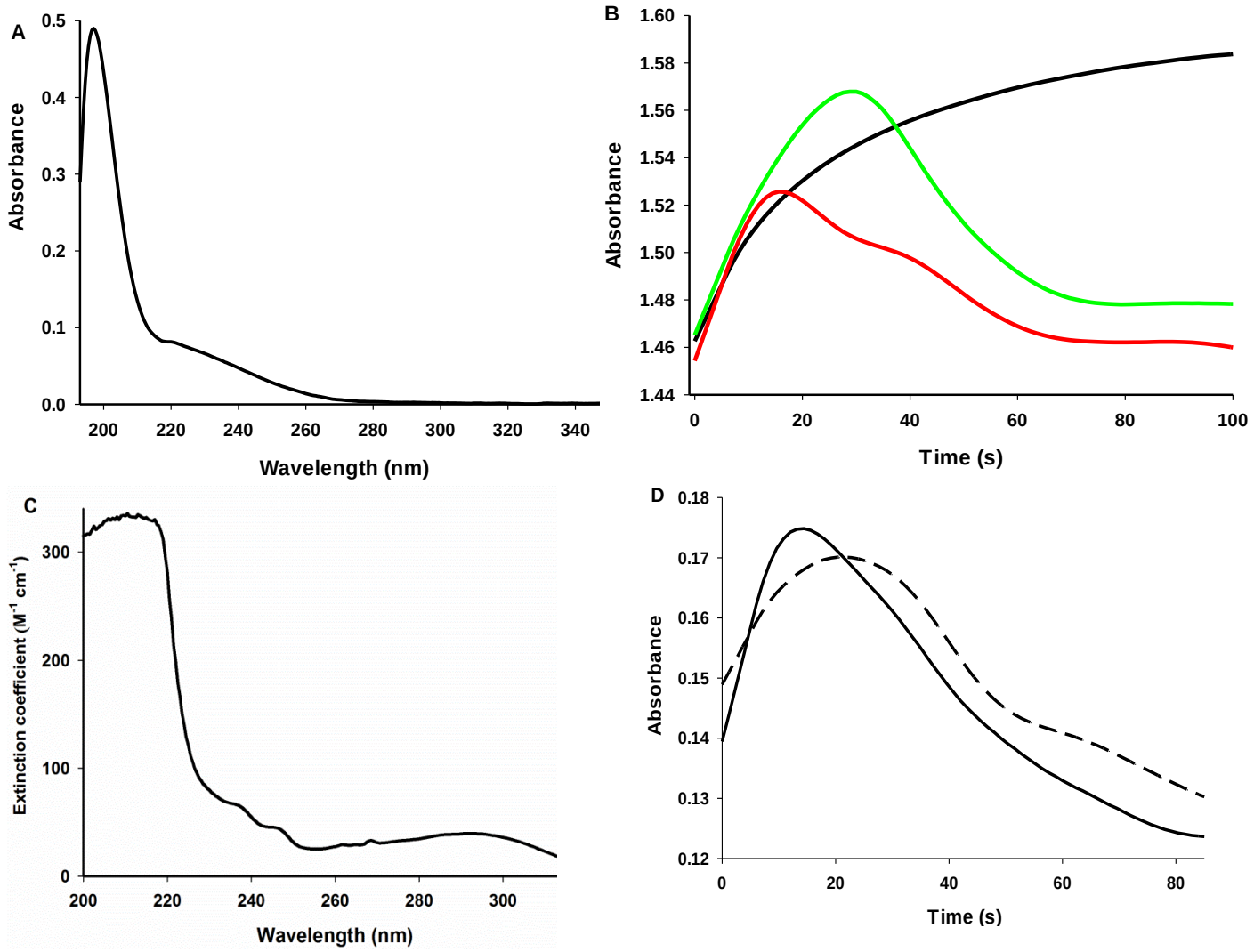

FIGURE 28. The absorbance spectrum of 2.5mg/ml of Δ^5–AD in methanol (A), the C5 double bond absorbs maximally at 200 nm with an extinction coefficient of 3800 $M^{-1}cm^{-1}$. The reaction progress curve of Δ^5–AD (B) followed at 238 nm (green), 256 nm (red) and 248 nm (black). The absorbance spectrum of 2.5mg/ml of Δ^5–AO in methanol (C); the carbonyl group absorbs maximally at 294 nm with an extinction coefficient of 43 $M^{-1}cm^{-1}$ and the isolated ethylenic bond absorbs maximally at 209 nm with an extinction coefficient of 335.4 $M^{-1}cm^{-1}$. The reaction progress curves of Δ^5–AO (D) followed at 235 nm (solid) and 248 nm (dashed).The reactions in (B) and (D) were done with 1µM enzyme and 9µM substrate in 25mM sodium phosphate, pH 8.0 at 20 ^oC.

3.8 The activation energy of reaction

The Arrhenius plots for the formation of product at 248 nm and intermediate at 238 nm (Figure 29) show that the data are linear within the temperature range specified in the experimental

procedures. The activation energy at 248 nm is 13.8 kcal/mole and that at 238 nm is 12.9 kcal/mole.

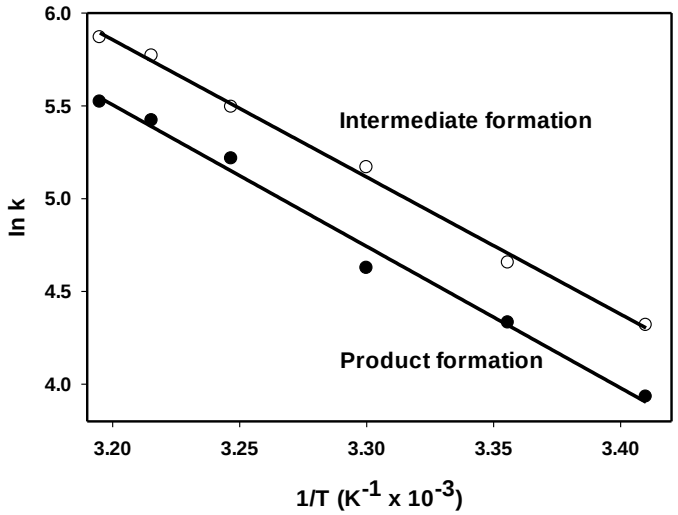

FIGURE 29. The Arrhenius plots for the formation of product (Δ^4-AD) followed at 248 nm yielded an E_a value of 13.8 ± 0.5 kcal/mol (●) and the formation of the conjugated heteroannular diene intermediate followed at 238 nm yielded an E_a value of 12.9 ± 0.4 kcal/mol (O).

3.9 The binding constant of equilenin to hGST A3-3

Equilenin was the non varied ligand concentration while hGST A3-3 concentrations ranged from 1 to 15 µM. This unconventional approach of obtaining K_D with a constant ligand concentration and increasing concentrations of enzyme is because free equilenin is the fluorogenic species. To avoid protein contribution to the signal, the excitation wavelength used was 325 nm corresponding to the signal produced only by free equilenin (Figure. 30a). This information was used to obtain the K_D by monitoring the decrease in fluorescence intensity. The data was fit to a three parameter hyperbolic decay curve (equation 5.), where F is the fluorescence intensity, $F\infty$ is the extrapolated intensity to infinite enzyme concentrations, F_o is the intensity in the absence of enzyme, $[E_T]$ is the total enzyme concentration and $[L_T]$ is the total ligand (equilenin) concentration (Figure 30b).

$$F = F\infty + \frac{\{(F_o - F) - k[E_T]\}K_D}{[E_T]} \qquad \text{equation 5}$$

Where $k = \frac{F_o - F\infty}{[L_T]}$

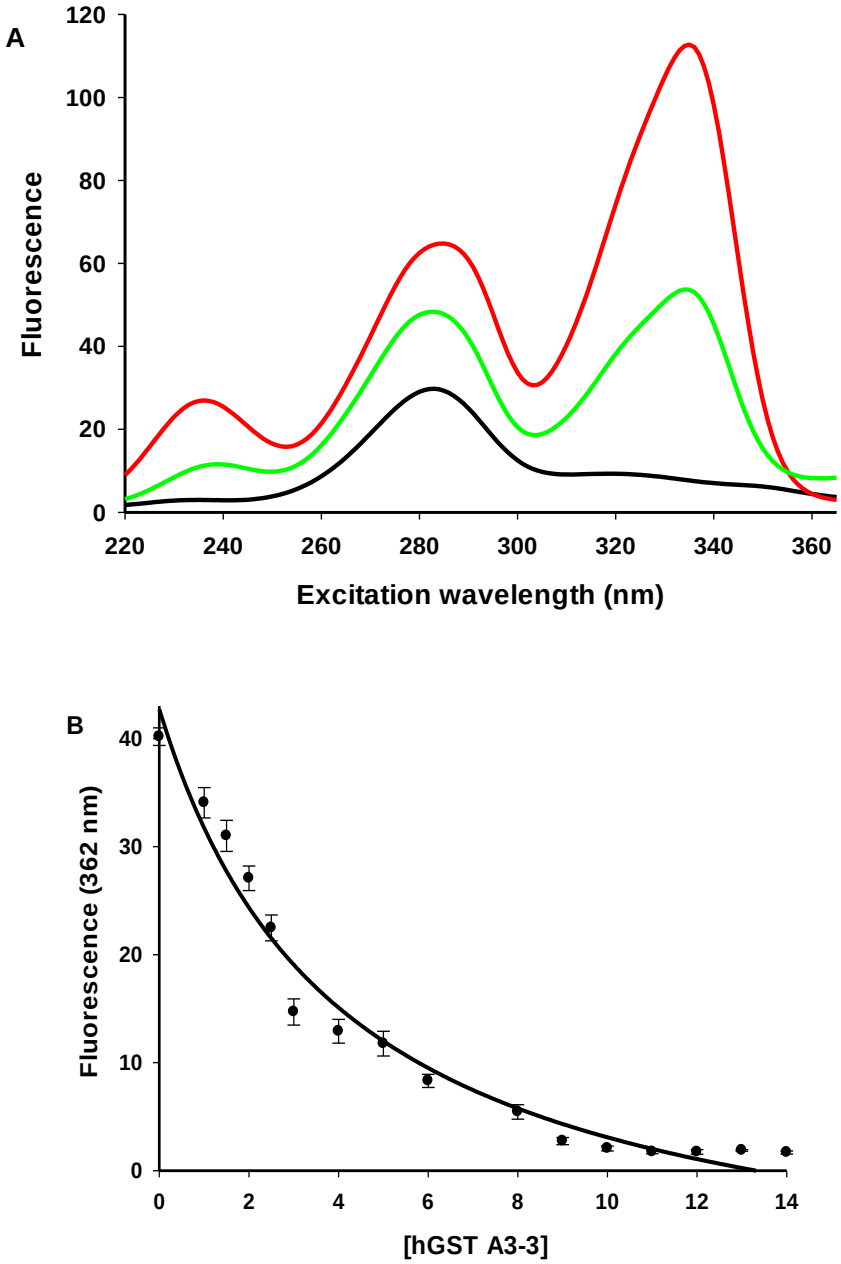

Figure 30. The fluorescence excitation (A) of equilenin and hGST A3-3, used to obtain a binding curve (B). The fluorescence data in (A) were collected for free equilenin (red), equilenin in the presence of hGST A3-3 (green) and free hGST A3-3 (black). A quenching effect is observed in the excitation spectra. The emission wavelength was set at 400 nm for (A) and excitation was set at 325 nm for (B). The data was fit to a three parameter hyperbolic decay curve yielding a K_D value of 3.93 ± 0.53 µM. Measurements were done in 1% methanol at pH 8.0 with 3 µM equilenin.

3.9 Solvent isotope effects

3.9.1 Isotopic exchange at 238 nm in D_2O

Experiments were conducted in which, Δ^5 –AD was varied independently in D_2O (KD_2PO_4 and K_2DPO_4 buffer system in D_2O) at 238 nm and the data were fitted by regression analysis (Figure 31).

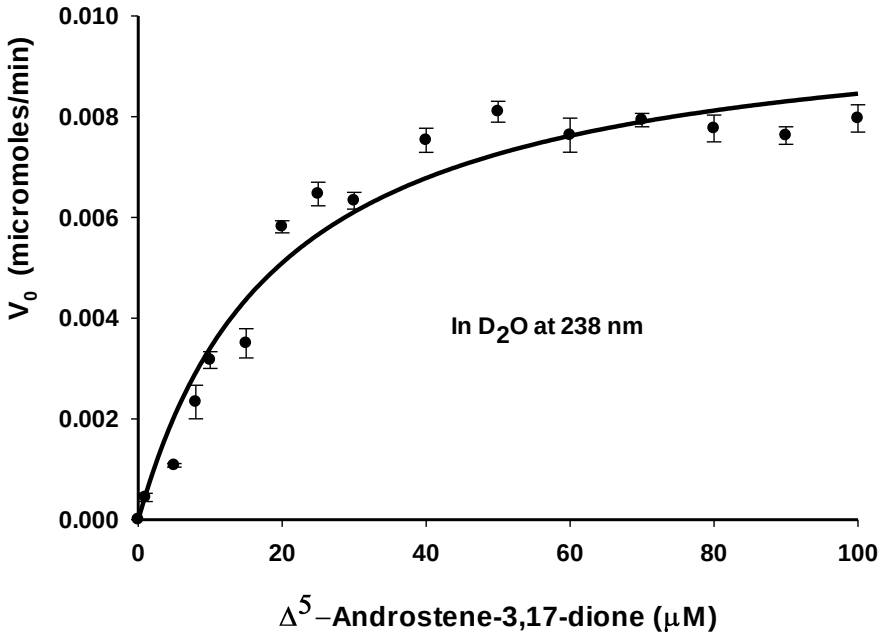

Figure 31. Michaelis-Menten kinetics for a random sequential mechanism were [Δ^5-AD] is varied between 0.5 µM-100 µM and [GSH] is kept constant at saturating conditions of 2mM at 238 nm in D_2O.

3.9.2 Determination of the kinetic parameters k_{cat} and k_{cat}/K_M at 238 nm in D_2O

Separate experiments were conducted to obtain the k_{cat} and k_{cat}/K_M values as described in the materials and methods (Figure 32a). The k_{cat} value obtained was 70.4 ± 3.5 s^{-1} and the k_{cat}/K_M was 1400 ± 155 mM^{-1} s^{-1} (Figure 32b).

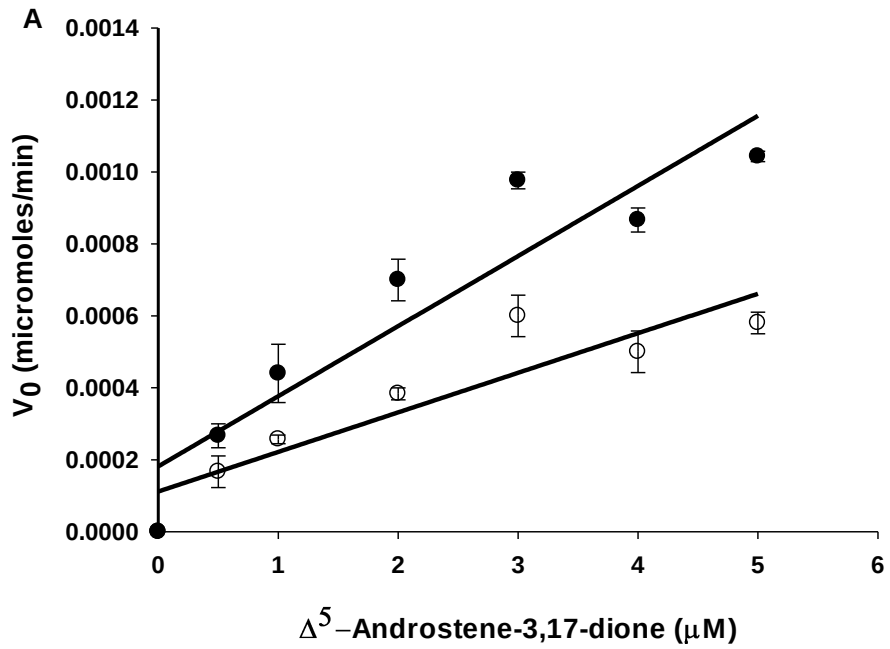

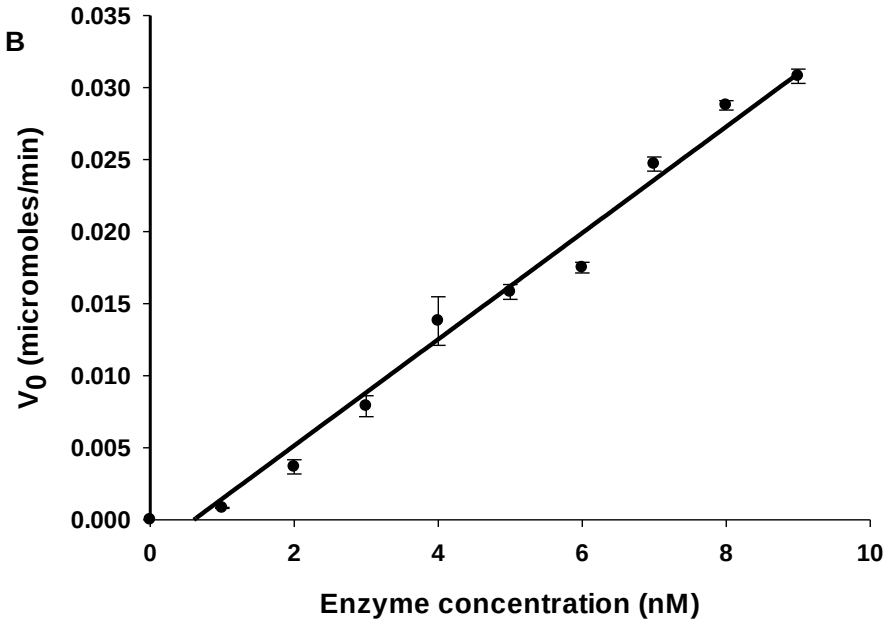

R	Rsqr	Adj Rsqr	Standard Error of Estimate
0.9875	0.9751	0.9742	0.0018

Figure 32. The k_{cat}/K_M values obtained for Δ^5-AD at two different enzyme concentrations 9 nM (●) and 4 nM (○) **(A)**. The k_{cat} obtained for Δ^5-AD under varying enzyme concentrations of 1-9 nM with both GSH and Δ^5-AD saturating at 2 nM and 200 μM respectively **(B)**.Both results were obtained at 238 nm in D_2O. The k_{cat} value obtained was 70.4 ± 3.5 s^{-1} and the k_{cat}/K_M was 1400 ± 155 mM^{-1} s^{-1}.

3.9.3 Michaelis-Menten kinetics at 238 nm in H_2O

The [Δ^5–AD] was varied while GSH was kept constant in order to access the kinetic constants associated with intermediate formation in H_2O (NaH_2PO_4 and Na_2HPO_4 buffer system in distilled water) as shown in figure 33.

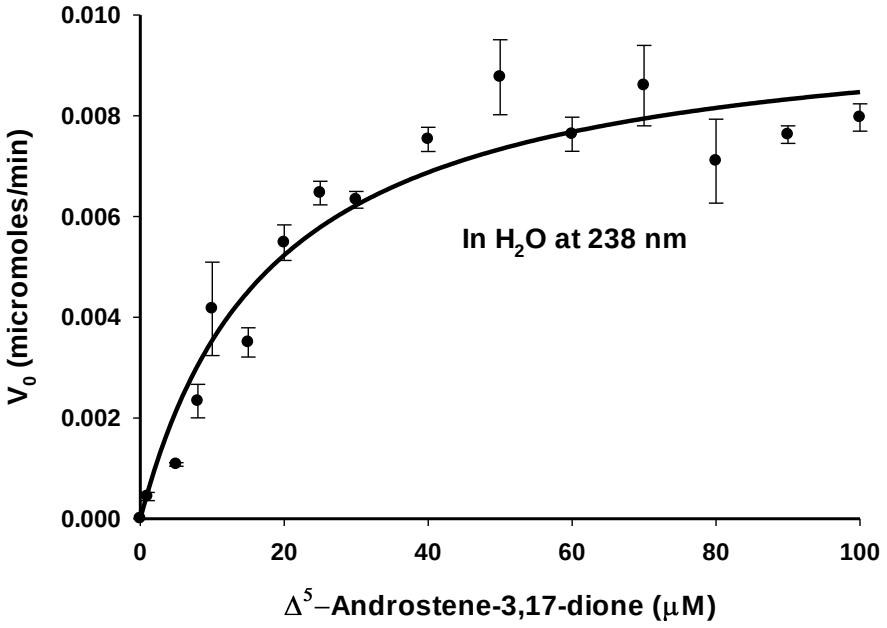

Figure 33. Michaelis-Menten Kinetics for a random sequential mechanism were [Δ^5-AD] is varied between 0.5 µM-100 µM and [GSH] is kept constant at saturating conditions of 2mM at 238 nm in H_2O.

3.9.4 Determination of the kinetic parameters k_{cat} and k_{cat}/K_M at 238 nm in H_2O

Separate experiments were conducted to obtain the k_{cat} and k_{cat}/K_M values as described in the materials and methods (Figure 34a). The k_{cat} value obtained was 75 ± 4 s^{-1} and the k_{cat}/K_M was 1700 ± 150 mM^{-1} s^{-1} (Figure 34b).

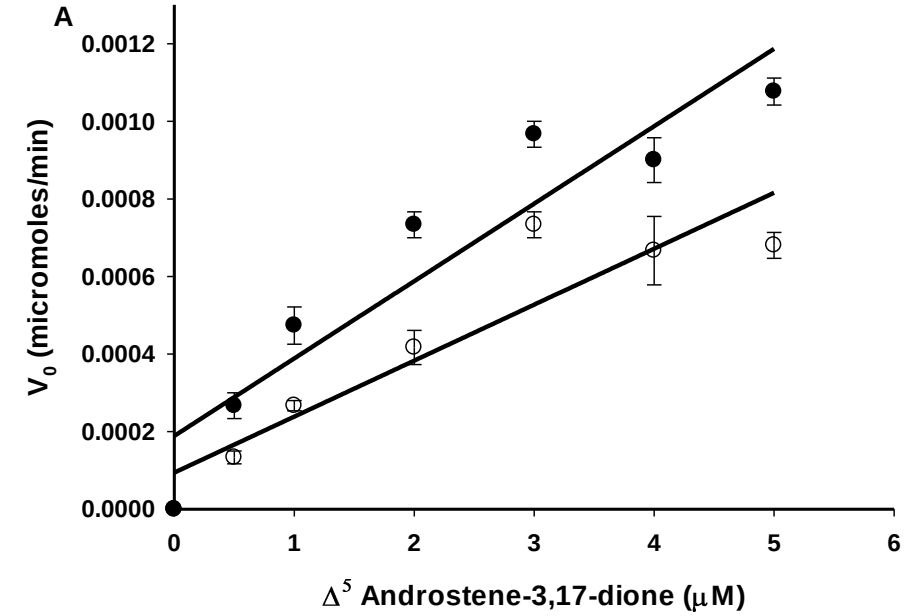

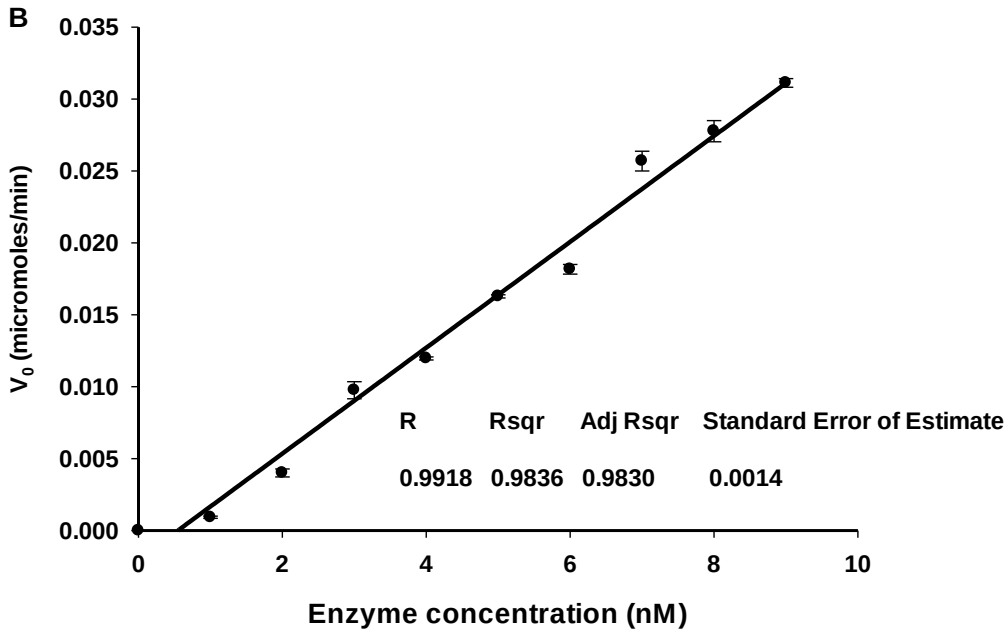

Figure 34. The k_{cat}/K_M values obtained for Δ^5-AD at two different enzyme concentrations 9 nM (●) and 4 nM (○) **(A)**. The k_{cat} obtained for Δ^5-AD under varying enzyme concentrations of 1-9 nM with both GSH and Δ^5-AD saturating at 2 nM and 200 μM respectively **(B)**.Both results were obtained at 238 nm in H_2O. The k_{cat} value obtained was 75 ± 4 s^{-1} and the k_{cat}/K_M was 1700 ± 150 mM^{-1} s^{-1}.

3.9.5 Isotopic exchange at 248 nm in D_2O

Experiments were conducted in which, Δ^5 –AD was varied independently in D_2O at 248 nm and the data were fitted by regression analysis (Figure 35).

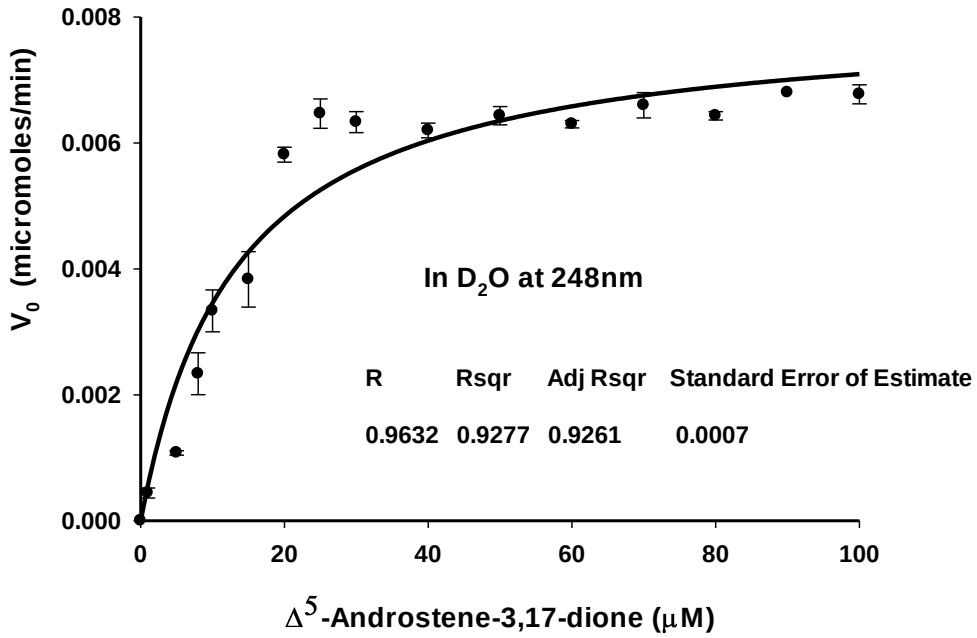

Figure 35. Michaelis-Menten Kinetics for a random sequential mechanism were [Δ^5-AD] is varied between 0.5 µM-100 µM and [GSH] is kept constant at saturating conditions of 2mM at 248 nm in D_2O.

3.9.6 Determination of the kinetic parameters k_{cat} and k_{cat}/K_M at 248 nm in D_2O

Separate experiments were conducted to obtain the k_{cat} and k_{cat}/K_M values as described in the materials and methods (Figure 36a). The k_{cat} value obtained was 41.7 ± 4.2 s^{-1} and the k_{cat}/K_M was 1100 ± 100 mM^{-1} s^{-1} (Figure 36b).

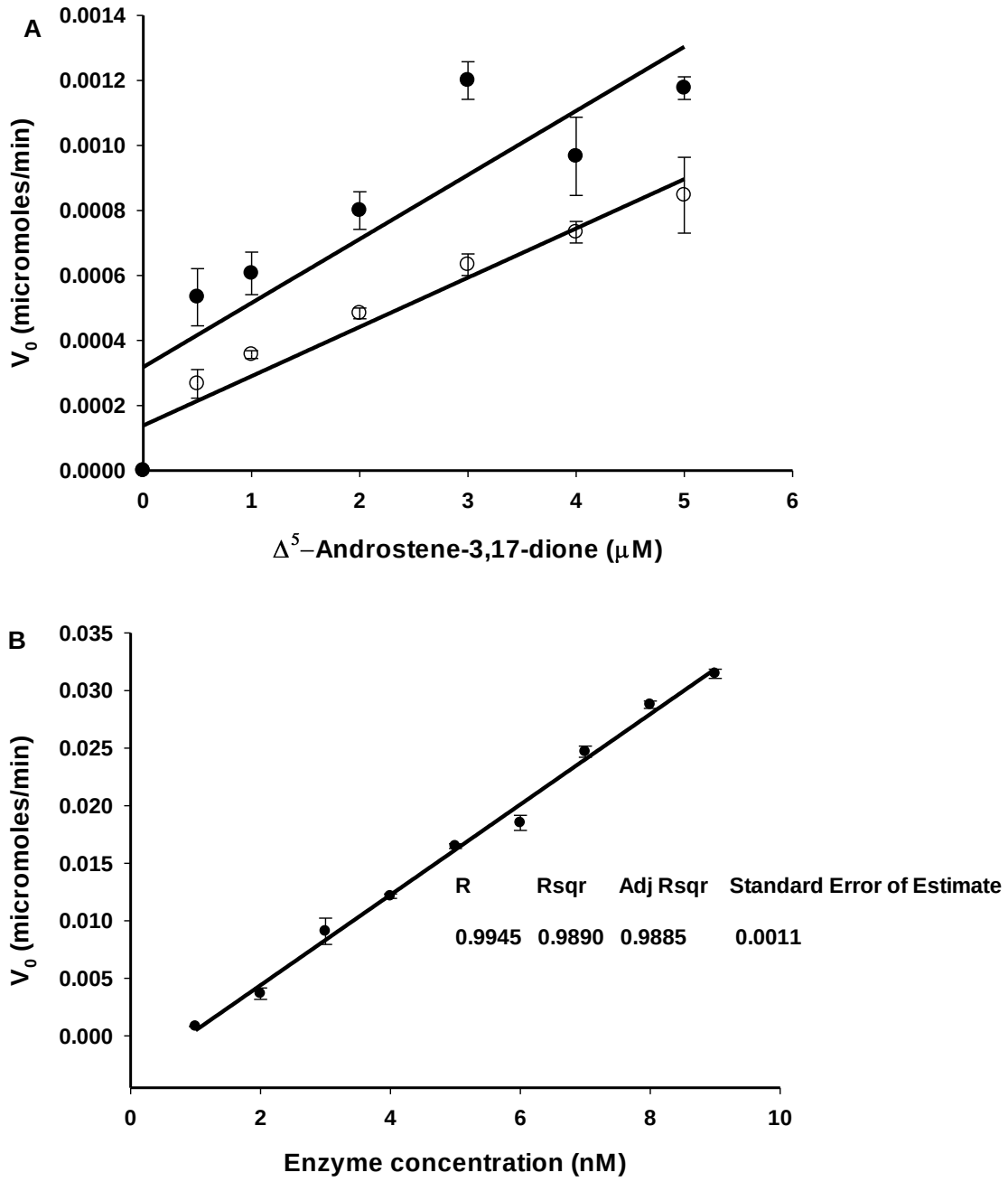

Figure 35. The k_{cat}/K_M values obtained for Δ^5-AD at two different enzyme concentrations 9 nM (●) and 4 nM (○) **(A)**. The k_{cat} obtained for Δ^5-AD under varying enzyme concentrations of 1-9 nM with both GSH and Δ^5-AD saturating at 2 nM and 200 μM respectively **(B)**.Both results were obtained at 248 nm in D_2O. The k_{cat} value obtained was 41.7 ± 4.2 s^{-1} and the k_{cat}/K_M was 1100 ± 100 mM^{-1} s^{-1}.

TABLE 3-2. *Solvent isotope exchange with Δ^5–AD at 238 nm and 248 nm.*
The enzyme activity with Δ^5–*AD* was measured with 2 mM saturating GSH in H_2O and D_2O at 20^oC. H_2O refers to 25 mM protiated phosphate buffer at *p*H 8.0 and D_2O refers to deuterated phosphate buffer at *p*D 8.0

Wavelength (nm)	k_{cat} (s^{-1})	K_M (μM)	$\frac{k_{cat}}{K_M}$ (mM^{-1} s^{-1})	K_S (μM)	Specific activity (μmol mg^{-1} min^{-1})
238 (H_2O)	75 ± 4	20.2 ± 3.4	1700 ± 150		
238 (D_2O)	70.4 ± 3.5	19.7 ± 2.3	1400 ± 155		
248 (D_2O)	41.7 ± 4.2	13.2 ± 1.8	1100 ± 100		51 ± 5
248 (H_2O)	51 ± 3	22.5 ± 4.3	2000 ± 198	9.3 ± 2.2[a]	76 ± 2
(GSH)		130 ± 21	370± 60	50 ± 10[b]	

[a]Determined with a constant Δ^5-AD concentration of 200 μM and varying GSH concentration
[b]Determined with a constant GSH concentration of 2 mM and varying Δ^5-AD concentration.

Chapter 4 Discussion

Energetics of proton abstraction reactions

The conversion of Δ^5-AD to Δ^4-AD in hormone production is a classic example of proton abstraction reactions that underpin a variety of biological processes such as isomerization, racemisation and transamination (Gerlt *et al*., 1991). This makes proton abstraction reactions of immense biological significance, however, these seemingly simple chemical transformations are energetically costly. Carbon acids (C-H bonds adjacent to a carbonyl or carboxylic acid functional group) are generally weak acids with pK_a values of the α-protons in the range 12 – 32 (Chiang and Kresge 1991). At the active site the general basic catalysts are not sufficiently basic with pK_a values usually ≤ 7 (Gerlt *et al*., 1991). The large pK_a difference between the substrate and the active site base poses a thermodynamic challenge. To overcome this great evil, the proffered hypothesis has been that the evolutionary gods have bestowed upon such enzymes, structural features capable of reducing this thermodynamic contribution to the activation energy.

The binding of the co-factor GSH to hGST A3-3 results in a reduction in the thiol pK_a from 9.17 to 6.31 as indicated in figure 26. Consequently at pH 8.0 the cofactor exists in its ionized state. The crystal structure of the ternary complex of hGST A3-3, GSH and the product Δ^4-AD reveals that GSH is 3.7Å from the C4 atom of Δ^4-AD (Tars *et al*., 2010) an ideal distance for proton abstraction. The consensus has been that the ionized thiol plays a similar role to Asp38 in the ketosteroid isomerase (KSI) catalyzed reaction, abstracting a proton from C4 of Δ^5-AD.

A comparison of the macroscopic rate constants in table 3-1 reveals that both the apparent second order and the first order rate constants for the two substrates are similar. The structure of Δ^5–AO eliminates hydrogen bonding interactions at C3 due to the absence of a carbonyl group; therefore the only stabilizing force in this molecule is the conjugate system of the vacant p-orbitals along C3-C4-C5-C6. A clear distinction concerning the major stabilizing force can therefore be made from kinetic data.

To probe the nature of the intermediate, fluorescence emission data (Figure. 27) was used to monitor the ionization state of an intermediate analogue equilenin. The breaking of the O-H bond in the aromatic phenol increases the number of non bonding electrons capable of making the $n \rightarrow \pi^*$ electronic transition. This transition requires less energy and as such a bathochromic shift is observed at pH 11 (Bevins *et al.,* 1986; Eames *et al.,* 1989; Kuliopulos *et al.,* 1989; Wang *et al.,* 1963). The results indicate that in the presence of hGST A3-3 the emission

spectrum resembles that of the un-ionized equilenin. In contrast, the binding of equilenin to KSI results in a spectrum that resembles the ionized state (Zeng *et al*, 1992). Since hGST A3-3 binds its substrate in the hydrophobic H-site, the generation of charges in the solvent-inaccessible hydrophobic environment is unfavourable without the formation of strong directional hydrogen bonding interactions (Zhao *et al.*, 1995). Our results indicate that there is no evidence of such directional hydrogen bonds in hGST A3-3 and the pK_a of equilenin remains invariant upon binding at the H-site. In the KSI mechanism, the D99A mutation decreases the k_{cat} value by $10^{3.7}$ (Wu *et al*., 1997), while the Y14F mutation decreases the k_{cat} value by $10^{4.7}$(Kuliopulos *et al*., 1989). If such a hydrogen bond was to be formed with a localized water molecule in the hGST A3-3 active site, then the k_{cat} of Δ^5 –AD would at least be three orders of magnitude greater than that of Δ^5 –AO. The implication is that the slight difference in the values of k_{cat} and $\frac{k_{cat}}{K_M}$ is not the consequence of a disruption in hydrogen bonding but instead the contribution of the C3 oxygen atom to the conjugate system of p-orbitals. In Δ^5-AD the vacant p-orbital at the C3 oxygen that forms during enolisation is closer to the oxygen nucleus and contributes ultimately to the overall stability of the intermediate.

The isomerization of Δ^5-AO at 235 nm follows the formation of the conjugated heteroannular diene intermediate (Figure 28). Both the substrate Δ^5-AO and suspected product, Δ^4-AO posses isolated double bonds (unconjugated) whose apparent λ_{max} is calculated to be 203 nm and 204 nm respectively, with extinction coefficients no greater than 4000 M^{-1} cm^{-1} (Bladon *et al*., 1952). However, the effect of conjugation results in a bathochromic and hyperchromic displacement of the principle absorption band resulting in an increased extinction coefficient of 17000 M^{-1} cm^{-1} (λ_{max}=235 nm) in the case of Δ^5-AO. Results in figure 28 (b and c) indicate that such transient intermediate species whose only form of stabilization is electron delocalization through a conjugate system do exist; furthermore the existence of the transient dienolate intermediate verifies its importance in the pathway. Both these species accumulate and gradually decay due to their transience in the isomerization process. The effect of the carbonyl group at C3 on the rate of isomerization only becomes significant in the presence of strong hydrogen bonds. In the absence of such strong bonds conjugation becomes the major stabilizing force with only a minimal contribution from the electronegative oxygen atom. The inability of hGST to offer further

stability by hydrogen bonding (as is the case with the KSI catalyzed reaction) means that the intermediate concentrations are not sufficient to account for a turnover similar to that of KSI.

The Marcus formalism-In proton and electron transfer reactions, rather than considering the activation energy as a single measurable quantity, the Marcus formalism (Cohen and Marcus 1968; Marcus 1969; Albery 1980; Gerlt and Gassman 1993; Marcus 2006) divides the activation energy $(\Delta G^{\dagger})$ into two components (i) the thermodynamic free energy barrier (ΔG^0) and (ii) the intrinsic kinetic barrier $(\Delta G^{\dagger}_{\text{int}})$ as shown in equation 6.

$$\Delta G^{\dagger} = \Delta G^{\dagger}_{\text{int}} + \frac{\Delta G^{o}}{2} + \frac{(\Delta G^{o})^2}{16\Delta G^{\dagger}_{\text{int}}} \qquad \text{equation 6}$$

Where $\Delta G^{\dagger}_{\text{int}}$ is the activation energy barrier in the absence of any thermodynamic contributions (i.e., when $\Delta G^0 = 0$). In proton transfer reactions, ΔG^0 is a function of ΔpK_a and is given by $\Delta G^0 = 2.303RT\Delta pK_a$ (ΔpK_a is the difference in the pK_a values between the proton donor and acceptor) (Gerlt and Gassman 1992). The position of the transition state occurs at the maximum value of eq. 3 and is given by equation 7 which equals the Brønsted coefficient β_c.

$$x^{\dagger} = \beta_c = 0.5 + \frac{\Delta G^{o}}{8\Delta G^{\dagger}_{\text{int}}} \qquad \text{equation 7}$$

In the hGST A3-3 catalyzed reaction the k_{cat} obtained for the isomerization of Δ^5–AD translates into an activation energy barrier of $\Delta G^{\dagger}$ =14.8 kcal/mol (according to the transition state theory). The hGST catalyzed isomerization reaction has been found to follow a random sequential mechanism (Pettersson and Mannervik 2001). If the model of scheme III for a random sequential mechanism is used (where 2 mM GSH and enzyme are incubated first to prevent initial random binding) then the k_{cat} is given by equation 8 (Cleland, 1975).

$$EG + S \underset{k_2}{\overset{k_1}{\rightleftharpoons}} EGS \underset{k_4}{\overset{k_3}{\rightleftharpoons}} EGI \underset{k_6}{\overset{k_5}{\rightleftharpoons}} EGP \begin{cases} \underset{k_8}{\overset{k_7}{\rightleftharpoons}} EP \underset{k_{10}}{\overset{k_9}{\rightleftharpoons}} E + P \\ \underset{k_{12}}{\overset{k_{11}}{\rightleftharpoons}} EG \underset{k_{14}}{\overset{k_{13}}{\rightleftharpoons}} E + G \end{cases}$$

Scheme III. E=Enzyme, G=Glutathione, S= Δ^5 –AD, I= intermediate and P= Product.

$$\frac{1}{k_{cat}} = \frac{1}{k'_3} + \frac{1}{k'_5} + \frac{1}{k'_{7,11}} \qquad \text{equation 8}$$

Where, k'_3 k'_5 and $k'_{7,11}$ are net rate constants with $k'_{7,11} = \frac{k_9 k_{13}(k_{11} + k_7)}{k_9 k_{13} + k_9 k_{11} + k_7 k_{13}}$.

The value of the apparent second order rate constant indicates that the hGST A3-3 catalyzed reaction is not diffusion controlled despite the high catalytic efficiency. This coupled with the fact that the product, Δ^4-AD (with a K_i of 25 μM) has the same affinity as the substrate (Johansson and Mannervik 2001) means that the net rate constants for dissociation are large (none limiting). Thus eq. 8 approximates to equation 9

$$\frac{1}{k_{cat}} \approx \frac{1}{k'_3} + \frac{1}{k'_5} \qquad \text{equation 9}$$

Given that $k_6 \ll (k_7 + k_{11})$

$$k_{cat} \approx \frac{k_3 k_5}{k_4 + k_5} \qquad \text{equation 10}$$

The microscopic rate constants reveal that the rate limiting steps are the chemical steps; proton abstraction from carbon 4, proton transfer to carbon 6 and proton transfer back to carbon 4 (equation 10). The reaction at 238 nm is best described by scheme IV,

$$EG + S \underset{k_2}{\overset{k_1}{\rightleftharpoons}} EGS \xrightarrow{k_3} EGI$$

Scheme IV. The reverse reaction from EGI to EGS (k_4) is assumed to be zero as initial rates are considered.

Results in Table 3-2 reveal that in H_2O, the k_{cat} for the overall reaction followed at 248 nm is comparable to the k_{cat} value for the reaction followed at 238 nm. Since this value represents k_3, the proton abstraction step is rate limiting. This allows us to use the macroscopic k_{cat} value as an approximation to the microscopic rate constant k_3 of proton abstraction in the Marcus equation. In assessing the contribution of the carbon 6 proton transfer step to the overall rate, solvent isotope effects are employed. The H/D isotopic exchange between solvent and substrate occurs at

the intermediate during the proton transfer step. In both reactions followed at 238 nm and 248 nm, the $\frac{^{H}k_{cat}}{^{D}k_{cat}} \approx 1$, suggesting that the carbon 6 proton transfer step is non limiting while the carbon 4 proton abstraction step is independent of H/D exchange with solvent .

This analysis, however, overlooks the possibility of protonation back to carbon 4 in the reverse reaction. The rate of carbon 4 protonation would be given by equation 11

$$k_r = \frac{k_2 k_4}{k_2 + k_3} \qquad \text{equation 11}$$

Where k_r is the net rate constant for reverse protonation at carbon 4, since the diffusion steps are rapid ($k_2 \gg k_3$) the value of $k_r \approx k_4$.The internal equilibrium constant between substrate and intermediate has been found (K_{int} = 0.3) (Hawkinson *et al*., 1994). This internal equilibrium constant indicates that the relative energies of the substrate and intermediate are similar. Since the free energy of reaction favours product formation (K_{eq} = 2400) (Pollack *et al*., 1989) the energy barrier for carbon 4 protonation back to reactant is much larger than the carbon 6 protonation for the forward reaction. Therefore the k_{cat} values for the forward reactions are minimally affected by the possible carbon 4 protonation.

If the pK_a of Δ^5–AD remains invariant upon binding the H-site, then the thermodynamic energy required for proton abstraction is ΔG^o = 9 kcal/mol (pK_a of bound GSH is 6.31). The value obtained for the intrinsic kinetic barrier from eq. 2 is $\Delta G^{\dagger}_{int}$ = 10 kcal/mole. Hawkinson *et al* (Hawkinson *et al*., 1994) calculated the intrinsic barrier for proton transfer from Δ^5–AD in solution to be $\Delta G^{\dagger}_{int}$ = 13 kcal/mol. This value was obtained by estimating the Brønsted β_c value of oxygen bases from tertiary amine and oxygen bases involved in the isomerization of 3-cyclohexanone. A β_c value of 0.6 was obtained representative of the acetate oxygen base used to catalyze the solution reaction. The actual β value for the acetate ion-catalyzed ketonisation is 0.54 (Yao *et al.*, 1999) verifying the accuracy of the Hawkinson approximation. Due credence must however encompass the role of the thiol as the base. Oxidized glutathione and similar thiols have β_c values ranging between 0.5 and 0.55 (Szajewski and Whitesides, 1980; Dalby and Jencks, 1997), since the basicity of thiols is expected to be greater than resonance stabilized

oxygen bases such as acetates, the upper limit value of this range is used and the Hawkinson approximation is still upheld. The strategy of hGST A3-3 appears in part to reduce the intrinsic kinetic barrier by 3 kcal/ mol. The Brønsted coefficient describing the position of the transition state is β_c = 0.6, a value that indicates a nearly symmetrical transition state. An alternative reaction pathway is utilized in which the pK_a perturbation is made to the cofactor rather than the substrate. This perturbation alone, contributes 3.8 kcal/mol to the enzyme catalyzed reaction; making GSH a stronger base by 2.6 pH units over Asp38, the proton abstractor in the KSI catalyzed reaction whose pK_a value is 3.75 (Yun *et al*., 2003) .

Revised Mechanism -The hGST A3-3 reaction pathway is initiated by proton abstraction at carbon 4 of Δ^5–AD (Figure 36). During proton abstraction, negative charge develops at the site of bond cleavage and the carbon 4 carbon transits from sp3 hybridization to sp2. This transition is energetically unfavourable because the electrons from the lower energy sp3 orbital are transferred to the vacant p-orbital of higher energy. At energy maxima, the transition state is nearly symmetrical but slightly favours the intermediate as indicated by the Brønsted coefficient (β_c = 0.6). As structural rearrangement progresses, electrons in the higher energy p-orbital are stabilized by the O3-C3-C4-C5-C6 conjugate system. Charge development has the effect of realigning the dipoles of active site water molecules thereby producing a negative entropic contribution due to solvent ordering (Gerlt and Gassman 1993)

The intrinsic kinetic barrier $\Delta G^{\dagger}_{\text{int}}$ refers to the energy that has to be overcome in making such an unfavourable electronic configuration as well as the negative entropic contribution associated with solvent ordering (Bernasconi, 1992). Conjugation alone has a minimal contribution to the overall stability of the intermediate. The strategy of hGST A3-3 is to lower $\Delta G^{\dagger}_{\text{int}}$ with a value of 13 kcal/mol in solution to, $\Delta G^{\dagger}_{\text{int}}$ = 10 kcal/mol at the active site. The enzyme utilizes an alternative reaction pathway that alters the co-factor pK_a thereby contributing 3.8 kcal/mol to the reaction. Although the altered pK_a of GSH contributes to the ΔG^{o} favourably, the enzyme has no structural features such as amino acids capable of forming hydrogen bonds and is thus incapable of effectively dealing with the developing charge. As the free energy of reaction favours product formation (K_{eq} = 2400) and the realization that the chemical steps are rate limiting, proton transfer to carbon 6 (resulting in product) is therefore a fast step.

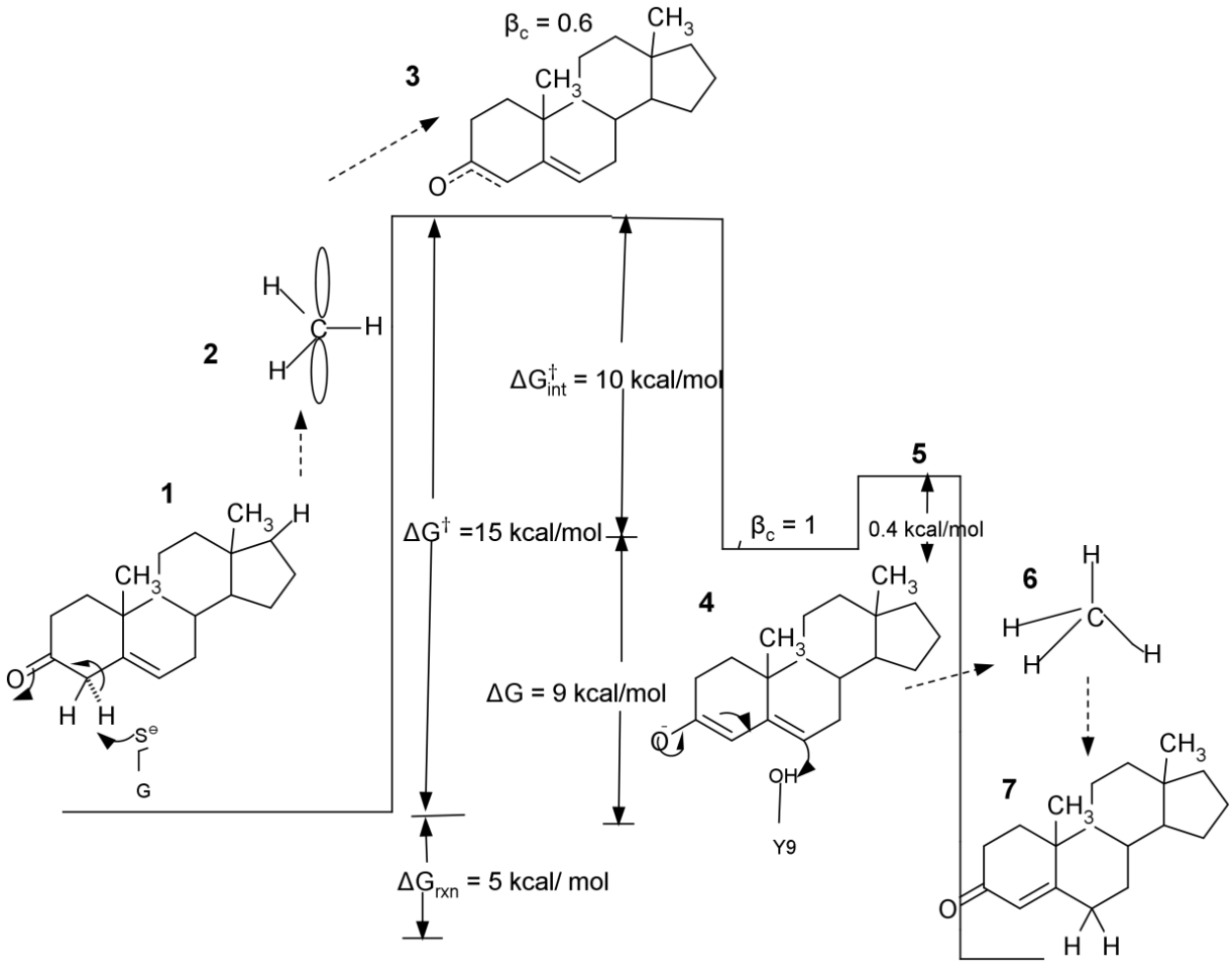

Figure 36. The proposed reaction pathway for the isomerization of Δ^5–AD by hGST A3-3, were the steps are numbered 1-7 and the thermodynamic parameters are calculated per enzyme subunit. At step 1, GSH abstracts the carbon 4 proton; at step 2 a change in hybridization at carbon 4 to a higher energy p-orbital; at step 3, a transition state that is nearly symmetrical but slightly favours the intermediate. At step 4 the structural realignments have advanced since the transition state, the high energy p-orbital electrons are stabilized by the now fully developed conjugate system. At step 5 the transfer of a proton to carbon 6 is kinetically insignificant, resulting in an enforced concerted mechanism and at step 6 a transfer of electrons from the p-orbital to the lower energy sp3 orbital resulting in step 7.

Solvent isotope exchange reveals that this energetic barrier is 0.4 kcal/mol. Since the kinetics studies follow product (and intermediate) formation, this energetic barrier does not include the regeneration of the protonated Tyr9 but merely the transfer of a proton to carbon 6. We propose that hGST A3-3 lowers the $\Delta G^{\dagger}_{int}$ by accelerating the rate of proton transfer to carbon 6 making this the fast step. The rapid transfer of the proton minimizes the extent of charge imbalance at the transition state and intermediate, ultimately reducing the negative entropic contribution

associated with solvent ordering at the active site. Since $\Delta G^{\dagger}_{int} = \Delta H^{\dagger}_{int} - T\Delta S^{\dagger}_{int}$ (Gerlt and Gassman 1993), a reduction in the loss of entropy contributes to lowering the activation energy.

The K_D value of 3.93 μM for equilenin (Figure. 30b) indicates that the protonated form of the intermediate has a similar affinity for binding as the substrate (as indicated by the K_S value). Although we could not obtain the K_D of ionized equilenin without compromising enzyme structure, a comparison of the K_D values of hGST A3-3 and KSI provided further insight. The K_D of equilenin for KSI is 1 μM (Hawkinson *et al*., 1994) a similar value to that of hGST A3-3. However, the rate of the KSI catalyzed reaction is greater than that of hGST A3-3 by three orders of magnitude, suggesting greater dienolate intermediate concentrations for the KSI reaction. Therefore, the critical difference is charge stabilization that allows KSI to ultimately achieve what Albery and Knowles term as "catalytic perfection." A computational analysis using a hybrid quantum mechanics/molecular mechanics approach is in agreement with this mechanism which proceeds via an intermediate (Calvaresi *et a.l,* 2012). The reported thermodynamic parameters of this computational study are, however, nearly two-fold greater than our reported values and may represent the dimeric protein instead of subunit values. Of recent, Ramos and co-workers (Dourado *et al,* 2014) have reconstructed the catalytic pathway by resorting to density functional theory. Their findings show that water molecules are neither necessary nor responsible for stabilizing the intermediate. They, however, attribute this stability to strong hydrogen bonds formed between the GSH-glycine main chain and the C3 oxygen. This is supported by kinetic studies in which the K_M value increases from 45 to 310 μM in the absence of GSH, suggesting a reduced affinity for Δ^5-AD due to the absence of this hydrogen bond. The use of K_M as an approximate measure for binding affinity becomes problematic with increased kinetic complexity. This value becomes a composite function of many microscopic rate constants whose contribution to the observed value may be significant, depending on the dominant enzyme-bound state. Nonetheless, if this approximation is accepted and further concession is made that this binding energy is realized most strongly at the transition-intermediate stages, the increase in the K_M value from 45 μM to 310 μM would only account for an energy difference of ~1 kcal/mol indicating that the contribution of the GSH-glycine main chain hydrogen bond with O3 contributes very little to the kinetic process.

Albery and Knowles analysis-In their pioneering work with triosephosphate isomerase (TIM), Albery and Knowles (Albery and Knowles 1977; Albery and Knowles 1976b; Albery and Knowles 1976a) provided a general framework that describes enzyme efficiency. The framework highlights the three main strategies employed by enzymes to adjust internal energetic states relative to external states namely; uniform binding, differential binding and catalysis of elementary steps.

The observed rate of isomerization of Δ^5–AD in solution at pH 8.0 translates into $\Delta G^{\dagger} = 24$ kcal/mol (Pollack *et al*., 1989). Since the K_S for Δ^5–AD is 9.3 µM, uniform binding alone lowers the energetic states of all bound species by 7 kcal/ mol. The next innovation is differential binding in which certain bound states are preferentially stabilized over the substrate. The inability of hGST A3-3 to effectively stabilize the intermediate by hydrogen bonding accounts for no significant energetic savings. The very unspecific hydrophobic pocket cannot effectively distinguish the substrate from the transition state and intermediate effectively to allow differential binding to occur. This is indicated by the comparable K_S values of the substrate and the intermediate analogue equilenin. The transition from $K_S = 9.3$ µM to $K_D = 3.9$ µM accounts for less than 0.6 kcal/ mol, even if the contribution of the GSH-glycine backbone is considered, this would bring the total change in $\Delta G^{\dagger}$ to ~17 kcal/mol. The next step is the catalysis of elementary steps. We have postulated that hGST A3-3 enhances the rate of proton transfer to carbon 6 aided by the reduction in the pK_a of GSH. The kinetic insignificance of this step minimizes charge imbalance at the transition state and intermediate thereby reducing $\Delta G^{\dagger}_{int}$ by 3 kcal/mol, bringing the total change in $\Delta G^{\dagger}$ to 14 kcal/mol in good agreement with the 14.8 kcal/ mol that has to be overcome in the enzyme catalyzed reaction (Figure 37).

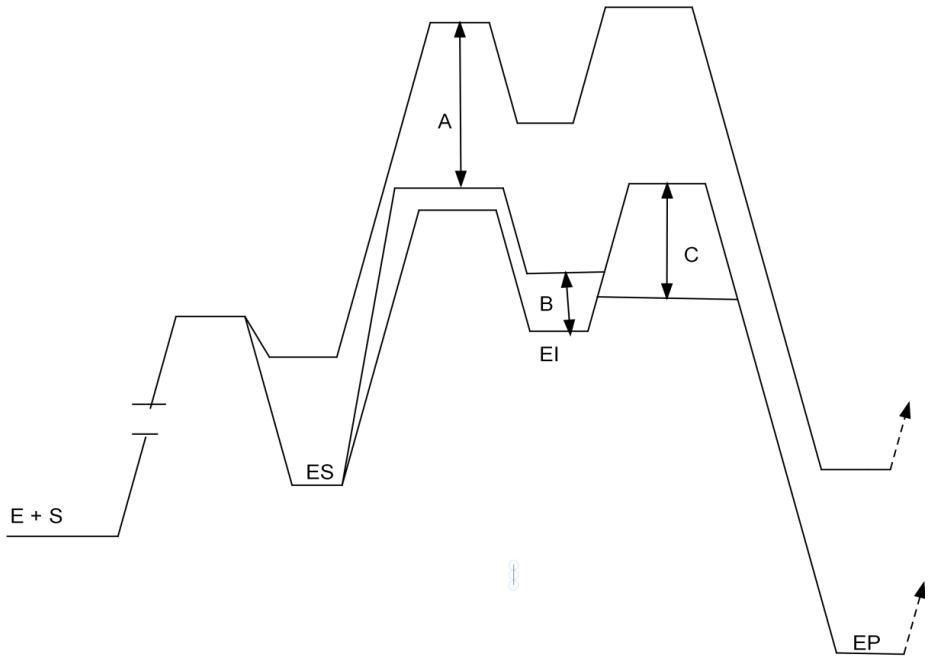

Figure 37. Free energy profiles illustrating the Albery and Knowles analysis where the letters E, S, I and P represent standard nomenclature for enzyme, substrate, intermediate and product respectively. The letter A, represents uniform binding of all species, B is the differential binding contributing very little to energy conservation and C is catalysis of elementary steps.

5 Conclusion

The mechanism in scheme I postulates the existence of a localized water molecule to stabilize a transient dienolate intermediate at the C3 oxygen similar to the roles of Tyr14 and Asp99 in the KSI catalyzed reaction; however neither our results nor the current structural data available support this view. The mechanism in scheme II proposes a reaction pathway that avoids the formation of the dienolate by placing a transient double bond at the-α,β positions; the mechanism implies perfect synchronization of the bond breaking and making process as anything less would result in an overcommitted β carbon with five bonds. Although this is within the realm of possibility, charge delocalization has been seen to lag behind proton transfer due to a lag in resonance development in carbon acids (Bernasconi, 1992) and specifically in enzymatic enolisation reactions (Yao *et al*., 1999). Furthermore electron movement against an electronegativity gradient and a conjugate system that offers stability is unlikely. As the chemical steps are rate limiting and the K_{eq} favours product formation, the energy barrier to product formation cannot exceed that of the decomposition back to substrate. Due to the instability of the dienolate intermediate whose only form of stabilization is charge delocalization; the collapse to

product which is strongly favoured thermodynamically may not be activation limited, making this step kinetically insignificant. We are of the view that uniform binding and catalysis of elementary steps are the main contributors to the rate enhancement observed, while the contribution of differential binding is negligible. The reaction proceeds through an enforced concerted mechanism (Jencks, 1981; Williams, 1994) which results from changes in a stepwise process where the energy well corresponding to an intermediate is nearly commensurate with a regular concerted mechanism.

References

Albery, W. J. The application of the Marcus relation to reactions in solution. *Annu. Rev. Phys. Chem.* **31,** 227–263 (1980).

Albery, W. J. and Knowles, J. R. Efficiency and evolution of enzyme catalysis. *Angew. Chemie Int. Ed. English* **16,** 285–293 (1977)

Albery, W. J. and Knowles, J. R. Free-energy profile for the reaction catalyzed by triosephosphate isomerase. *Biochemistry* **15,** 5627–5631 (1976).

Albery, W. J. and Knowles, J. R. Evolution of enzyme function and the development of catalytic efficiency. *Biochemistry* **15,** 5631–5640 (1976).

Allardyce, C.S., McDonagh, P.D., Lian, L., Wolf, C.R., and Roberts, G., (1999). The role of tyrosine-9 and the C-terminal helix in the catalytic mechanism of Alpha-class glutathione S-transferases. *Biochem. J. 343 , 525*.

Armstrong, R. N. (1997). Structure, catalytic mechanism, and evolution of the glutathione transferases. *Chem. Res. Toxicol, 10*(1), 2-18.

Arvanites, A. C., and Boerth, D. W. (2001). Modeling of the mechanism of nucleophilic aromatic substitution of fungicide chlorothalonil by glutathione. *Mol Modeling Annu, 7*(7), 245-256.

Babbitt, P.C., Gerlt, J.A., (1997b). Understanding Enzyme Superfamilies: Chemistry as the fundamental determinant in the evolution of new catalytic activities. *J. Biol. Chem 272 , 30591-30594*.

Balchin, D., Fanucchi, S., Achilonu, I., Adamson, R.J., Burke, J., Fernandes, M., Gildenhuys, S., and Dirr, H.W., (2010). Stability of the domain interface contributes towards the catalytic function at the H-site of class alpha glutathione transferase A1-1. *Biochim. Biophys. Acta*; *1804* , 2228-2233.

Benson, A.M., Talalay, P., Keen, J.H., and Jakoby, W.B., (1977). Relationship between the soluble glutathione-dependent delta 5-3-ketosteroid isomerase and the glutathione S-transferases of the liver. *Proc. Natl. Acad. Sci. U. S. A. 74 , 158-162.*

Bornscheuer, U.T., Kazlauskas, R.J., (2004b). Catalytic Promiscuity in Biocatalysis: Using Old Enzymes to Form New Bonds and Follow New Pathways. *Angewandte Chemie International Edition 43* , 6032-6040.

Caccuri, A. M., Antonini, G., Board, P. G., Parker, M. W., Nicotra, M., Lo Bello, M., Federici, G., and Ricci, G. (1999) Proton release on binding of glutathione to alpha, mu, and delta class glutathione transferases. *Biochem. J.* 344, 419–425

Cleland, W. W. (1963) The kinetics of enzyme-catalyzed reactions with two or more substrates or products. I. Nomenclature and rate equations. *Biochim. Biophys. Acta* 67, 104–137

Cleland, W. W. (1975) Partition analysis and concept of net rate constants as tools in enzyme kinetics. *Biochemistry*. *14*, 3220–3224

Cohen, A. O., & Marcus, R. A. (1968). Slope of free energy plots in chemical kinetics. *J Phys Chem*, *72*(12), 4249-4256.

Dalby, K. N. and Jencks, W. P. (1997) General acid catalysis of the reversible addition of thiolate anions to cyanamide. *J. Chem. Soc. Perkin Trans. 2* 1555–1564.

Dirr, H., Reinemer, P., and Huber, R. (1994). X-ray crystal structures of cytosolic glutathione S-transferases. *Eur.J. Biochem*, *220*(3), 645-661.

Dirr, H.W., Wallace, L.A., (1999). Role of the C-terminal helix 9 in the stability and ligandin function of class α glutathione transferase A1-1. *Biochemistry 38* , 15631-15640.

Fried, S.D., Boxer, S.G., (2011). Evaluation of the Energetics of the Concerted Acid–Base Mechanism in Enzymatic Catalysis: The Case of Ketosteroid Isomerase. *J. Phys. Chem. B 116* , 690-697.

Gerlt, J. A., and Gassman, P. G. (1993). An explanation for rapid enzyme-catalyzed proton abstraction from carbon acids: importance of late transition states in concerted mechanisms. *J Am Chem Soc*, *115*(24), 11552-11568.

Gu, Y., Guo, J., Pal, A., Pan, S., Zimniak, P., Singh, S.V., and Ji, X., (2004). Crystal structure of human glutathione S-transferase A3-3 and mechanistic implications for its high steroid isomerase activity. *Biochemistry 43 , 15673-15679.*

Hanukoglu, I. (1992). Steroidogenic enzymes: structure, function, and role in regulation of steroid hormone biosynthesis. *J Steroid Biochem Mol Bioly*. *43*(8), 779-804.

Hawkinson, D. C., Pollack, R. M., and Ambulos, N. P., Jr. (1994) Evaluation of the internal equilibrium constant for 3-oxo 5-steroid isomerase using the D38E and D38N mutants: the energetic basis for catalysis. Biochemistry 33, 12172–12183

Heaps, N. A., and Poulter, C. D. (2011). Type-2 Isopentenyl Diphosphate Isomerase: Evidence for a Stepwise Mechanism. *J Am Chem Soc*, *133*(47), 19017-19019.

Honaker, M. T., Acchione, M., Sumida, J. P., and Atkins, W. M. (2011). Ensemble Perspective for Catalytic Promiscuity; Calorimetric analysis of the active site conformational landscape of a detoxification enzyme. *J Biol Chem*. *286*(49), 42770-42776.

Johansson, A., Mannervik, B., (2001). Human glutathione transferase A3-3, a highly efficient catalyst of double-bond isomerization in the biosynthetic pathway of steroid hormones. *J. Biol. Chem. 276 , 33061-33065.*

Johnson, K. A. and Goody, R. S. (2011). The original Michaelis constant: translation of the 1913 Michaelis–Menten paper. *Biochemistry*, *50*(39), 8264-8269.

Listowski, *I. (1993) in Hepatic transport and bile secretion: physiology and pathology (Tavoloni, N. and Berk, P. D., eds) pp. 397–405*

Mannervik, B., (2005). Glutathione transferase: Glutathione transferases and gamma-glutamyl transpeptidases, *Methods Enzymol.401* , 254.

Marcus, R. A. (1969). Unusual slopes of free energy plots in kinetics. *J Am Chem Soc*, *91*(26), 7224-7225.

Miller, W. L., & Auchus, R. J. (2010). The molecular biology, biochemistry, and physiology of human steroidogenesis and its disorders. *Endocr rev*.*32*(1), 81-151.

Montgomery, R., Conway, T. W., Spector, A. A., and Chappell, D. (1996) Biochemistry: A Case-oriented Approach, 6th Ed., pp. 587–618, Mosby Year Book, Inc., St. Louis, MO

Moss, G. P. (1989). IUPAC-IUB joint commission on biochemical nomenclature (JCBN). The nomenclature of steroids. Recommendations 1989. *Eur J Biochem*, *168*, 429-458.

Oakley, A.J. (2005). Glutathione transferases: new functions. *Curr. Opin. Struct. Biol. 15 , 716-723.*

Pettersson, P. L., and Mannervik, B. (2001) The role of glutathione in the isomerization of delta 5-androstene-3,17-dione catalyzed by human glutathione transferase A1-1. *J. Biol. Chem*. *276*, *11698–11704*

Pollack, R. M., Zeng, B., Mack, J. P. G., and Eldin, S. (1989) Determination of the microscopic rate constants for the base-catalyzed conjugation of 5-androstene-3,17-dione. *J. Am. Chem. Soc. 111, 6419–6423*

Pollack, R.M. (2004). Enzymatic mechanisms for catalysis of enolization: ketosteroid isomerase. *Bioorg. Chem. 32 , 341-353.*

Qi, L. and Pollack, R. M. (1998). Catalytic contribution of phenylalanine-101 of 3-oxo-Δ5-steroid isomerase. *Biochemistry*, *37*(19), 6760-6766.

Raffalli-Mathieu, F., Orre, C., Stridsberg, M., Hansson, E. M., & Mannervik, B. (2008). Targeting human glutathione transferase A3-3 attenuates progesterone production in human steroidogenic cells. *Biochem. J*, *414*, 103-109.

Szajewski, R. P. and Whitesides, G. M. (1980) Rate constants and equilibrium constants for thiol-disulfide interchange reactions involving oxidized glutathione. *J. Am. Chem. Soc.* **102,** 2011–2026.Tars,

K., Olin, B., and Mannervik, B., (2010). Structural basis for featuring of steroid isomerase activity in alpha class glutathione transferases. *J. Mol. Biol. 397 , 332-340.*

Tawfik, O. K. A. D. S. (2010). Enzyme promiscuity: a mechanistic and evolutionary perspective. *Annu.Rev.Biochem, 79*, 471-505.

Tian, X. Q., Chen, T. C., Matsuoka, L. Y., Wortsman, J. and Holick, M. F. (1993) Kinetic and thermodynamic studies of the conversion of previtamin D3 to vitamin D3 in human skin. *J. Biol. Chem.* 268, 14888–14892.

Todd, A.E., Orengo, C.A., and Thornton, J.M. (2002). Plasticity of enzyme active sites. *Trends Biochem. Sci. **27** , 419-426.*

Wallace, L.A., Dirr, H.W., (1999). Folding and assembly of dimeric human glutathione transferase A1-1. *Biochemistry **38** , 16686-16694*.

Wang, S. F., Kawahara, F. S. and Talalay, P. The mechanism of the delta5-3-ketosteroid isomerase reaction: absorption and fluorescence spectra of enzyme-steroid complexes. *J. Biol. Chem.* **238,** 576–585 (1963).

Wilce, M. C., and Parker, M. W. (1994). Structure and function of glutathione S-transferases. *Biochimica et biophysica acta*, *1205*(1), 1.

Williams, A. (1994). The diagnosis of concerted organic mechanisms. *Chem Soc Reviews*, *23*(2), 93-100.

Yun, Y. S. *et al.* Origin of the different pH activity profile in two homologous ketosteroid isomerases. *J. Biol. Chem.* **278,** 28229–28236 (2003).

Zeng, B., Bounds, P. L., Steiner, R. F., and Pollack, R. M. (1992). Nature of the intermediate in the 3-oxo-. DELTA. 5-steroid isomerase reaction. *Biochemistry*, *31*(5), 1521–1528.

Zeng, B., and Pollack, R. M. (1991). Microscopic rate constantsfor the acetate ion catalyzed isomerization of 5-androstene-3,17-dione to 4-androstene-3,17-dione: A model for steroid isomerase. *J. Am. Chem. Soc.*, ***113***(10), 3838–3842.

Zhao, Q., Mildvan, A. S., and Talalay, P. (1995). Enzymic and Nonenzymic Polarizations of. alpha.,. beta.-Unsaturated Ketosteroids and Phenolic Steroids. Implications for the Roles of Hydrogen Bonding in the Catalytic Mechanism of. DELTA. 5-3-Ketosteroid Isomerase. *Biochemistry*, ***34***(2), 426–434.

Appendix

Original research publication	The Isomerization of Δ^5–Androstene-3,17-dione by the Human Glutathione Transferase A3-3 Proceeds via a Conjugated Heteroannular Diene Intermediate. *J. Biol. Chem. 289, 32243-32252*



Enzymology:

The Isomerization of Δ^5-Androstene-3,17-dione by the Human Glutathione Transferase A3-3 Proceeds via a Conjugated Heteroannular Diene Intermediate

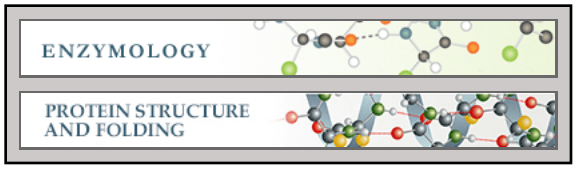

Jonathan L. Daka, Ikechukwu Achilonu and Heini W. Dirr

J. Biol. Chem. 2014, 289:32243-32252.
doi: 10.1074/jbc.M114.601609 originally published online September 23, 2014

Access the most updated version of this article at doi: 10.1074/jbc.M114.601609

Find articles, minireviews, Reflections and Classics on similar topics on the JBC Affinity Sites.

Alerts:
- When this article is cited
- When a correction for this article is posted

Click here to choose from all of JBC's e-mail alerts

This article cites 44 references, 7 of which can be accessed free at
http://www.jbc.org/content/289/46/32243.full.html#ref-list-1

Downloaded from http://www.jbc.org/ at UNIVERSITY OF WITWATERSRAND on November 17, 2014

THE JOURNAL OF BIOLOGICAL CHEMISTRY VOL. 289, NO. 46, pp. 32243–32252, November 14, 2014
© 2014 by The American Society for Biochemistry and Molecular Biology, Inc. Published in the U.S.A.

The Isomerization of Δ^5-Androstene-3,17-dione by the Human Glutathione Transferase A3-3 Proceeds via a Conjugated Heteroannular Diene Intermediate*

Received for publication, July 31, 2014, and in revised form, September 22, 2014 Published, JBC Papers in Press, September 23, 2014, DOI 10.1074/jbc.M114.601609

Jonathan L. Daka, Ikechukwu Achilonu, and Heini W. Dirr[1]

From the Protein Structure-Function Research Unit, School of Molecular and Cell Biology, University of the Witwatersrand, Johannesburg 2050, South Africa

Background: Isomerization reactions are important biochemical transformations required to support life, but the enzymatic pathways are not fully understood.
Results: We propose a mechanism for the isomerization of androst-5-enes by glutathione transferase A3-3.
Conclusion: The glutathione transferase-catalyzed isomerization of androst-5-enes proceeds via an enforced concerted mechanism.
Significance: An understanding of the mechanism allows further insight into proton abstraction reactions in biological systems.

The seemingly simple proton abstraction reactions underpin many chemical transformations, including isomerization reactions, and are thus of immense biological significance. Despite the energetic cost, enzyme-catalyzed proton abstraction reactions show remarkable rate enhancements. The pathways leading to these accelerated rates are numerous and on occasion partly enigmatic. The isomerization of the steroid Δ^5-androstene-3,17-dione by the glutathione transferase A3-3 in mammals was investigated to gain insight into the mechanism. Particular emphasis was placed on the nature of the transition state, the intermediate suspected of aiding this process, and the hydrogen bonds postulated to be the stabilizing forces of these transient species. The UV-visible detection of the intermediate places this species in the catalytic pathway, whereas fluorescence spectroscopy is used to obtain the binding constant of the analog intermediate, equilenin. Solvent isotope exchange reveals that proton abstraction from the substrate to form the intermediate is rate-limiting. Analysis of the data in terms of the Marcus formalism indicates that the human glutathione transferase A3-3 lowers the intrinsic kinetic barrier by 3 kcal/mol. The results lead to the conclusion that this reaction proceeds through an enforced concerted mechanism in which the barrier to product formation is kinetically insignificant.

A natural consequence of the evolution of species in response to their environmental pressures has been the refinement and optimization of biological macromolecules, thus improving the functioning and adaptability of the entire organism. Enzymes are one such group of macromolecules that have been optimized to allow a more efficient flow of energy and material through a system. They display greater effectiveness than simple organic catalysts and have been the subject of much fascination because of their remarkable catalytic prowess.

In aerobic organisms, the deleterious effect of xenobiotic compounds, both of endogeneous and exogenous origin, is prevented by a superfamily of soluble dimeric proteins known as the glutathione transferases (EC 2.5.1.18) (1, 2). The detoxification reaction involves the conjugation of the toxicant with the tripeptide co-substrate glutathione (GSH), where the ionized thiol group of GSH attacks the electrophilic center of the compound. Although the soluble glutathione transferases have been grouped in different classes (alpha, pi, mu, theta, sigma, zeta, and omega), they retain a common fold, with each subunit possessing a conserved thioredoxin-like domain with a GSH binding site (G-site) and a less conserved all-α-helical hydrophobic site (H-site) for the binding of diverse nonpolar electrophiles (3). In 1976 Benson and Talalay (4) showed that a major GSH-dependent enzyme displays high isomerase activity with 3-ketosteroids, and 25 years later Johansson and Mannervik (5) identified the human glutathione transferase A3-3 (hGST A3-3) as displaying the highest isomerase activity over other members of the same class because of amino acid variations in the H-site.

The production of steroid hormones such as testosterone and progesterone from cholesterol proceeds via a complex series of oxidation and isomerization reactions (6). A critical step in this biosynthetic pathway is the isomerization of the β,γ double bond of Δ^5-androstene-3,17-dione (Δ^5-AD)[2] to the α,β isomer Δ^4-androstene-3,17-dione (Δ^4-AD); a labile hydrogen from carbon 4 adjacent to the carbonyl functional group of Δ^5-AD, is abstracted and transferred to carbon 6. In bacteria this conversion is catalyzed by ketosteroid isomerase (KSI) (7), whereas in mammalian tissue, hGST A3-3 and KSI have been shown to perform a similar task, with GSH acting as a cofactor

* This work was supported by the University of the Witwatersrand, Grants 60810, 65510, and 68898 from the South African National Research Foundation, and Grant 64788 from the South African Research Chairs Initiative of the Dept. of Science and Technology and National Research Foundation.
[1] To whom correspondence should be addressed: Protein Structure-Function Research Unit, School of Molecular and Cell Biology, University of the Witwatersrand, Johannesburg 2050, South Africa. Tel.: 27-11-717-6352; E-mail: heinrich.dirr@wits.ac.za.

[2] The abbreviations used are: Δ^5-AD, Δ^5-androstene-3,17-dione; Δ^4-AD, Δ^4-androstene-3,17-dione; KSI, ketosteroid isomerase; hGST, human glutathione *S*-transferase.

Downloaded from http://www.jbc.org/ at UNIVERSITY OF WITWATERSRAND on November 17, 2014

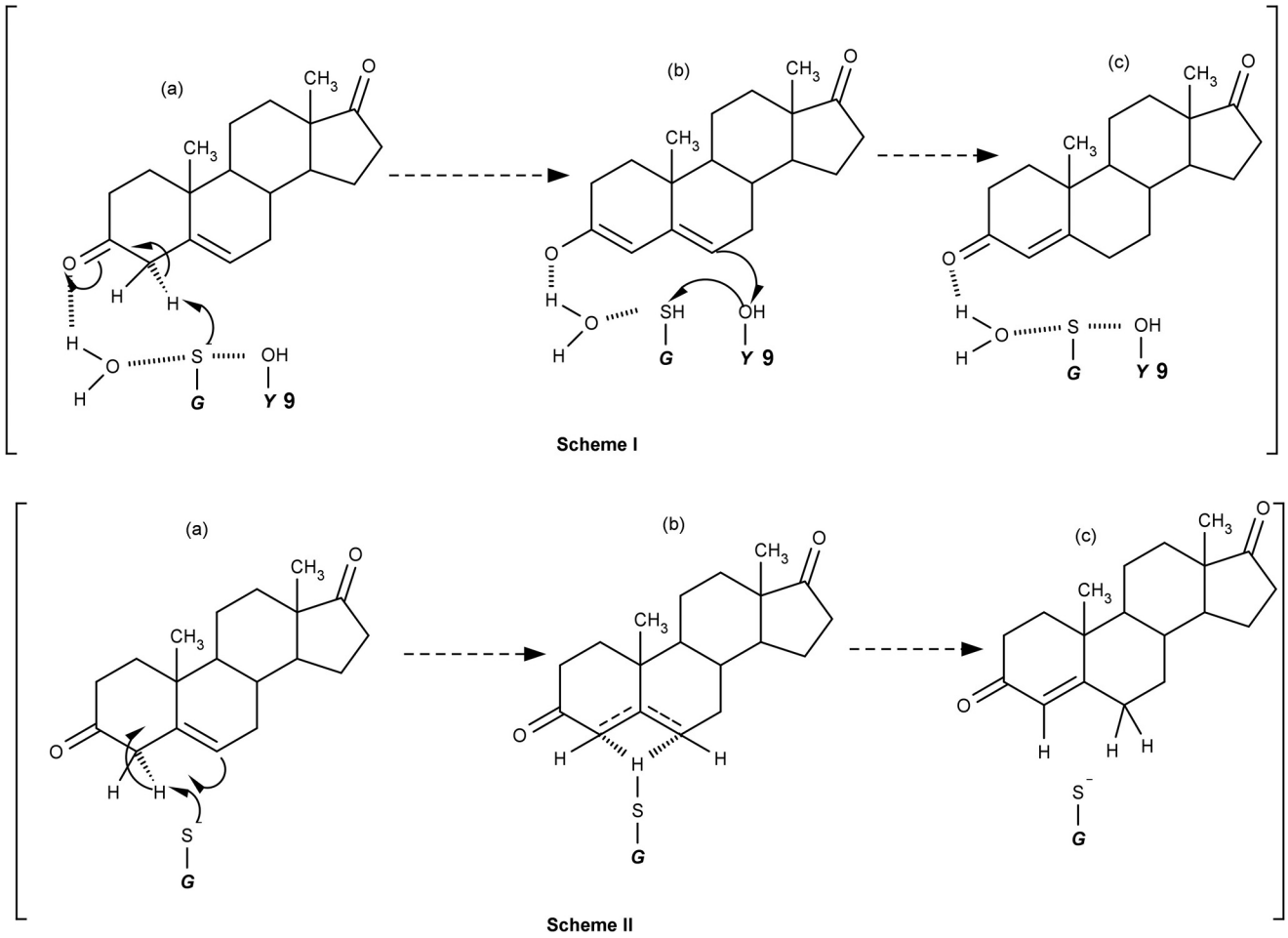

FIGURE 1. **Proposed reaction mechanisms for Δ^5-AD isomerization by hGST A3-3.** In **Scheme I**, adapted from Gu *et al.* (10), GSH abstracts the carbon 4 proton, and a water molecule acts as a hydrogen bond donor, stabilizing the negative charge on the dienolate intermediates (*a* and *b panels*). The keto form is regenerated by the transfer of negative charge via a conjugation system of π bonds with Tyr-9 acting as a proton shuttle (*c*). In **Scheme II**, adapted from Tars *et al.* (11), GSH abstracts a proton from carbon 4 while simultaneously transferring it to carbon 6. The keto group at carbon 3 is unaffected, and the reaction proceeds without the formation of the dienolate intermediate via a concerted single step mechanism.

in the hGST A3-3-catalyzed pathway but as an activator in the KSI-mediated reaction (8). Although the bacterial KSI-catalyzed conversion of Δ^5-AD has been elucidated (9), both the hGST A3-3 and mammalian KSI-catalyzed reactions remain enigmatic.

There has been much contention over the GST A3-3 catalytic conversion of Δ^5-AD to Δ^4-AD. Ji and co-workers (10) have proposed a mechanism, shown in Fig. 1, **Scheme I**, that proceeds by a stepwise pathway via the formation of a dienolate intermediate, stabilized by electron delocalization through a conjugate system of vacant *p*-orbitals along an O-C3-C4-C5-C6 pathway. It is thought that electron delocalization alone is insufficient to explain the observed catalytic rates, and a water molecule that would act as a hydrogen bond donor to the carbonyl oxygen to further stabilize the dienolate intermediate has been proposed. Structural data based on the crystal structure of a ternary complex of hGST A3-3, GSH, and the product Δ^4-AD provide no evidence of such a stabilizing water molecule, prompting Mannervik and co-workers (11) to suggest that both the bond-breaking process at carbon 4 and the bond-making process at carbon 6 is concerted and is devoid of a stable dienolate intermediate, as shown in Fig. 1, **Scheme II**. The implication is that the carbonyl oxygen plays no role in the stabilization process and electron delocalization proceeds directly from carbon 3 to carbon 6 in concert with proton transfer to carbon 6.

We sought to investigate the two proposed mechanisms in order to establish the most plausible reaction pathway. We hypothesized that if the model proposed by Mannervik and co-workers (11) is correct, there should be neither evidence of intermediate formation nor the presence of an existing water molecule at carbon 3. Furthermore we obtained the dissociation constant (K_D) for the analog intermediate, equilenin, and used this value to approximate the relative stabilities of the bound substrate and the proposed intermediate. This information, together with the pK_a values of both the free and the enzyme-bound GSH, was used to explain how the hGST A3-3 enhances the rate of proton abstraction reactions in steroidogenesis, where the Marcus formalism (12) is employed. We have further provided a molecular mechanism consistent with these results that fully explains the observed rate enhancements, with particular focus on the nature of the intermediate.

Downloaded from http://www.jbc.org/ at UNIVERSITY OF WITWATERSRAND on November 17, 2014

EXPERIMENTAL PROCEDURES

Materials—GSH, equilenin, 19-nortestosterone, D_2O, and K_2DPO_4 were obtained from Sigma-Aldrich. The steroid Δ^5-androstene-3,17-dione was obtained from Steraloids Inc. (Newport, RI). All other reagents were of analytical grade.

Heterologous Protein Expression and Purification—High level expression of the wild-type hGST A3-3 was based on the pET11a vector (GenScript, Inc.) in BL21(DE3) pLysS *Escherichia coli* cells. The cells were grown in 2× TY (1.6% (w/v) tryptone, 1% (w/v) yeast extract, 0.5% (w/v) NaCl) at 37 °C to an A_{600} of 0.4. A final concentration of 1 mM isopropyl-β-D-thiogalactoside was used to induce protein expression. After 4 h of growth, the cells were harvested and lysed by ultrasonication. Protein purification was by immobilized metal affinity chromatography using nickel-Sepharose (Amersham Biosciences) eluted with 20 mM Tris buffer containing 0.5 M imadazole at pH 7.4. An additional purification step using benzamidine-Sepharose produced thrombin-free pure protein. The purity was determined using SDS-polyacrylamide gel electrophoresis, and the protein was dialyzed against 20 mM sodium phosphate buffer, pH 8, containing 1 mM EDTA and 0.02% sodium azide. The concentration of the dimer was determined at 280 nm using the protein subunit molar extinction coefficient of 23,900 M^{-1} cm^{-1} (5).

Determination of the pK_a of the Thiol Group of Free and Enzyme-bound GSH—The spectrum of free GSH in solution was obtained at different pH values, and the ionization of the thiol group was monitored by measuring the absorbance of the thiolate at 239 nm. The spectrum of GSH bound to hGST A3-3 was obtained within the pH range of 5.2 to 9.3 using 0.1 M mono-, di-, and trisodium phosphate to cover the pH range and was corrected for both free GSH by subtracting the spectrum of free GSH within this pH range and free enzyme at the storage buffer pH of 7.4 from the enzyme-bound spectrum. The enzyme concentration was 9 μM, and the GSH concentration was kept at 250 μM.

Fluorescence Measurements with Equilenin—All fluorescence measurements were done at 20 °C with a scan rate of 200 nm/min using the Jasco FP-6300 fluorimeter with the excitation and emission slit widths set at 5 and 10 nm, respectively. The emission spectrum was scanned from 300 to 500 nm with an average of three scans and all spectra corrected for buffer. The nature of the intermediate at the active site of hGST A3-3 was probed using an excitation wavelength of 292 nm in 25 mM sodium phosphate buffer at pH 8 and pH 11 in a total volume of 300 μl with 1% methanol. The equilenin and protein concentrations used were 3 and 9 μM, respectively. The dissociation constant for the binding of equilenin to hGST A3-3 was determined by fluorescence titration of 3 μM equilenin with varying enzyme concentrations ranging between 1 and 15 μM in 25 mM sodium phosphate buffer, pH 8, with 1% methanol. The dependent variable was the emission of free equilenin measured at 363 nm.

Absorbance Measurements with 19-Nortestosterone—Spectral measurements were made in quartz cuvettes with a 1-cm light path. A concentration of 33 μM of 19-nortestosterone with 19.6 μM enzyme was used. The spectrum of the ketosteroid was measured against a 25 mM sodium phosphate buffer blank in 1% methanol. The spectrum of the mixture of ligand and enzyme was measured against a blank containing the enzyme at 19.6 μM with the same buffer composition.

Detection of the Dienolate Intermediate—Zeng and Pollack (13) determined the maximum absorbance wavelength for the externally generated dienolate intermediate to be 238 nm. The UV-visible spectroscopic detection of the dienolate intermediate was followed at 238 nm in 25 mM sodium phosphate buffer at 20 °C and pH 8.0. A total concentration of 10 μM was used for the substrate with 1 μM enzyme concentration.

Solvent Isotope Effects with Δ^5-AD—Steady-state kinetic parameters at 238 and 248 nm were obtained in both D_2O and H_2O in 25 mM phosphate buffer at 20 °C (using potassium deuterium phosphate for D_2O with a pD of 8.0).

The concentrations of substrate were varied from 0.5 to 100 μM. The data were fitted to the Michaelis-Menten equation using SigmaPlot v11 (Systat Software, Inc.). The activity of hGST A3-3 toward Δ^5-AD for the isomerization reaction at 248 nm was determined with a molar extinction coefficient of 16,300 M^{-1} cm^{-1} for Δ^4-AD (8), and the molar extinction coefficient for the formation of the dienolate intermediate was 13,800 M^{-1} cm^{-1} (13). All measurements were done per enzyme subunit with 2 mM GSH at pH 8.

Determination of the Activation Energy—Isomerase activity was recorded from 15 to 40 °C in a thermostatted Varian Cary UV-visible spectrophotometer with a Cary dual cell Peltier accessory. Steady-state kinetic parameters were obtained at 248 and 238 nm with three replicate measures collected for each temperature. The activation energy was determined as described by Tian *et al.* (14) by using the Arrhenius equation ($\ln k = \ln A - E_a/RT$), where k is the rate constant (catalytic turnover), R is the molar gas constant, T is the temperature in degrees Kelvin, E_a is the activation energy, ln is the natural logarithm, and A is the pre-exponential factor. Linear plots of $\ln k$ *versus* $1/T$ yield a slope of $-E_a/R$ from which E_a can be obtained directly. The relationship between the Arrhenius equation and the Eyring transition state equation, k_BT/h exp $(-\Delta G^{\ddagger}/RT)$, yields $\Delta H^{\ddagger} = E_a - RT$, where k_B is the Boltzmann constant, h is the Plank constant, $\Delta G^{\ddagger}$ is the Gibbs free energy of activation, and $\Delta H^{\ddagger}$ is the enthalpy of activation.

RESULTS

The pK_a Value of GSH upon Binding—The binding of the cofactor GSH to hGST A3-3 results in a reduction of the thiol pK_a from the solution value of 9.1 to 6.3 in the active site (Fig. 2). Previous studies on hGST A1-1, a variant of hGST A3-3, indicate a similar reduction for both the isomerization reaction (15) and the typical conjugation reaction (16), equivalent to a reduction in ΔG^0 of 3.8 kcal/mol ($\Delta G^0 = 2.303\ RT\Delta pK_a$).

The Nature of the Intermediate at the Active Site of hGST A3-3—At pH 8.0, free equilenin displays a λ_{max} of 362 nm with a resulting red shift at pH 11 to 425 nm (Fig. 3*A*). The ionization of the aromatic phenol results in the release of electrons previously held in the O–H σ bond, thereby increasing the number of nonbonding electrons capable of making the $n \rightarrow \pi^*$ electronic transition. In the presence of hGST A3-3, the fluorescence emission spectrum resembles the protonated state with a

Downloaded from http://www.jbc.org/ at UNIVERSITY OF WITWATERSRAND on November 17, 2014

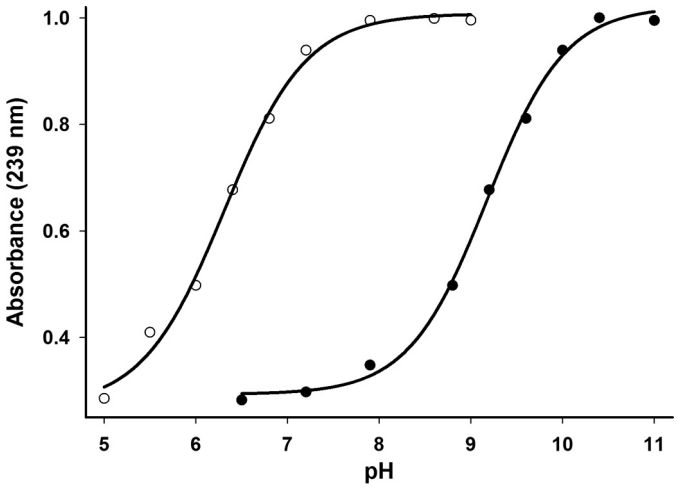

FIGURE 2. **The deprotonation of GSH expressed as a function of pH in the presence and absence of hGST A3-3.** Nonlinear regression analysis of the data yielded a pK_a value of 9.17 ± 0.04 for free GSH (●) and a pK_a value of 6.31 ± 0.07 for the active site-bound GSH (○).

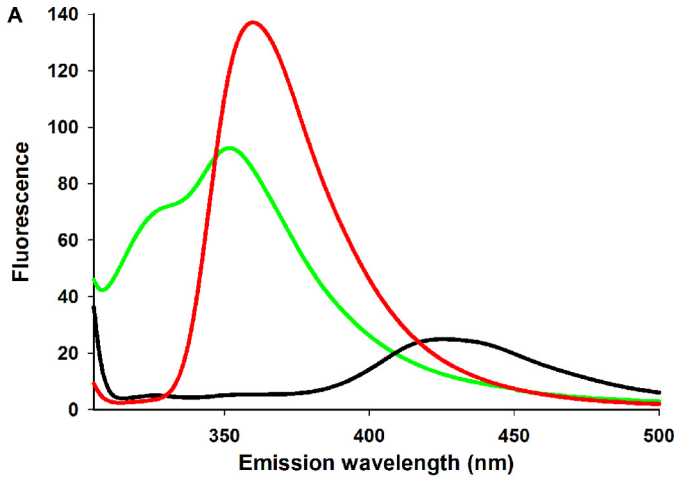

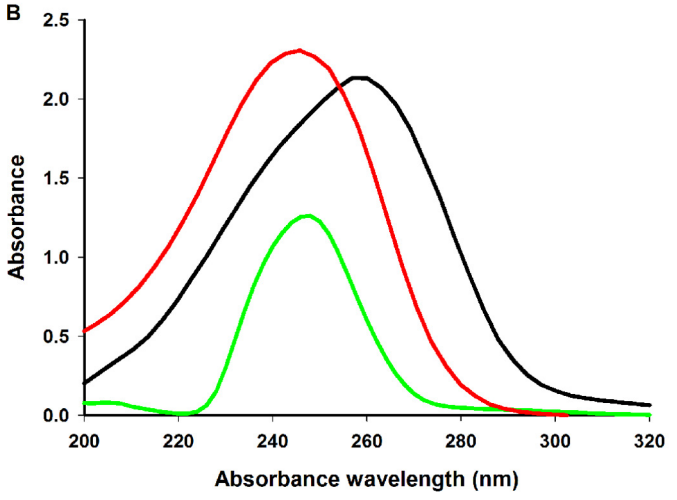

FIGURE 3. *A*, fluorescence emission spectra of equilenin as an indicator of the intermediate ionization state at the active site. Free equilenin (3.8 μM) is observed at pH 8.0 (*red*) and pH 11.0 (*black*) and in the presence of 9 μM enzyme (*green*). Equilenin was dissolved in 1% methanol, and excitation was set at 292 nm. *B*, the absorbance spectra of 19-nortestosterone (36.6 μM) observed in solution at pH 8.0 (*red*), in 10 M HCl (*black*), and in the presence of 19 μM enzyme (*green*).

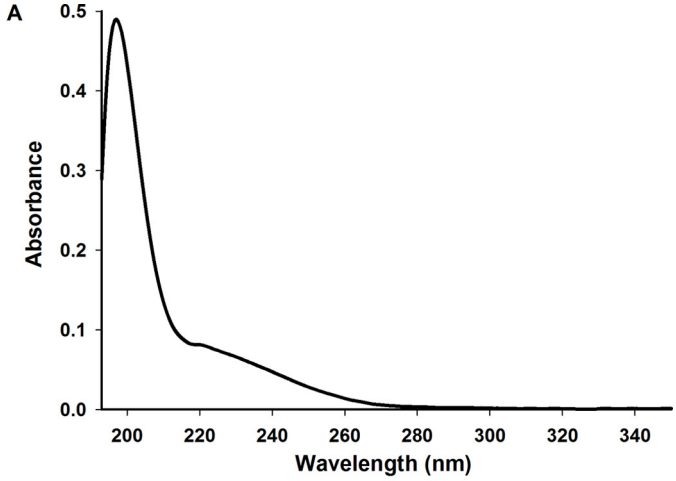

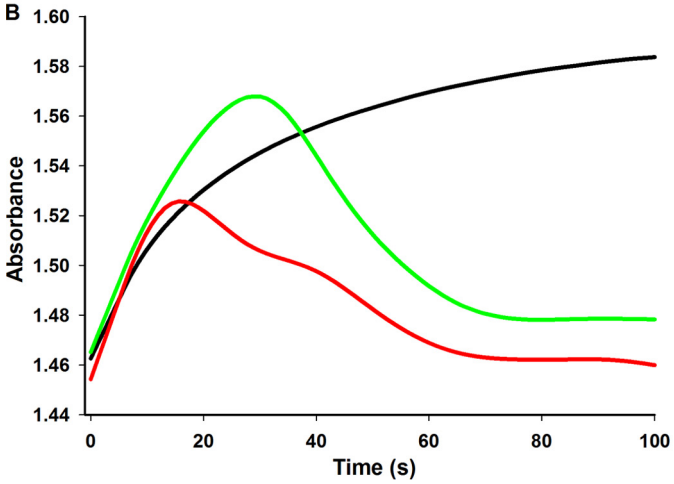

FIGURE 4. *A*, the absorbance spectrum of 150 μM Δ^5-AD in methanol. The isolated ethylenic bond absorbs maximally at 200 nm. *B*, the reaction progress curves of Δ^5-AD followed at 238 nm (*green*), 256 nm (*red*), and 248 nm (*black*).The reactions were done with 1 μM enzyme and 9 μM substrate in 25 mM sodium phosphate, pH 8.0, at 20 °C.

slight shift to 350 nm (Fig. 3*A*). The α,β-unsaturated ketosteroid 19-nortestosterone has a principle absorption maximum at 248 nm in water. A 10-nm shift is observed when the enone chromophore is exposed to 10 M HCl. In the presence of enzyme, the shift is not observed and the absorption maximum remains at 248 nm with a reduction in the concentration of free ligand (Fig. 3*B*).

UV-visible Detection of the Intermediate—The substrate Δ^5-AD displays a λ_{max} of 200 nm because of the isolated double bond (Fig. 4*A*). The principle chromophore at 238 nm however is the conjugated heteroannular diene that is characteristic of the intermediate. Ionization to the enolate frees the O–H-bonding electrons, which make the $n \rightarrow \pi^*$ transition. This transition shifts λ_{max} to 256 nm with a corresponding hyperchromic shift from 13,800 M^{-1} cm^{-1} to 15,000 M^{-1} cm^{-1} (17). The enzymatic conversion of Δ^5-AD was followed at 238, 256, and 248 nm (Fig. 4*B*). The reaction at 248 nm for Δ^5-AD follows product formation, with the chromophoric region being the conjugated α,β-3-ketone isomer. Therefore the reaction does not show a decrease in absorbance, whereas the two progress curves at 238 and 256 nm produce an initial rise in the absor-

Downloaded from http://www.jbc.org/ at UNIVERSITY OF WITWATERSRAND on November 17, 2014

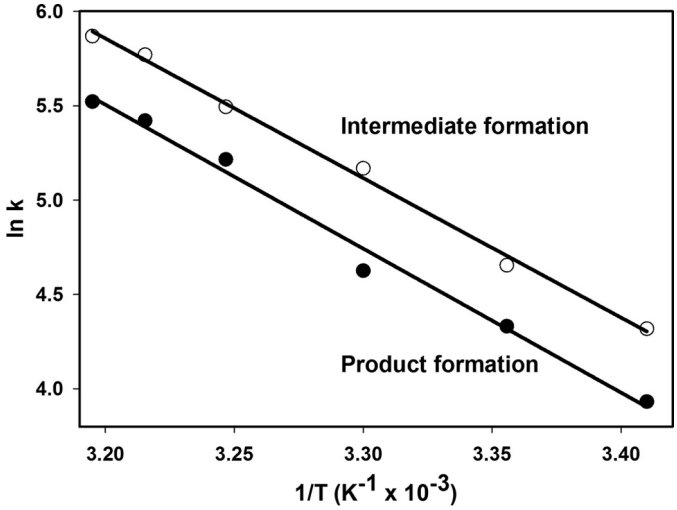

FIGURE 5. The Arrhenius plots for the formation of product (Δ^4-AD) followed at 248 nm yielded an E_a value of 13. 8 ± 0.5 kcal/mol (●) and the formation of the conjugated heteroannular diene intermediate followed at 238 nm yielded an E_a value of 12.9 ± 0.4 kcal/mol (○).

bance followed by a gradual decay corresponding to a decrease in intermediate concentrations.

The Activation Energy of Reaction—The Arrhenius plots for the formation of product at 248 nm and intermediate at 238 nm (Fig. 5) show that the data are linear within the temperature range specified in the experimental procedures. The activation energy at 248 nm is 13.8 kcal/mol and at 238 nm is 12.9 kcal/mol.

Solvent Isotope Effects with Δ^5-AD—Experiments were conducted in which the concentration of Δ^5-AD was varied in H_2O and D_2O, and the initial rates data were fit to Equation 1 describing a random sequential mechanism that is characteristic of GSTs (15).

$$v = \frac{V[A][B]}{K_m^B K_s^A + K_m^B[A] + K_m^A[B] + [A][B]} \quad \text{(Eq. 1)}$$

Steady-state kinetic parameters obtained from the fits are shown in Table 1, where K_s^A is the dissociation constant for the nonvaried substrate and K_m^A and K_m^B are the Michaelis constants for the substrates (18).

The Binding Constant of Equilenin for hGST A3-3—Equilenin was the nonvaried ligand concentration, whereas the hGST A3-3 concentrations ranged from 1 to 15 μM. This unconventional approach of obtaining K_D with a constant ligand concentration and increasing concentrations of enzyme was used because free equilenin is the fluorogenic species. To avoid a protein contribution to the signal, the excitation wavelength used was 325 nm corresponding to the signal produced only by free equilenin (Fig. 6*A*). This information was used to obtain the K_D by monitoring the decrease in fluorescence intensity. The data were fit to a three-parameter hyperbolic decay curve (Equation 2), where F is the fluorescence intensity, $F\infty$ is the extrapolated intensity to infinite enzyme concentrations, F_o is the intensity in the absence of enzyme, $[E_T]$ is the total enzyme concentration, and $[L_T]$ is the total ligand (equilenin) concentration (Fig. 6*B*). The K_D value calculated was 3.93 ± 0.53 μM,

TABLE 1

Solvent isotope exchange with Δ^5–AD at 238 and 248 nm

The enzyme activity with Δ^5-AD was measured with 2 mM saturating GSH in H_2O and D_2O at 20 °C. H_2O refers to 25 mM protiated phosphate buffer at pH 8.0, and D_2O refers to deuterated phosphate buffer at pD 8.0.

Wavelength (nm)	k_{cat}	K_m	k_{cat}/K_m	K_s	Specific activity
	s^{-1}	μM	$mM^{-1}\ s^{-1}$	μM	$\mu mol\ mg^{-1}\ min^{-1}$
H_2O (238)	75 ± 4	20.2 ± 3.4	1700 ± 150		
D_2O (238)	70.4 ± 3.5	19.7 ± 2.3	1400 ± 155		
D_2O (248)	41.7 ± 4.2	13.2 ± 1.8	1100 ± 100		51 ± 5
H_2O (248)	51 ± 3	22.5 ± 4.3	2000 ± 198	9.3 ± 2.2[a]	76 ± 2
GSH (248)		130 ± 21	370 ± 60	50 ± 10[b]	

[a] Determined with a constant Δ^5-AD concentration of 200 μM and varying the GSH concentration.

[b] Determined with a constant GSH concentration of 2 mM and varying the Δ^5-AD concentration.

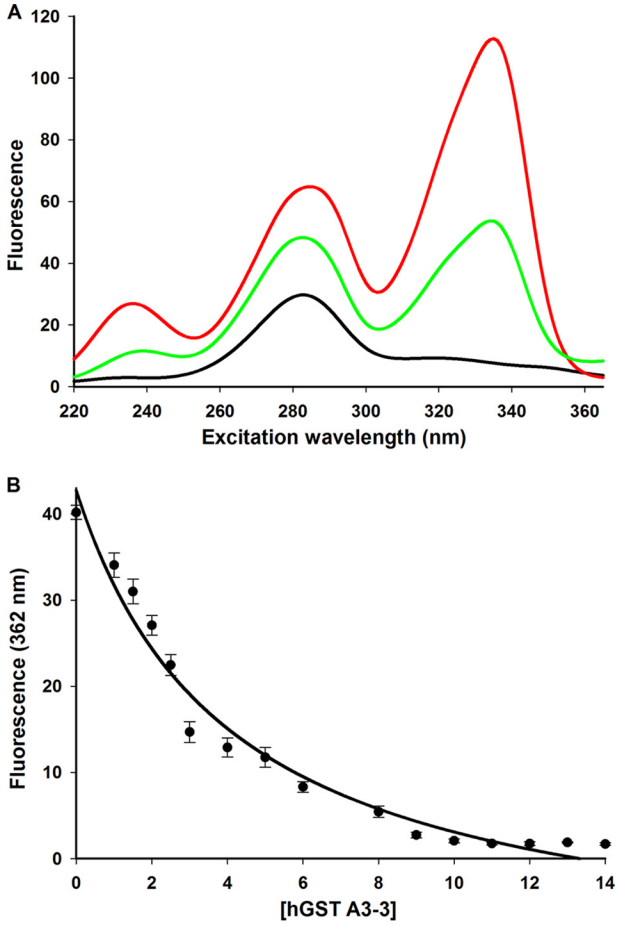

FIGURE 6. **The fluorescence excitation (*A*) of equilenin and hGST A3-3 used to obtain a binding curve (*B*).** The fluorescence data in *A* were collected for free equilenin (*red*), equilenin in the presence of hGST A3-3 (*green*), and free hGST A3-3 (*black*). A quenching effect is observed in the excitation spectra. The emission wavelength was set at 400 nm for *A*, and excitation was set at 325 nm for *B*. The data were fit to a three-parameter hyperbolic decay curve yielding a K_D value of 3.93 ± 0.53 μM. Measurements were done in 1% methanol at pH 8.0 with 3 μM equilenin.

$$F = F_\infty + \frac{\{(F_o - F) - k[E_T]\}K_D}{[E_T]} \quad \text{(Eq. 2)}$$

where $k = F_o - F\infty/[L_T]$.

DISCUSSION

Energetics of Proton Abstraction Reactions—Carbon acids (C–H bonds adjacent to a carbonyl or carboxylic acid func-

Downloaded from http://www.jbc.org/ at UNIVERSITY OF WITWATERSRAND on November 17, 2014

tional group) are generally very weak acids with pK_a values of the α-protons in the range of 12 to 32 (19). At the active site, the general base catalysts are not sufficiently basic, with pK_a values usually ≤7 (20). The large pK_a difference between the substrate and the active site base poses a thermodynamic challenge. To overcome this challenge, enzymes have evolved structural features capable of reducing this thermodynamic contribution to the activation energy.

The binding of the cofactor GSH to hGST A3-3 results in a reduction in the thiol pK_a from 9.17 to 6.31. Consequently at pH 8.0 the cofactor exists in its ionized state. The crystal structure of the ternary complex of hGST A3-3, GSH and the product Δ^4-AD reveals that the thiol group of GSH is 3.7 Å from the carbon 4 atom of Δ^4- AD (11), an ideal distance for proton abstraction. The consensus has been that the ionized thiol plays a role similar to Asp-38 in the KSI-catalyzed reaction, abstracting a proton from the carbon 4 of Δ^5-AD.

The use of chromophoric steroids as a tool to probe the nature of intermediates in ketosteroid isomerization was first reported by Wang *et al.* (21). Fluorescence emission data were used to monitor the ionization state of the phenolic analog intermediate equilenin (Fig. 3*A*). The breaking of the O–H bond in the aromatic phenol increases the number of nonbonding electrons capable of making the $n \rightarrow \pi^*$ electronic transition. This transition requires less energy, and as such a bathochromic shift is observed at pH 11 (21–24). The results indicate that in the presence of hGST A3-3 the emission spectrum resembles that of the un-ionized equilenin. In contrast, the binding of equilenin to KSI results in a spectrum that resembles the ionized state (25). The enone chromopore is responsible for the UV spectral behavior of the ketosteroid competitive inhibitor 19-nortestosterone (Fig. 3*B*). A 10-nm transition of the absorption maximum of this compound from 248 to 258 nm is attributed to enolization, protonation, or strong hydrogen bonding, mimicking its own behavior in strong acid (21, 23, 25, 26).

Our results shown in Fig. 3 indicate that these shifts in wavelength do not occur in the enzyme active site. As hGST A3-3 binds its substrate in the hydrophobic H-site, the generation of charge that accompanies dienolate formation is unfavorable in the solvent-inaccessible hydrophobic environment without the formation of strong directional hydrogen-bonding interactions (26). Our results support the current structural data and show no evidence of such directional hydrogen bonds; consequently the existence of the dienolate would either be a transient feature in a thermodynamically driven pathway, where the final product is more stable, or it would be a nonexistent feature if the end product was merely its own formation. In the KSI mechanism, Asp-99 and Tyr-14 stabilize the intermediate by hydrogen bonding, the D99A mutation decreases the k_{cat} value by $10^{3.7}$ (27), and the Y14F mutation decreases the k_{cat} value by $10^{4.7}$ (23). These mutations result in catalytic turnovers that compare well with the observed turnover value for hGST A3-3, suggesting that this enzyme may be devoid of such strong hydrogen-bonding interactions. The thiolate of GSH acts as the base catalyst but without an equivalent acidic residue at the C3 oxygen, a general, concerted, acid-base catalysis that enhances intermediate stabilization in the enolization step would not occur.

To verify the transient existence of the dienolate in a thermodynamically favored reaction, the isomerization of Δ^5-AD was followed at 238 nm. This wavelength detects the formation of the conjugated heteroannular diene intermediate. The substrate Δ^5-AD possesses an isolated double bond (unconjugated) for which the apparent λ_{max} is calculated to be 203 nm, with an extinction coefficient no greater than 4000 M^{-1} cm^{-1} (28). The principle absorption wavelength for Δ^5-AD is λ_{max} = 200 nm, with a calculated extinction coefficient of 3800 M^{-1} cm^{-1} (Fig. 4*A*). However, the effect of conjugation results in a bathochromic and hyperchromic displacement of the principle absorption band resulting in an increased extinction coefficient of 13,800 M^{-1} cm^{-1} (λ_{max} = 238 nm). The product, Δ^4-AD, has an α,β-ethylenic center conjugated with the 3-keto group. The effect of alkyl substituents on the double bond chromophore is a bathochromic displacement. This displacement, however, does not occur with the same regularity among the three chromophoric regions that constitute the three species in the catalytic pathway: (i) the isolated double bond in the substrate Δ^5-AD, (ii) the conjugated diene in the intermediate species, and (iii) the α,β-unsaturated ketone of the product Δ^4-AD (29). There is a 30–40-nm shift in wavelength in moving from an isolated double bond to a conjugated diene and an additional 11–15-nm wavelength shift from the conjugated diene to the α,β-unsaturated ketone (28–30), with such changes attributed to bond strain and alterations in the planarity of the resonating system. The results in Fig. 4*B* indicate that such transient intermediate species, for which the only form of stabilization is electron delocalization through a conjugate system, do exist. Furthermore, the existence of the transient dienolate intermediate verifies its importance in the catalytic pathway. The intermediate species accumulates and gradually decays because of its transience in the isomerization process. The effect of the carbonyl group at carbon 3 on the rate of isomerization becomes significant only in the presence of strong hydrogen bonds. In the absence of such strong bonds, conjugation becomes the major stabilizing force with only a minimal contribution from the electronegative oxygen atom. The inability of hGST to offer further stability by hydrogen bonding (as is the case with the KSI-catalyzed reaction) means that the intermediate concentrations are not sufficient to account for a turnover similar to that of KSI.

The Marcus Formalism—In proton and electron transfer reactions, rather than considering the activation energy as a single measurable quantity, the Marcus formalism (12, 31–34) divides the activation energy ($\Delta G^{\dagger}$) into two components, (i) the thermodynamic free energy barrier (ΔG^0) and (ii) the intrinsic kinetic barrier ($\Delta G^{\dagger}_{int}$), as shown in Equation 3,

$$\Delta G^{\dagger} = \Delta G^{\dagger}_{int} + \frac{\Delta G^0}{2} + \frac{(\Delta G^0)^2}{16\Delta G^{\dagger}_{int}} \qquad \text{(Eq. 3)}$$

where $\Delta G^{\dagger}_{int}$ is the activation energy barrier in the absence of any thermodynamic contributions (*i.e.* when $\Delta G^0 = 0$). In proton transfer reactions, ΔG^0 is a function of ΔpK_a and is given by $\Delta G^0 = 2.303\ RT\Delta pK_a$ (ΔpK_a is the difference in the pK_a values

Downloaded from http://www.jbc.org/ at UNIVERSITY OF WITWATERSRAND on November 17, 2014

between the proton donor and acceptor) (35). The position of the transition state occurs at the maximum value of Equation 3 and is given by Equation 4, which equals the Brønsted coefficient, β_c.

$$x^{\dagger} = \beta_c = 0.5 + \frac{\Delta G^0}{8\Delta G^{\dagger}_{int}} \quad \text{(Eq. 4)}$$

In the hGST A3-3-catalyzed reaction, the k_{cat} obtained for the isomerization of Δ^5-AD translates into an activation energy of 13.8 kcal/mol from the Arrhenius plots in Fig. 5 and a calculated $\Delta G^{\dagger} = 14.8$ kcal/mol (according to the Eyring transition state equation). The hGST-catalyzed isomerization reaction has been found to follow a random sequential mechanism (15). If the model of Reaction 1 (E = enzyme, G = glutathione, S = Δ^5-AD, I = intermediate, and P = product) for a random sequential mechanism is used (where 2 mM GSH and enzyme are incubated first to prevent initial random binding), then the k_{cat} is given by Equation 5 (36).

$$EG + S \underset{k_2}{\overset{k_1}{\rightleftharpoons}} EGS \underset{k_4}{\overset{k_3}{\rightleftharpoons}} EGI \underset{k_6}{\overset{k_5}{\rightleftharpoons}} EGP \left\{ \begin{array}{l} \underset{k_8}{\overset{k_7}{\rightleftharpoons}} EP \underset{k_{10}}{\overset{k_9}{\rightleftharpoons}} E + P \\ \underset{k_{12}}{\overset{k_{11}}{\rightleftharpoons}} EG \underset{k_{14}}{\overset{k_{13}}{\rightleftharpoons}} E + G \end{array} \right.$$

REACTION 1

$$\frac{1}{k_{cat}} = \frac{1}{k'_3} + \frac{1}{k'_5} + \frac{1}{k'_{7,11}} \quad \text{(Eq. 5)}$$

where k'_3, k'_5, and $k'_{7,11}$ are net rate constants, with $k'_{7,11} = k_9k_{13}(k_{11} + k_7)/k_9k_{13} + k_9k_{11} + k_7k_{13}$. The value of the apparent second order rate constant indicates that the hGST A3-3-catalyzed reaction is not diffusion-controlled, despite the high catalytic efficiency. This coupled with the fact that the product, Δ^4-AD (with a K_i of 25 μM), has the same affinity as the substrate (5) means that the net rate constants for dissociation are large (non-limiting). Thus Equation 5 approximates to Equation 6.

$$\frac{1}{k_{cat}} \approx \frac{1}{k_3'} + \frac{1}{k_5'} \quad \text{(Eq. 6)}$$

Given that $k_6 \ll (k_7 + k_{11})$,

$$k_{cat} \approx \frac{k_3k_5}{k_4 + k_5} \quad \text{(Eq. 7)}$$

The microscopic rate constants reveal that the rate-limiting steps are the chemical steps: proton abstraction from carbon 4, proton transfer to carbon 6, and proton transfer back to carbon 4 (Equation 7). The reaction at 238 nm is best described by Reaction 2. The reverse reaction from *EGI to EGS* (k_4) is assumed to be zero as initial rates are considered.

$$EG + S \underset{k_2}{\overset{k_1}{\rightleftharpoons}} EGS \overset{k_3}{\rightleftharpoons} EGI$$

REACTION 2

The results shown in Table 1 reveal that in H_2O, the k_{cat} for the overall reaction followed at 248 nm is comparable with the k_{cat} value for the reaction followed at 238 nm. Because this value represents k_3, the proton abstraction step is rate-limiting. This allows us to use the macroscopic k_{cat} value as an approximation to the microscopic rate constant k_3 of the proton abstraction in the Marcus equation. In assessing the contribution of the carbon 6 proton transfer step to the overall rate, solvent isotope effects are employed. The H/D isotopic exchange between solvent and substrate occurs at the intermediate during the proton transfer step. In both reactions followed at 238 and 248 nm, $(^{H}k_{cat})/(^{D}k_{cat}) \approx 1$, suggesting that the carbon 6 proton transfer step is nonlimiting, whereas the carbon 4 proton abstraction step is independent of H/D exchange with solvent.

This analysis however overlooks the possibility of protonation back to carbon 4 in the reverse reaction. The rate of carbon 4 protonation would be given by Equation 8,

$$k_r = \frac{k_2k_4}{k_2 + k_3} \quad \text{(Eq. 8)}$$

where k_r is the net rate constant for reverse protonation at carbon 4; because the diffusion steps are rapid ($k_2 \ll k_3$), the value of $k_r \approx k_4$. The internal equilibrium constant between substrate and intermediate has been found ($K_{int} = 0.3$) (37). This internal equilibrium constant indicates that the relative energies of the substrate and intermediate are similar. Because the free energy of reaction favors product formation ($K_{eq} = 2400$) (17), the energy barrier for carbon 4 protonation back to reactant is much larger than the carbon 6 protonation for the forward reaction. Therefore the k_{cat} values for the forward reactions are minimally affected by the possible carbon 4 protonation.

If the pK_a of Δ^5-AD remains invariant upon binding the H-site, then the thermodynamic energy required for proton abstraction is $\Delta G^0 = 9$ kcal/mol (pK_a of bound GSH is 6.31). The value obtained for the intrinsic kinetic barrier from Equation 2 is $\Delta G^{\dagger}_{int} = 10$ kcal/mol. Hawkinson *et al.* (37) calculated the intrinsic barrier for proton transfer from Δ^5-AD in solution to be ($\Delta G^{\dagger}_{int} = 13$ kcal/mol. This value was obtained by estimating the Brønsted β_c value of oxygen bases from tertiary amine and oxygen bases involved in the isomerization of 3-cyclohexanone. A β_c value of 0.6 was obtained, representative of the acetate oxygen base used to catalyze the solution reaction. The actual β value for the acetate ion-catalyzed ketonization is 0.54 (38), verifying the accuracy of the Hawkinson approximation. Due credence must however encompass the role of the thiol as the base. Oxidized glutathione and similar thiols have β_c values ranging between 0.5 and 0.55 (39, 40); because the basicity of thiols is expected to be greater than resonance-stabilized oxygen bases such as acetates, the upper limit value of this range was used, and the Hawkinson approximation was still upheld. The strategy of hGST A3-3 appears in part to reduce the intrinsic kinetic barrier by 3 kcal/mol. The Brønsted coefficient describing the position of the transition state is $\beta_c = 0.6$, a value that indicates a nearly symmetrical transition state.

Revised Mechanism—The hGST A3-3 reaction pathway is initiated by proton abstraction at carbon 4 of Δ^5-AD (Fig. 7). During proton abstraction, a negative charge develops at the

Downloaded from http://www.jbc.org/ at UNIVERSITY OF WITWATERSRAND on November 17, 2014

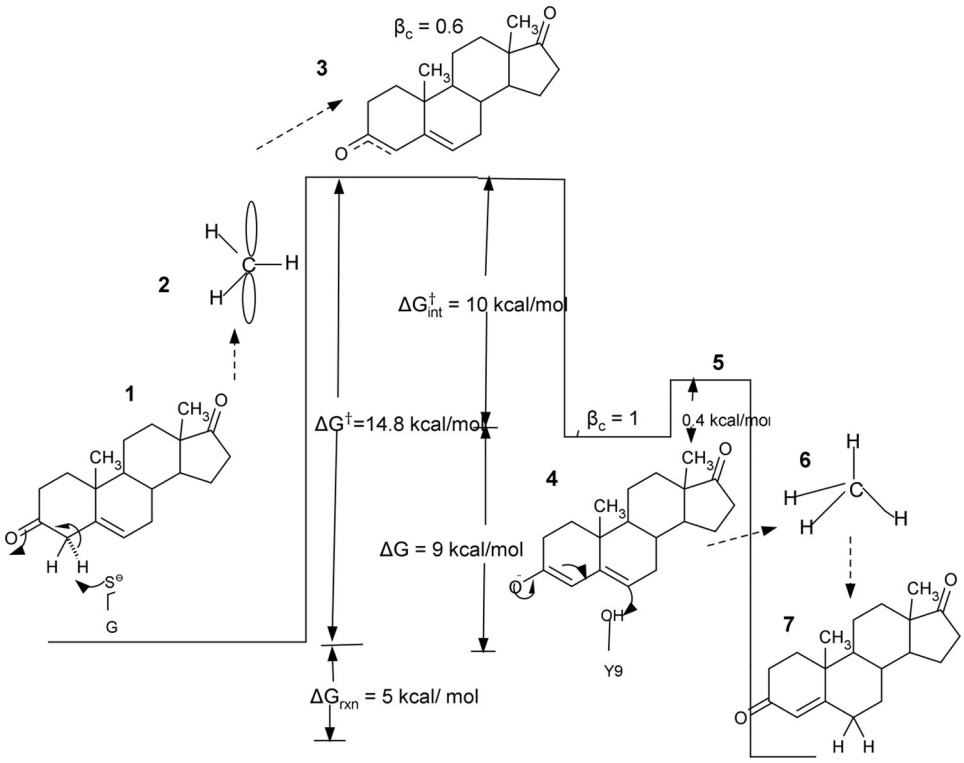

FIGURE 7. **The proposed reaction pathway for the isomerization of Δ^5-AD by hGST A3-3, were the *steps* are numbered *1–7* and the thermodynamic parameters are calculated per enzyme subunit.** At *step 1*, GSH abstracts the carbon 4 proton; at *step 2* a change in hybridization at carbon 4 to a higher energy *p*-orbital; at *step 3*, a transition state occurs that is nearly symmetrical but slightly favors the intermediate. At *step 4* the structural realignments have advanced since the transition state, and the high energy *p*-orbital electrons are stabilized by the now fully developed conjugate system. At *step 5* the transfer of a proton to carbon 6 is kinetically insignificant, resulting in an enforced concerted mechanism, and at *step 6* a transfer of electrons from the *p*-orbital to the lower energy sp3 orbital resulting in *step 7*.

site of bond cleavage, and the carbon 4 carbon transits from sp3 hybridization to sp2. This transition is energetically unfavorable because the electrons from the lower energy sp3 orbital are transferred to the vacant *p*-orbital of higher energy. At the energy maxima, the transition state is nearly symmetrical but slightly favors the intermediate, as indicated by the Brønsted coefficient ($\beta_c = 0.6$). As structural rearrangement progresses, electrons in the higher energy *p*-orbital are stabilized by the O3-C3-C4-C5-C6 conjugate system. Charge development has the effect of realigning the dipoles of active site water molecules, thereby producing a negative entropic contribution due to solvent ordering (33). The intrinsic kinetic barrier $\Delta G^{\dagger}_{int}$ refers to the energy that has to be overcome in making such an unfavorable electronic configuration as well as the negative entropic contribution associated with solvent ordering (41). Conjugation alone has a minimal contribution to the overall stability of the intermediate. The strategy of hGST A3-3 is to lower $\Delta G^{\dagger}_{int}$ with a value of 13 kcal/mol in solution to $\Delta G^{\dagger}_{int} = 10$ kcal/mol at the active site. The enzyme utilizes an alternative reaction pathway that alters the cofactor pK_a, thereby contributing 3.8 kcal/mol to the reaction. Although the altered pK_a of GSH contributes to the ΔG^0 favorably, the enzyme has no structural features such as amino acids capable of forming hydrogen bonds and is thus incapable of effectively dealing with the developing charge. As the free energy of reaction favors product formation ($K_{eq} = 2400$) and the realization that the chemical steps are rate-limiting, proton transfer to carbon 6 (resulting in product) is therefore a fast step. Solvent isotope exchange reveals that this energetic barrier is 0.4 kcal/mol. As the kinetics studies follow product (and intermediate) formation, this energetic barrier does not include the regeneration of the protonated Tyr-9 but merely the transfer of a proton to carbon 6. We propose that hGST A3-3 lowers the $\Delta G^{\dagger}_{int}$ by accelerating the rate of proton transfer to carbon 6, making this the fast step. The rapid transfer of the proton minimizes the extent of charge imbalance at the transition state and intermediate, ultimately reducing the negative entropic contribution associated with solvent ordering at the active site. because $\Delta G^{\dagger}_{int} = \Delta H^{\dagger}_{int} + T\Delta S^{\dagger}_{int}$ (33), a reduction in the loss of entropy contributes to lowering the activation energy. The K_D value of 3.93 μM for equilenin (Fig. 6*B*) indicates that the protonated form of the intermediate has an affinity for binding similar to that of the substrate (as indicated by the K_S value). Although we could not obtain the K_D of ionized equilenin without compromising enzyme structure, a comparison of the K_D values of hGST A3-3 and KSI provided further insight. The K_D of equilenin for KSI is 1 μM (37), a value similar to that of hGST A3-3. However, the rate of the KSI-catalyzed reaction is greater than that of hGST A3-3 by 3 orders of magnitude, suggesting greater dienolate intermediate concentrations for the KSI reaction. Therefore, the critical difference is charge stabilization. A computational analysis using a hybrid quantum mechanics/molecular mechanics approach is in agreement with this mechanism, which proceeds via an intermediate (42). The reported thermodynamic parameters of

Downloaded from http://www.jbc.org/ at UNIVERSITY OF WITWATERSRAND on November 17, 2014

this computational study are however nearly 2-fold greater than our reported values and may represent the dimeric protein instead of subunit values. Recently, Ramos and co-workers (43) have reconstructed the catalytic pathway by resorting to density functional theory, and their findings show that water molecules are neither necessary nor responsible for stabilizing the intermediate. They however attribute this stability to strong hydrogen bonds formed between the GSH-glycine main chain and the C3 oxygen (43). This is supported by kinetic studies in which the K_m value increases from 45 to 310 μM in the absence of GSH, suggesting a reduced affinity for Δ^5-AD due to the absence of this hydrogen bond. The use of K_m as an approximate measure for binding affinity becomes problematic with increased kinetic complexity. This value becomes a composite function of many microscopic rate constants, and its contribution to the observed value may be significant depending on the dominant enzyme-bound state. Nonetheless, if this approximation is accepted and further concession is made that this binding energy is realized most strongly at the transition-intermediate stages, the increase in the K_m value from 45 to 310 μM would only account for an energy difference of ~1 kcal/mol, indicating that the contribution of the GSH-glycine main chain hydrogen bond with O3 contributes very little to the kinetic process.

The mechanism shown in Fig. 1, **Scheme I**, postulates the existence of a localized water molecule to stabilize a transient dienolate intermediate at the C3 oxygen similar to the roles of Tyr-14 and Asp-99 in the KSI-catalyzed reaction; however, neither our results nor the currently available structural data support this view. The mechanism shown in Fig. 1, **Scheme II**, proposes a reaction pathway that avoids the formation of the dienolate by placing a transient double bond at the α,β-positions. The mechanism implies perfect synchronization of the bond-breaking and -making process, as anything less would result in an overcommitted β-carbon with five bonds. Although this is within the realm of possibility, charge delocalization has been seen to lag behind proton transfer due to a lag in resonance development in carbon acids (41) and specifically in enzymatic enolization reactions (38). Furthermore electron movement against an electronegativity gradient and a conjugate system that offers stability is unlikely. As the chemical steps are rate-limiting and the K_{eq} favors product formation, the energy barrier to product formation cannot exceed that of the decomposition back to substrate. Because of the instability of the dienolate intermediate, in which only form of stabilization is charge delocalization, the collapse to product, which is strongly favored thermodynamically, may not be activation-limited, making this step kinetically insignificant. We are of the view that reaction proceeds through an enforced, concerted mechanism (44, 45) that results from changes in a stepwise process, where the energy that corresponds well to an intermediate is nearly commensurate with a regular, concerted mechanism.

Acknowledgments—We thank Professor Emeritus Ralph Pollack for valuable and insightful suggestions on certain aspects of the experimental design and Monika Nowakowska for assistance rendered with the thermostated Varian Cary UV-visible spectrophotometer.

REFERENCES

1. Armstrong, R. N. (1997) Structure, catalytic mechanism, and evolution of the glutathione transferases. *Chem. Res. Toxicol.* **10,** 2–18
2. Mannervik, B., and Danielson, U. H. (1988) Glutathione transferase-structure and catalytic activity. *CRC Crit. Rev. Biochem.* **23,** 283–337
3. Dirr, H., Reinemer, P., and Huber, R. (1994) X-ray crystal structures of cytosolic glutathione *S*-transferases. *Eur. J. Biochem.* **220,** 645–661
4. Benson, A. M., and Talalay, P. (1976) Role of reduced glutathione in the Δ(5)-3-kitosteroid isomerase reaction of liver. *Biochem. Biophys. Res. Commun.* **69,** 1073–1079
5. Johansson, A. S., and Mannervik, B. (2001) Human glutathione transferase A3-3, a highly efficient catalyst of double-bond isomerization in the biosynthetic pathway of steroid hormones. *J. Biol. Chem.* **276,** 33061–33065
6. Montgomery, R., Conway, T. W., Spector, A. A., and Chappell, D. (1996) Biochemistry: A Case-oriented Approach, 6th Ed., pp. 587–618, Mosby Year Book, Inc., St. Louis, MO
7. Talalay, P., and Wang, V. S. (1955) Enzymic isomerization of Δ5-3-ketosteroids. *Biochim. Biophys. Acta* **18,** 300–301
8. Benson, A. M., Talalay, P., Keen, J. H., and Jakoby, W. B. (1977) Relationship between the soluble glutathione-dependent Δ5-3-ketosteroid isomerase and the glutathione *S*-transferases of the liver. *Proc. Natl. Acad. Sci. U.S.A.* **74,** 158–162
9. Hawkinson, D. C., Eames, T. C., and Pollack, R. M. (1991) Energetics of 3-oxo-Δ 5-steroid isomerase: source of the catalytic power of the enzyme. *Biochemistry* **30,** 10849–10858
10. Gu, Y., Guo, J., Pal, A., Pan, S. S., Zimniak, P., Singh, S. V., and Ji, X. (2004) Crystal structure of human glutathione *S*-transferase A3-3 and mechanistic implications for its high steroid isomerase activity. *Biochemistry* **43,** 15673–15679
11. Tars, K., Olin, B., and Mannervik, B. (2010) Structural basis for featuring of steroid isomerase activity in α class glutathione transferases. *J. Mol. Biol.* **397,** 332–340
12. Marcus, R. A. (1969) Unusual slopes of free energy plots in kinetics. *J. Am. Chem. Soc.* **91,** 7224–7225
13. Zeng, B., and Pollack, R. M. (1991) Microscopic rate constants for the acetate ion catalyzed isomerization of 5-androstene-3,17-dione to 4-androstene-3,17-dione: a model for steroid isomerase. *J. Am. Chem. Soc.* **113,** 3838–3842
14. Tian, X. Q., Chen, T. C., Matsuoka, L. Y., Wortsman, J., and Holick, M. F. (1993) Kinetic and thermodynamic studies of the conversion of previtamin D3 to vitamin D3 in human skin. *J. Biol. Chem.* **268,** 14888–14892
15. Pettersson, P. L., and Mannervik, B. (2001) The role of glutathione in the isomerization of delta 5-androstene-3,17-dione catalyzed by human glutathione transferase A1-1. *J. Biol. Chem.* **276,** 11698–11704
16. Caccuri, A. M., Antonini, G., Board, P. G., Parker, M. W., Nicotra, M., Lo Bello, M., Federici, G., and Ricci, G. (1999) Proton release on binding of glutathione to alpha, mu, and delta class glutathione transferases. *Biochem. J.* **344,** 419–425
17. Pollack, R. M., Zeng, B., Mack, J. P. G., and Eldin, S. (1989) Determination of the microscopic rate constants for the base-catalyzed conjugation of 5-androstene-3,17-dione. *J. Am. Chem. Soc.* **111,** 6419–6423
18. Cleland, W. W. (1963) The kinetics of enzyme-catalyzed reactions with two or more substrates or products. I. Nomenclature and rate equations. *Biochim. Biophys. Acta* **67,** 104–137
19. Chiang, Y., and Kresge, A. J. (1991) Enols and other reactive species. *Science* **253,** 395–400
20. Gerlt, J. A., Kozarich, J. W., Kenyon, G. L., and Gassman, P. G. (1991) Electrophilic catalysis can explain the unexpected acidity of carbon acids in enzyme-catalyzed reactions. *J. Am. Chem. Soc.* **113,** 9667–9669
21. Wang, S. F., Kawahara, F. S., and Talalay, P. (1963) The mechanism of the Δ5-3-ketosteroid isomerase reaction: absorption and fluorescence spectra of enzyme-steroid complexes. *J. Biol. Chem.* **238,** 576–585
22. Bevins, C. L., Pollack, R. M., Kayser, R. H., and Bounds, P. L. (1986) Detection of a transient enzyme-steroid complex during active-site-directed irreversible inhibition of 3-oxo-Δ 5-steroid isomerase. *Biochemistry* **25,** 5159–5164
23. Kuliopulos, A., Mildvan, A. S., Shortle, D., and Talalay, P. (1989) Kinetic

Downloaded from http://www.jbc.org/ at UNIVERSITY OF WITWATERSRAND on November 17, 2014

and ultraviolet spectroscopic studies of active-site mutants of Δ5-3-ketosteroid isomerase. *Biochemistry* **28,** 149–159
24. Eames, T. C., Pollack, R. M., and Steiner, R. F. (1989) Orientation, accessibility, and mobility of equilenin bound to the active site of steroid isomerase. *Biochemistry* **28,** 6269–6275
25. Zeng, B. F., Bounds, P. L., Steiner, R. F., and Pollack, R. M. (1992) Nature of the intermediate in the 3-oxo-Δ 5-steroid isomerase reaction. *Biochemistry* **31,** 1521–1528
26. Zhao, Q., Mildvan, A. S., and Talalay, P. (1995) Enzymic and nonenzymic polarizations of. α,β-unsaturated ketosteroids and phenolic steroids: implications for the roles of hydrogen bonding in the catalytic mechanism of Δ 5-3-ketosteroid isomerase. *Biochemistry* **34,** 426–434
27. Wu, Z. R., Ebrahimian, S., Zawrotny, M. E., Thornburg, L. D., Perez-Alvarado, G.C., Brothers, P., Pollack, R. M., and Summers, M. F. (1997) Solution structure of 3-oxo-Δ5-steroid isomerase. *Science* **276,** 415–418
28. Bladon, P., Henbest, H. B., and Wood, G. W. (1952) Studies in the sterol group. Part LV. Ultra-violet absorption spectra of ethylenic centres. *J. Chem. Soc.* **517,** 2737–2744
29. Woodward, R. B. (1941) Structure and the absorption spectra of α,β-unsaturated ketones. *J. Am. Chem. Soc.* **63,** 1123–1126
30. Dorfman, L. (1953) Ultraviolet absorption of steroids. *Chem. Rev.* **53,** 47–144
31. Cohen, A. O., and Marcus, R. A. (1968) Slope of free energy plots in chemical kinetics. *J. Phys. Chem.* **72,** 4249–4256
32. Albery, W. J. (1980) The application of the Marcus relation to reactions in solution. *Annu. Rev. Phys. Chem.* **31,** 227–263
33. Gerlt, J. A., and Gassman, P. G. (1993) Understanding the rates of certain enzyme-catalyzed reactions: proton abstraction from carbon acids, acyl transfer reactions, and displacement reactions of phosphodiesters. *Biochemistry* **32,** 11943–11952
34. Marcus, R. A. (2006) Enzymatic catalysis and transfers in solution. I. Theory and computations, a unified view. *J. Chem. Phys.* **125,** 194504
35. Gerlt, J. A., and Gassman, P. G. (1992) Understanding enzyme-catalyzed proton abstraction from carbon acids: details of stepwise mechanisms for β-elimination reactions. *J. Am. Chem. Soc.* **114,** 5928–5934
36. Cleland, W. W. (1975) Partition analysis and concept of net rate constants as tools in enzyme kinetics. *Biochemistry* **14,** 3220–3224
37. Hawkinson, D. C., Pollack, R. M., and Ambulos, N. P., Jr. (1994) Evaluation of the internal equilibrium constant for 3-oxoΔ 5-steroid isomerase using the D38E and D38N mutants: the energetic basis for catalysis. *Biochemistry* **33,** 12172–12183
38. Yao, X., Gold, M. A., and Pollack, R. M. (1999) Transition state imbalance in proton transfer from phenyl ring-substituted 2-tetralones to acetate ion. *J. Am. Chem. Soc.* **121,** 6220–6225
39. Szajewski, R. P., and Whitesides, G. M. (1980) Rate constants and equilibrium constants for thiol-disulfide interchange reactions involving oxidized glutathione. *J. Am. Chem. Soc.* **102,** 2011–2026
40. Dalby, K. N., and Jencks, W. P. (1997) General acid catalysis of the reversible addition of thiolate anions to cyanamide. *J. Chem. Soc. Perkin Trans.* **2,** 1555–1564
41. Bernasconi, C. F. (1992) The principle of nonperfect synchronization: more than a qualitative concept? *Acc. Chem. Res.* **25,** 9–16
42. Calvaresi, M., Stenta, M., Garavelli, M., Altoé, P., and Bottoni, A. (2012) Computational evidence for the catalytic mechanism of human glutathione *S*-transferase A3-3: a QM/MM investigation. *ACS Catal.* **2,** 280–286
43. Dourado, D. F., Fernandes, P. A., Mannervik, B., and Ramos, M. J. (2014) Isomerization of Δ5-androstene-3,17-dione into Δ4-androstene-3,17-dione catalyzed by human GST A3-3: a computational study identifies a dual role for glutathione. *J. Phys. Chem. A* **118,** 5790–5800
44. Williams, A. (1994) The diagnosis of concerted organic mechanisms. *Chem. Soc. Rev.* **23,** 93–100
45. Jencks, W. P. (1981) Ingold lecture: how does a reaction choose its mechanism? *Chem. Soc. Rev.* **10,** 345–375

Downloaded from http://www.jbc.org/ at UNIVERSITY OF WITWATERSRAND on November 17, 2014